INFORMATION TO USERS

This manuscript has been reproduced from the microfilm master. UMI films the text directly from the original or copy submitted. Thus, some thesis and dissertation copies are in typewriter face, while others may be from any type of computer printer.

The quality of this reproduction is dependent upon the quality of the copy submitted. Broken or indistinct print, colored or poor quality illustrations and photographs, print bleedthrough, substandard margins, and improper alignment can adversely affect reproduction.

In the unlikely event that the author did not send UMI a complete manuscript and there are missing pages, these will be noted. Also, if unauthorized copyright material had to be removed, a note will indicate the deletion.

Oversize materials (e.g., maps, drawings, charts) are reproduced by sectioning the original, beginning at the upper left-hand corner and continuing from left to right in equal sections with small overlaps.

Photographs included in the original manuscript have been reproduced xerographically in this copy. Higher quality 6" x 9" black and white photographic prints are available for any photographs or illustrations appearing in this copy for an additional charge. Contact UMI directly to order.

Bell & Howell Information and Learning
300 North Zeeb Road, Ann Arbor, MI 48106-1346 USA
800-521-0600

UMI®

HIGH SOLIDS DENSITY GYPSUM PRODUCTION THROUGH AN IMPROVED NEUTRALIZATION PROCESS FOR ZINC PLANT EFFLUENT

Sidney J. Omelon

Department of Mining and Metallurgical Engineering
McGill University
Montreal, Canada

July, 1998

A Thesis submitted to the Faculty of Graduate Studies and Research in partial fulfillment of the requirements of the degree of Master of Engineering

National Library
of Canada

Acquisitions and
Bibliographic Services

395 Wellington Street
Ottawa ON K1A 0N4
Canada

Bibliothèque nationale
du Canada

Acquisitions et
services bibliographiques

395, rue Wellington
Ottawa ON K1A 0N4
Canada

Your file Votre référence

Our file Notre référence

0-612-55122-9

Canada

Abstract

A common wastewater treatment process practiced by zinc production facilities is the single-stage mixing of acidic wastewaters with slaked lime, inducing the reactive precipitation of fine (~1μm) gypsum ($CaSO_4.2H_2O$) and other solids with a solids density less than 10%. These solids report to a tailings pond for containment.

Tailings pond life would be increased if the solids density of the precipitated solids was improved. Previous work at McGill University suggested that a staged neutralization process with solids recycle and seeded with gypsum would produce large-sized gypsum crystals with a high solids density. A continuous lab-scale process run with synthetic zinc plant effluent produced large (~100μm) gypsum crystals with a solids density of 50±3%.

Meissner's method of calculating mean activity coefficients allowed for the calculation of gypsum solubility in mixed, strong sulphate electrolyte solutions.

Résumé

Le traitement des eaux usées de l'usine de production de zinc est normalement un procédé simple qui mélange l'effluent acide sulfaté avec la soude. Les fines (~ 1 µm) du gypse ($CaSO_4.2H_2O$) et les autres solides sont produit. Ils ont un pourcentage de solides qui est inférieur à 10 %. Les solids sont envoyés dans un parc à résidus.

La durée de vie des parcs à résidus peut être augmenter si le pourcentage de solides de les precipites est amelioré. Des études menées à l'Université McGill ont montré qu'il est possible de générer des particules de gypse de plus grosse taille en utilisant un procédé combinant neutralisation par étapes, semence avec la gypse et recyclage d'une partie du solides formé. Un procédé continu marchait dans la laboratoire avec d'eaux usée synthétique qui a produit de larges (~ 100 µm) particules de gypse et un pourcentage en solides de 50±3%.

Acknowlegments

First and foremost, I acknowledge and thank my project principal and supervisor, Dr. Demopoulos. I am most grateful to him for the opportunity to be the student to work on this project, and for the many hours and energy he has spent with me from which many amazing things have grown.

I express much gratitude to CEZinc, the Noranda Technology Center and NSERC for their financial contributions to this project.

Ever and extremely thankful and grateful I am to Monique Riendeau, Helen Campbell, and Glenn Poirier for their invaluable skills, technical help with analysis and SEM imaging, time, patience and insight.

The work, company and conversations (Frostbite trips too) with Anne le Guen and Alex Brassard were invaluable to this project; their contributions to this work are extremely appreciated. Thanks to Joachim Broomberg for his company and his help with the Résumé.

Thanks are also extended to:

- The ever-present Dutch contingent: Dave "Lange" Droppert, Raf Dabekaussen, Niels "Knorrie" Verbaan, Prof. G. van Weert, and my colleagues, especially Amy Nelson, Frank Principe, Trina Dreher, the Hydromet. group, Colin Hardie and his printer, the coffee-chocolate club champion James Anson, the dessert-deserving Louisa Davis, as well as the super-spirited undergrads with whom much decompressing took place.

- Other amazing engineering/research role-models of Dr. Cooke, Dr. Munz, Des Brophy, Ben Shaw, Dr. and Mr. Jan Kwak and Dr. Laplante.

- Debbie Morzajew, Nigel Ayoung-Chee, Sima Gupta, Gunther Leichtle and the other wonders of the EMF lab.

- My roommates: Jane, Jon, Candice, Debbie, Trina and Maia, who endured endless biological drawer experiments and an overtired roommate.

This is dedicated to the memories of Dave Brophy and Professor Fuller, as well as to Tom O'Connor and Judy Pharo, to whom I am thankful for asking the questions that helped me define my characteristically convoluted path, to my Mom and Dad for the opportunity to take it and to special Champignon who walked some of the more brutal parts with me.

TABLE OF CONTENTS

8 APPENDICES ....

1 INTRODUCTION

The treatment of plant wastewater does not often receive much process attention. The most simple and common acidic wastewater neutralization process is usually employed before the neutral effluent is discharged past the plant battery limits. In particular, the zinc industry commonly treats its acidic sulphate waste streams by mixing them with an inexpensive base and calcium source, such as slaked lime or limestone in an agitated process vessel. The hydroxide ions of the slaked lime neutralize the acidic stream, and gypsum is produced by the reactive precipitation of calcium with sulphate and water:

$$Ca(OH)_{2(aq)} + H_2SO_4 \rightarrow CaSO_4 \cdot 2H_2O_{(s)}$$

Zinc, iron, magnesium and manganese ions are also present in the wastewater; some of these precipitate out as hydroxides or other solid salts at the final neutral pH. The solids precipitated by this process are separated in large thickeners, as the fine particles settle out slowly. The low solids density underflow (<10%) reports to a tailings pond for containment, while the overflow is used as process water or discharged to the environment.

The volumetric flowrate of underflow to the tailing pond would be reduced if the solids density of the precipitated product could be increased. Research conducted by the hydrometallurgy group at McGill suggested that a new neutralization process, based on crystallization theory, could be developed that would produce higher solids density precipitate. A controlled, seeded neutralization process with solids recycle was proposed to increase the precipitated gypsum particle size, settling velocity and solids density. This masters' thesis is the result of the joint NSERC-CEZinc funded project to study the reactive crystallization of gypsum and design a new neutralization process for synthetic zinc plant effluent.

The thesis is divided into five parts. The first chapter describes the setup and use of a model that predicts gypsum solubility in acidic sulphate aqueous electrolyte, with a literature review of past publications relating to the prediction of gypsum solubility. Knowledge of gypsum solubility data is important for the design of a gypsum precipitation process, and if scale production is of concern.

The next chapter discusses the precipitation of solid salts, and gypsum in particular, from solution. The relevant crystallization theory is presented, and the published literature reviewed. The experiments used to determine the critical supersaturation above which gypsum spontaneously precipitates from sulphuric acid solutions are reported, with a discussion of the results.

The new seeded, controlled neutralization process concept was tested with pure sulphuric acid solutions in a semi-batch format. The neutralization of two pH ranges (pH 0.5 to 1, and pH 1 to 7) were tested with slaked lime and calcium carbonate as neutralization agents. Chapter 4 discusses relevant crystallization process information and presents the results of the semi-batch tests, which suggested that a continuous controlled neutralization process with solids recycle could produce gypsum with increased size and solids density.

Chapter 5 outlines the process of selecting the optimum solids loading, neutralization agent, neutralization agent concentration, reactor setup and process design for the continuous neutralization of synthetic zinc plant wastewater. The results of this process are compared to the results of other process alternatives. The average solids density of the precipitate produced by a seeded, staged neutralization process with solids recycle that neutralized synthetic zinc plant wastewater from pH 1 to 5 with slaked lime was 50±3%. The other process alternatives produced precipitate with lower solids density. An analysis of the solution chemistry indicated that less zinc reported to the solids precipitated by the staged, seeded neutralization with solids recycle than by the single stage neutralization process with no seeding or solids recycle. This could provide an option of increasing the zinc recovery from the waste streams.

The Appendices constitute the last section. They expand on relevant gypsum crystallization and other subjects that contribute to the understanding of the complex problem of gypsum precipitation.

2 PREDICTING GYPSUM SOLUBILITY IN AQUEOUS ELECTROLYTE SOLUTIONS

2-1 INTRODUCTION

The use of mathematical modeling has increased in research and industry to save time and costs. Some models are successfully developed from first principles, and others are hybrids that include empirical relations. One interesting frontier of mathematical modeling for the chemical and metallurgical process industries involves the modeling of aqueous electrolytes. Aqueous thermodynamics is an interesting mix of theory and empirical relations; the models that strive to predict thermodynamic data are many and varied in their methods.

Knowledge of electrolyte solubility data is important as it is the first step of the successful development of a crystallization process (Price, 1997). As the goal of this project was the development of a neutralization process involving the precipitation of gypsum from an acidic electrolyte, a model was developed to predict the solubility of gypsum for a particular range of sulphate electrolyte compositions and temperatures.

2-1-1 Modeling Aqueous Electrolyte Systems – A Brief Review

Central to the successful modeling of aqueous electrolyte systems is the calculation of the activity coefficients of the ionic species in solution. Many methods have been developed to predict electrolyte activity coefficients. The method of Debye and Hückel is based on different empirical parameters. However, this model is effective only for single ion systems of dilute concentrations. Davies (1938), Pitzer (1973) and Janz (1983) developed more comprehensive methods of calculating ion activity coefficients; these also lose precision in predicting the activity coefficients for polyvalent, mixed and concentrated systems. Yadav et al. (1995) used the method of Davies to predict gypsum solubility in binary electrolyte systems, but had to regress equation parameters with experimental data in order to produce good results.

Meissner published a valuable novel method of calculating mean ion activity coefficients for polyvalent electrolytes in low and high ionic strength solutions (Meissner et al., 1972, 1973, 1980, Kusik et al., 1978). The model presented in this work uses Meissner's method to calculate the mean activity coefficient of gypsum in mixed sulphate electrolyte solutions in order to predict its solubility. Figure 2-1 compares experimental gypsum solubility values, literature data, values calculated with PHREEQE (Parkhurst et al, 1998) a program that uses the Debye-Hückel or Davies equations to model aqueous electrolyte systems, and values calculated in this work by Meissner's method. It is clear that the Davies equation results become less accurate at higher ionic strengths.

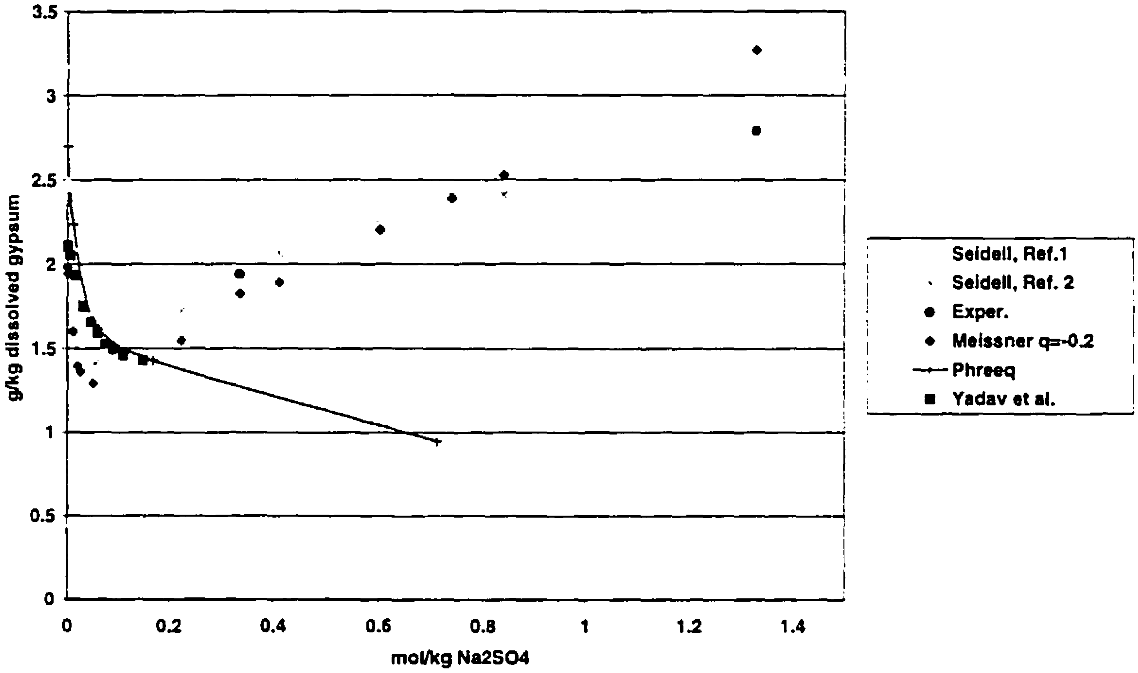

Figure 2-1: Comparison of calculated and experimental gypsum solubility values in sodium sulphate solutions

2-1-2 Modeling electrolyte solubility

The solubility product of an electrolyte compound in aqueous solution is defined:

$$K_{sp} = (\Pi\alpha_i^{vi})(\alpha_w^{k}) \qquad (2\text{-}1)$$

K_{sp} is the thermodynamic solubility product, α_i is the activity of each dissociated ion "i" from a given electrolyte, and v_i = the number of moles of ion "i" generated upon complete dissociation of one mole of electrolyte. α_i is defined as $\alpha_i = \gamma_i m_i$, γ_i= the activity coefficient of ion "i", m_i = molality of ion "i". The activity of water (α_w) is included in the solubility product expression when there are k hydration waters in the solid.

The mean activity coefficient ($\gamma_{\pm}$) can be used to calculate the mean activity of an electrolyte species: $\alpha_{\pm}^{vi} = \gamma_{\pm}^{vi}\, m_{+}^{vi\,+} m_{-}^{vj\,-}$ (where m_{+}/m_{-} = moles of cations/anions, v_{i+}/v_{i-} = the moles of cations/anions produced per mole of compound, $v_i = v_{i+} + v_{i-}$). Knowledge of the mean activity coefficient of the ionic pair of interest, correct thermodynamic solubility product, and activity of water is important to the calculation of the saturated salt concentration, and therefore the successful modeling of the electrolyte solubility (Demopoulos et al., 1987).

2-1-3 Modeling gypsum solubility – calculation of activity coefficients

The solubility of gypsum ($CaSO_4.2H_2O$) is defined with single or mean activity coefficients:

$$K_{sp} = \gamma_{Ca2+} [Ca^{2+}]\ \gamma_{SO42-} [SO_4^{2-}]\ \alpha_w^2 \qquad (2\text{-}2)$$

or

$$K_{sp} = \gamma^2_{\pm CaSO4} [Ca^{2+}]\ [SO_4^{2-}]\ \alpha_w^2 \qquad (2\text{-}3)$$

Many programs exist that predict the solubility of gypsum in sea water and ground water, each using the methods of Pitzer, Davies or Debye-Hückel to calculate the individual activities of calcium and sulphate ions (Moreno et al. (1963), He et al. (1993), Calmanovici et al. (1993), Yadav et al. (1995)). Once calibrated with experimental data of the ionic strength of interest, these methods can be fairly accurate. Power et al. (1966) predicted gypsum solubility in aqueous sodium chloride solutions with an equation that calculated mean activity coefficients, however, above an ionic strength of one, this relation also required an empirical correction factor.

Meissner's method calculates mean activity coefficients from solution composition information, an empirical value for each component electrolyte, and the ionic strength of the solution, where the ionic strength is defined:

$$I_i = \frac{1}{2}\sum_i m_i z_i^2 \qquad (2\text{-}4)$$

where m_i is the molality of ion "i" and z_i is the charge of ion "i".

2-1-4 Meissner's method of calculating mean activity coefficients

Meissner's semi-empirical method of calculating mean activity coefficients utilizes a parameter termed the reduced activity coefficient Γ (where $\Gamma = \gamma_{\pm}^{1/z+z-}$, z= the charge of the ion). The Γ parameter arises from a family of distinct curves over a range of ionic strengths (Figure 2-2).

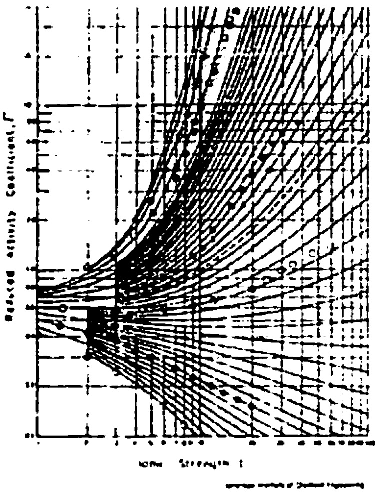

Figure 2-2: Meissner's reduced activity coefficient parameter Γ vs. ionic strength I (from Meissner, 1980).

These curves are defined by an empirical parameter q_o. Each ion pair has a characteristic q_o value, which is a number that ranges from –2.6 to 9.0. The calculation of the mean activity coefficient in single or mixed electrolyte systems of different ionic strengths requires knowledge of the q_o values for all of the compounds. The q_o values, electrolyte molalities, ionic strength and temperature are used to determine the reduced activity coefficient Γ, from which the mean activity coefficient $\gamma_{\pm}$ of a species is calculated.

Filippou produced a FORTRAN IV program that used Meissner's method to calculate the activity of H_2SO_4 in the system $ZnSO_4$-$Fe_2(SO_4)_3$-H_2O (Filippou, 1989, Filippou et al., 1993). The program calculated the activity of sulphuric acid in solutions below 200 g/l H_2SO_4, 100 g/l Zn^{2+}, and 30 g/l Fe^{3+}. Parts of this program were used to develop a program that uses Meissner's method to calculate the gypsum mean activity coefficient and gypsum solubility in an extended range of sulphate electrolytes (H^+, Zn^{2+},

Mg^{2+}, Na^+, NH_4^+, Fe^{2+}, Mn^{2+}), concentrations (up to an ionic strength of 20) and temperatures up to 65°C.

Meissner published a calculation of gypsum solubility in water using his method of calculating mean activity coefficients (Meissner, 1980). Meissner used the Gibbs equation to calculate the activity of water for his calculation:

$$-\log \alpha_w^o = \frac{2I^o}{z_1 z_2} + 2\int_1^{\Gamma^o} \Gamma_{12}^o \, d\ln\Gamma_{12}^o \qquad (2-4)$$

Meissner's calculations assumed that the dissolved gypsum lattice ions do not influence the ionic strength of the solution because gypsum is sufficiently insoluble. The solubility of gypsum is however, high enough that low ionic strength systems are affected by the dissolved divalent calcium and sulphate ions. This in turn affects the mean activity coefficient of calcium sulphate. The gypsum solubility model presented here uses a modified version of Meissner's published method, incorporating an iterative method to include the dissolved gypsum ions in the calculation of the gypsum activity coefficient. As will be demonstrated, gypsum solubilities in mixed neutral electrolyte solutions up to ionic strength 20 at room temperature are calculated with good accuracy with this model (Section 2-3).

2-1-5 Calculating gypsum solubility with Meissner's method

The molal concentrations and q_o values of the system electrolytes, as well as the temperature and solubility constant of gypsum as a function of temperature are required for calculating gypsum solubility. The following sections discuss these values.

2-1-5-1 Solution density

The electrolyte solution density is required to calculate the ion molalities that are required for the use of Meissner's method from the molarity input values. An empirical equation presented by Filippou (1989) was used to calculate the electrolyte solution density (ρ):

$$\rho = (1.0027 + 6\text{x}10^{-4} \text{ x } \Sigma(\text{g electrolyte species})) \text{ x } (1.009 - 4.5 \text{ x } (T(°C)-25)) \qquad (2-5)$$

2-1-5-2 q_o values

Central to the working of the Meissner model is the empirical value of q_o for each electrolyte ion-pair. It may be determined by generating a single experimental point on the Γ vs. I family of curves, calculated using either solution vapour pressures or solubilities in mixed solutions, or by other published estimation methods (Kusik (1978), Meissner (1980)). The q_o values for all of the electrolytes used in this work are summarized in Table 2-1.

Table 2-1: q_o values of electrolytes used in the gypsum solubility model

Salt	Gypsum	$ZnSO_4$	$MgSO_4$	H_2SO_4	$FeSO_4$	$MnSO_4$	Na_2SO_4	$(NH_4)_2SO_4$
q_o	0.2	0.05	0.5	Eq (2-6,7)	0.0	0.14	-0.19	-0.25

Some of these q_o values were obtained from literature (Kusik, 1978). The q_o value for sulphuric acid is a function of ionic strength; it was developed by Tozawa et al. (1986), and later improved by Filippou (1993):

$$q^o_{H_2SO_4} = \begin{cases} -8.23\exp\left\{-\sqrt{I_n}\right\} & for\, 0.5 \le I_n \le 6.0\, mol/l \\ -81.14\exp\left\{-1.93\sqrt{I_n}\right\} & for\, 6.0 \le I_n \le 10.8\, mol/l \end{cases} \qquad (2.6), (2\text{-}7)$$

It may be the speciation of sulphuric acid at different ionic strengths that requires the use of different q_o values. For gypsum, Meissner published a q_o value of 0.5 (Meissner, 1980), however, 0.11 was used by Demopoulos, et al. (1987). In light of these different values, experimental values of gypsum solubility at different sodium sulphate concentrations were compared to the values calculated with different gypsum q_o values. In Figure 2-3, a gypsum q_o of –0.2 calculates the closest fit to the reported solubility values for this system (Section 2-3-1). However, Figures 2-4, 2-5, and 2-6, show that a value of 0.2 best fits the experimental data of zinc, magnesium and ammonium sulphate systems (Section 2-3-1). A gypsum q_o value of 0.2 was used for the mixed electrolyte test calculations as well (Sections 2-3-3, 2-3-4).

2-1-5-3 Gypsum solubility product

An accurate solubility product is required to determine gypsum supersaturation for the model. The Electric Power Research Institute developed a model for the evaluation of recirculating cooling water systems (Banz et al., 1985). They expressed gypsum solubility as a function of temperature in degrees Celcius up to 65°C:

$$\log K_{sp} = -(4.944/T) - 37.75 \log T + 105.4 \qquad (2\text{-}8)$$

This relation, which calculates a gypsum K_{sp} at 25°C of 2.4×10^{-5} was used in the model presented.

2-1-5-4 The effect of temperature

Meissner's method includes an equation for correcting the mean activity coefficient for temperature. This was included in the model; the results are not included as the majority of the test work occurred at room temperature. The results were compared to experimental values with acceptable results.

2-2 EXPERIMENTAL - Generating gypsum solubility values

2-2-1 Objective

The gypsum solubility values generated by the program are compared to those that were either retrieved from literature or determined in the lab. The classic dissolution method was used in the lab to determine gypsum solubility in different electrolytes.

2-2-2 Experimental Procedure

All electrolyte solutions were composed of deionized water produced by Cole-Parmer Universal and Research columns. When used in series, the columns are rated to remove all ionized minerals down to a level of 4 ppb or less, as well as CO_2 and silica, producing water ionically equivalent to triple distilled water. Electrolyte solutions were produced with reagent grade chemicals that were measured with a Mettler AE200 balance that reports to the tenth of a milligram.

The dissolution process began with 100ml solutions of test electrolyte contained in a closed Erlenmeyer flask. A 2 g charge of dry synthetic gypsum (Sigma, ACS reagent, 99.7%) was added to the electrolyte. Magnetic stirrers maintained the solids in suspension for a minimum of two hours in some of the tests. The slurry was gravity filtered through Whatman Qualitative 2 paper filters and quickly diluted to best preserve the calcium content of solution. 100x dilutions were made for atomic adsorption analysis of calcium concentration.

A dissolution time of two hours was considered enough time for the system to reach equilibrium. Some crystallization papers quoted 2-5 hours as the time required for solid-liquid electrolyte systems to reach equilibrium, however, Power (1966) noted rapid solubility changes with time for their gypsum dissolution experiments, and Liu et al.

(1971) commented that only a few minutes were required to reach equilibrium for their gypsum dissolution experiments. Experimental error may have arisen from calcium concentration analysis and solution preparation.

2-2-3 Analysis

The diluted solutions were analyzed with a Perkin Elmer 3110 Atomic Absorption Spectrometer to determine calcium concentration. It was assumed that the concentration of dissolved calcium represented the molar concentration of dissolved gypsum. Measurement repeats were within 2% of the concentration value.

2-3 RESULTS

2-3-1 Modeling binary sulphate systems

Figures 2-3, 2-4, 2-5 and 2-6 compare the experimental, literature and calculated gypsum solubility values for neutral sodium, zinc, magnesium and ammonium sulphate electrolyte systems at room temperature. The literature sources (Seidell et al. (1958), Silcock, (1979), Yadav et al. (1995)) did not include error information; the experimental data include error bars for the first standard deviation with at least 2 repeats for the data points. For all but the sodium sulphate system, a gypsum q_o value of 0.2 bets fit the solubility data. The sodium sulphate system at these concentrations was best modeled with a gypsum q_o value of -0.2 (Figure 2-1).

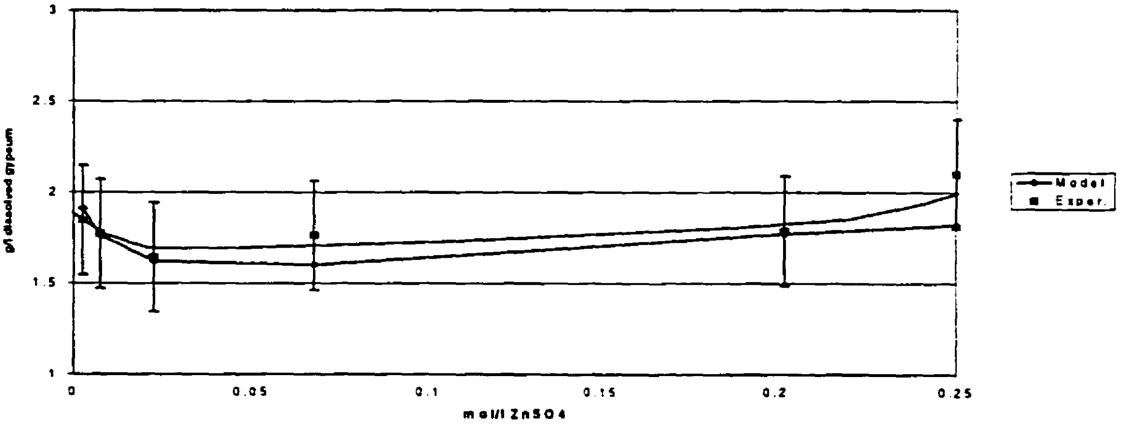

Figure 2-3: Comparison of experimental and calculated gypsum solubility in zinc sulphate electrolyte, T=21°C, $q^{o}_{gypsum} = 0.2$

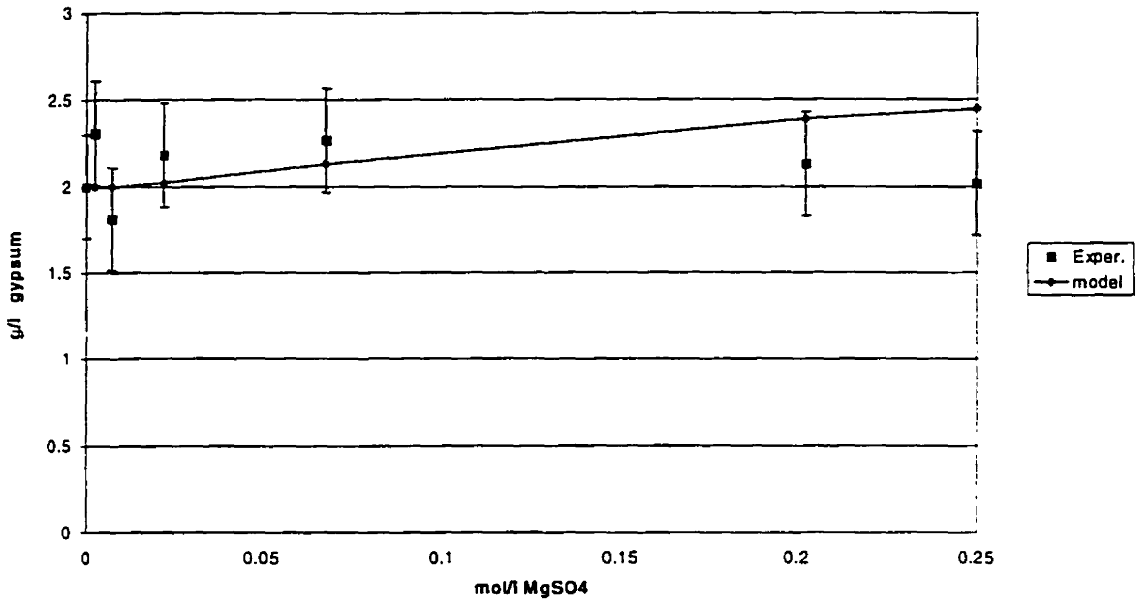

Figure 2-4: Comparison of experimental and calculated gypsum solubility in magnesium sulphate electrolyte. T=21°C, $q^{o}_{gypsum} = 0.2$

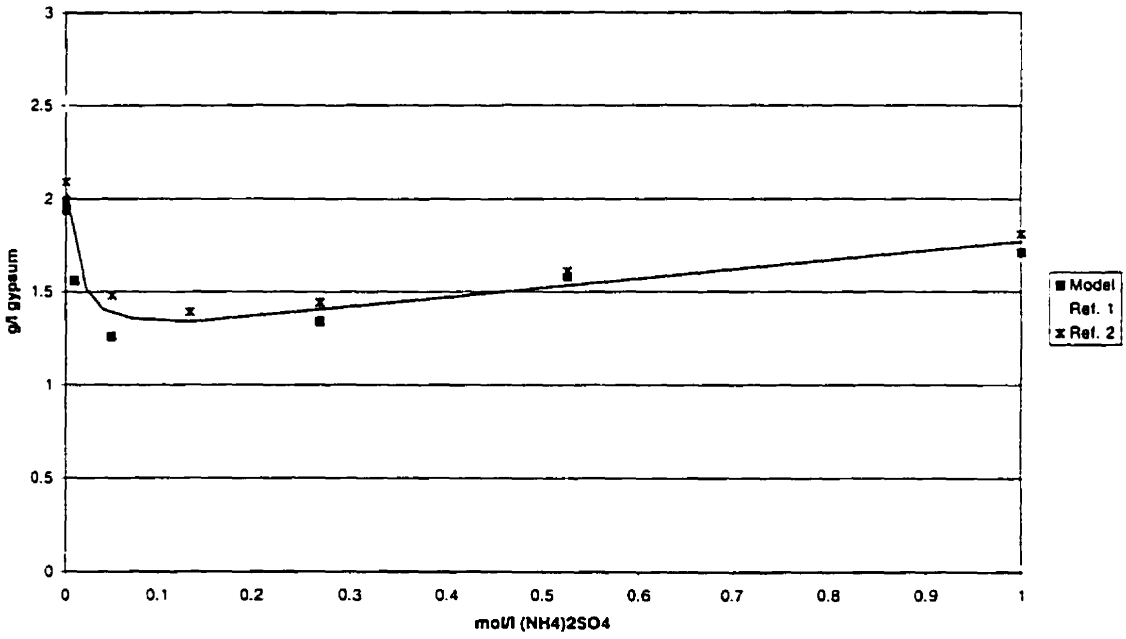

Figure 2-5: Comparison of literature and calculated gypsum solubility in ammonium sulphate electrolyte, T=21°C, $q^{o}_{gypsum} = 0.2$

2-3-2 Modeling strong binary sulphate systems

The model was tested on the same binary systems at cation molalities of 1 to 5 at room temperature, with the ionic strength reaching 20 for 5 m concentrations of zinc sulphate.

Figures 2-6, 2-7, and 2-8 compare the calculated gypsum solubility with the experimental and literature values.

A gypsum q_o value of 0.2 was used to model all three strong electrolyte systems.

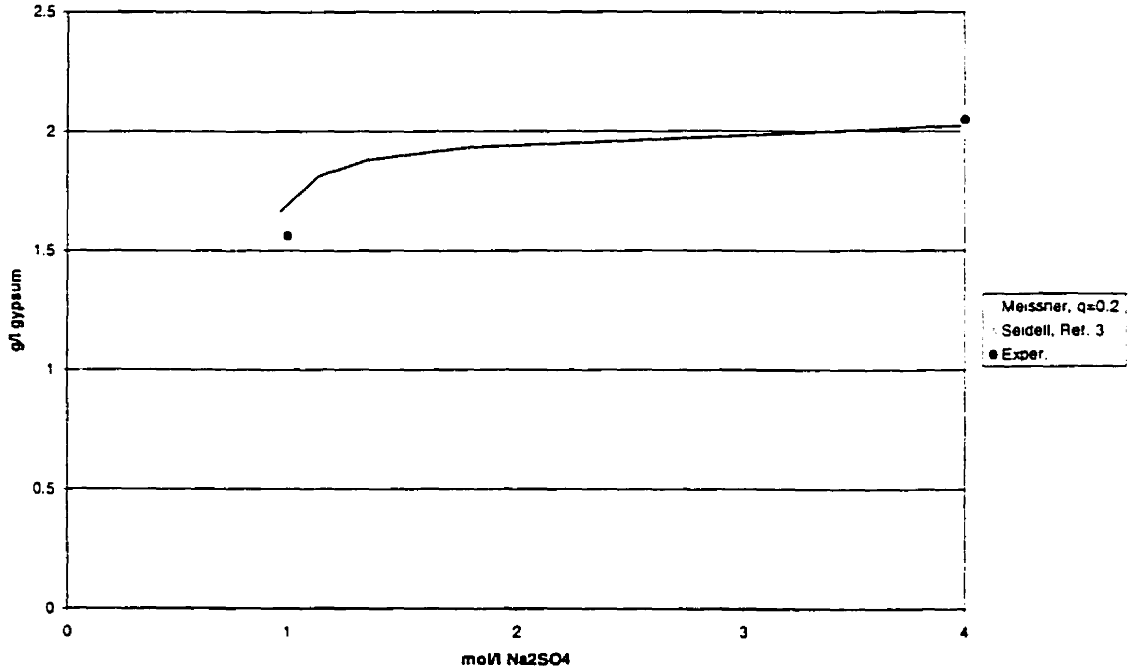

Figure 2-6: Comparison of experimental and calculated gypsum solubility in sodium sulphate electrolyte at high ionic strength, T=21°C, $q^{o}_{gypsum} = 0.2$

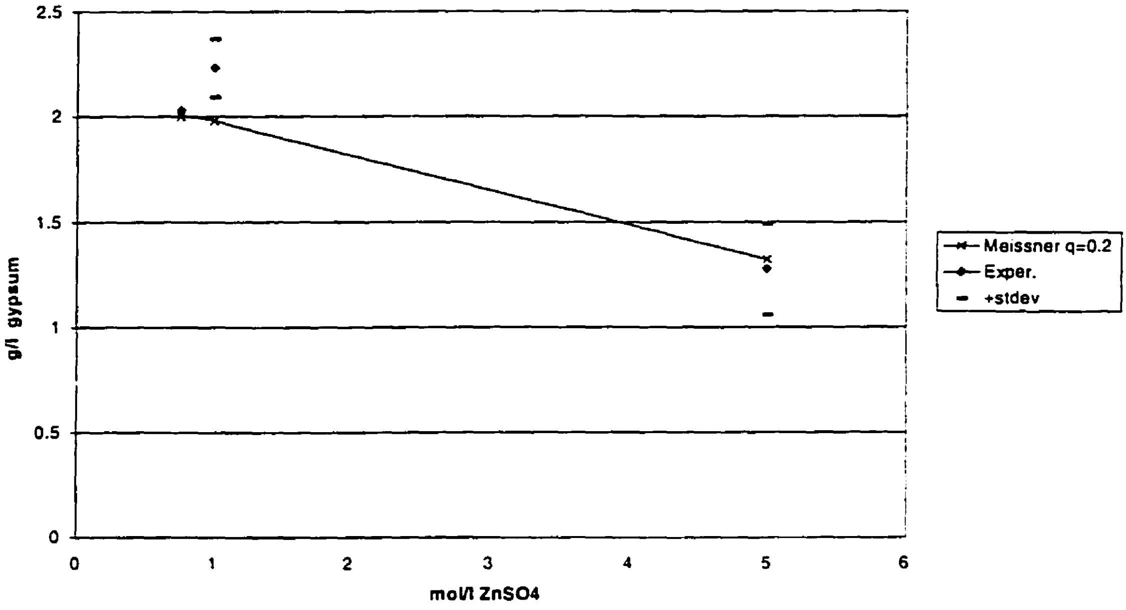

Figure 2-7: Comparison of experimental and calculated gypsum solubility in zinc sulphate electrolyte at high ionic strength, T=21°C, $q^{o}_{gypsum} = 0.2$

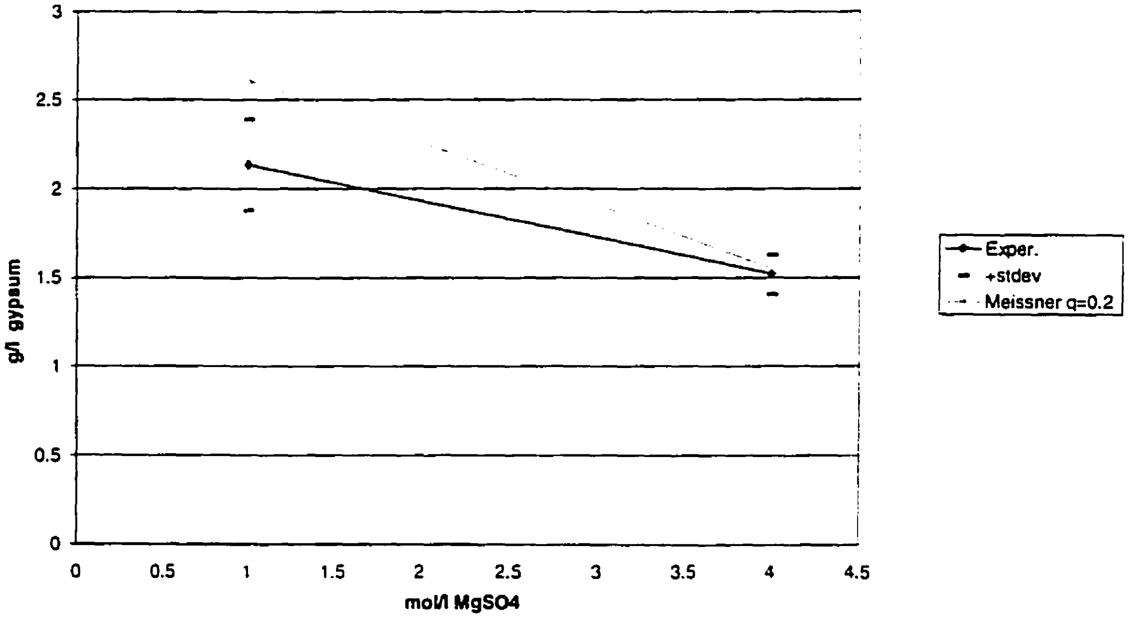

Figure 2-8: Comparison of experimental and calculated gypsum solubility in magnesium sulphate electrolyte at high ionic strength, T=21°C, $q^{o}_{gypsum} = 0.2$

2-3-3 Modeling strong acidic zinc sulphate quaternary systems

The model's ability to calculate gypsum solubility in acidic, mixed solutions with zinc sulphate as the most concentrated species and another sulphate electrolyte at lower concentrations was also tested. The solubility of gypsum in 1 and 20 g/l sulphuric acid solutions of 60, 100 and 120 g/l zinc sulphate was measured and calculated for different concentrations (2-8 g/l Na^+ or NH_4^+) of sodium sulphate and ammonium sulphate. The predicted results were within 1 standard deviation of the experimental results for all except the strong acid solutions. Figure 2-9 compares the experimental data and model results for an acidic (0.75 g/l acid) zinc sulphate (120 g/l Zn^{2+}) system with varying sodium sulphate concentrations (0-8 g/l Na^+).

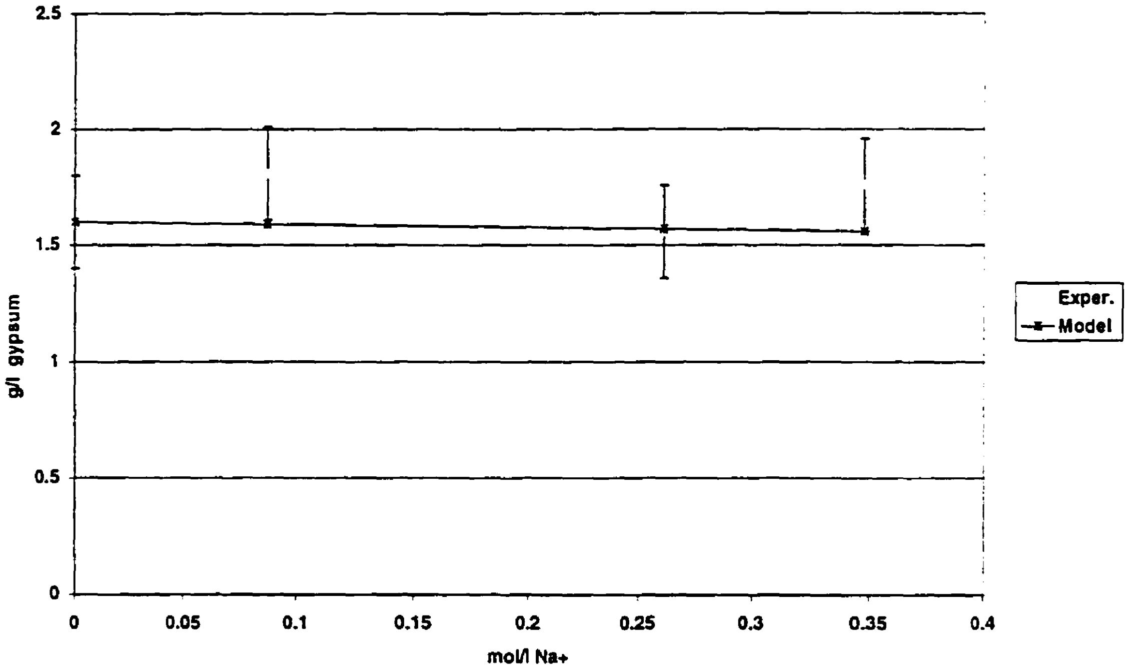

Figure 2-9: Comparison of experimental and calculated gypsum solubility in acidic (0.75 g/l H_2SO_4)-$ZnSO_4$ (120 g/l)-Na_2SO_4 electrolyte, T=21°C, $q^{o}_{gypsum} = 0.2$

2-3-4 Modeling strong quaternary mixed sulphate systems

Gypsum solubility in equimolar and non-equimolar solutions of neutral mixed sulphate electrolyte, each with a total ionic strength of one, were tested and compared to the values predicted by the model. The equimolar solutions consist of three mixed sulphate salts (sodium, zinc, magnesium or ammonium) each contributing an ionic strength value of 0.33. The predicted values were within the first standard deviation of the experimental results except for the zinc, sodium and ammonium sulphate mix.
The non-equimolar solubility tests compared the predicted and experimental values of gypsum solubility in a neutral mixed sulphate electrolyte of zinc, magnesium and sodium sulphate in ionic strength proportion of 0.8:0.1:0.1 (Figure 2-10). The predicted solubility followed the same trend as the experimental results but the solubility of gypsum was underestimated in all three cases.

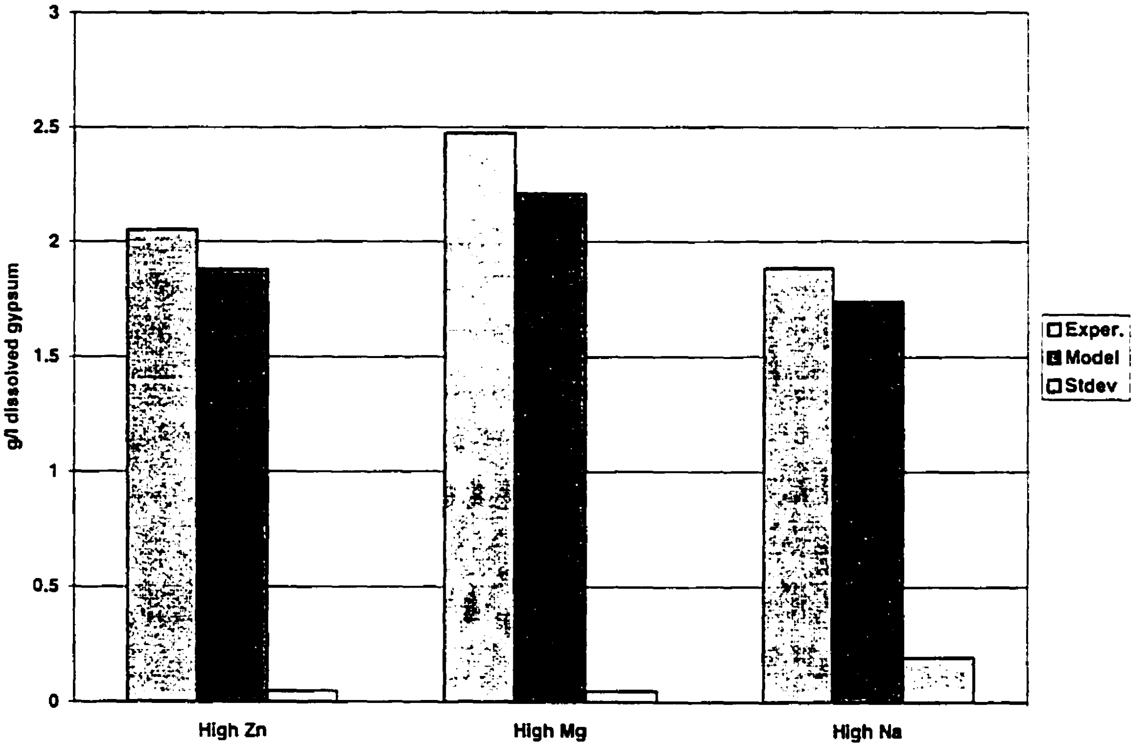

Figure 2-10: Comparison of experimental and calculated gypsum solubility in neutral mixed ($ZnSO_4$-$MgSO_4$-Na_2SO_4) sulphate electrolyte, total ionic strength of 1, salt fraction = 0.8:0.1:0.1, T=21°C, $q^o_{gypsum} = 0.2$

2-4 DISCUSSION

2-4-1 Gypsum q_o values

Although the low and high ionic strength systems are modeled well with a calcium sulphate q_o value of 0.2, it is curious that a different value is required to model the sodium sulphate system at low concentrations. An empirical method of determining q_o for a compound requires a solubility test at high solution ionic strength of the singular electrolyte, and using that information to determine the q_o curve that best fits the point on the family of reduced activity coefficient curves (Figure 2-2) (Kusik, 1978). This is more accurate at higher ionic strengths, where the family of curves diverges. Unfortunately, the ionic strength of a saturated gypsum solution is not high enough to determine an accurate q_o with this method. A trial and error method was used to determine a gypsum q_o value of 0.2, as the value suggested by Meissner did not produce very accurate results.

A possible reason for the discrepancy in accurate q_o values for gypsum may stem from the tendency of calcium and sodium to form aqueous complexes to different degrees at different ionic strengths. Gardner et al. (1970) calculated the mean activity coefficient of calcium sulphate as a function of temperature, and concluded that there was a strong interaction between the ions of the electrolyte. They observed that a straight-line correlation between the concentration of dissolved gypsum with an ionic strength expression deviated at low ionic strength and temperature, possibly due to gypsum lattice ion association. Yadav et al. (1995) comment that the solubility of gypsum is a combined function of ionic strength, stability of ion pairs and the magnitude of common ions present in solution.

Nakayama et al. (1967) calculated activity coefficients and dissociation constants for calcium sulphate at low ionic strengths using Debye-Hückel theory. Their results indicate that calcium cations form complexes in solutions of low ionic strength, but the degree of dissociation was a function of ionic strength and ion types. They determined that the gypsum solubility product was a function of ionic strength, but they did not include the activity of water in the solubility product calculation. Baltpurvins (1997) suggested that calcium cations form thermodynamically stable complexes with many anions, thereby altering the speciation and possible affecting the mean activity coefficient of gypsum.

Demopoulos et al. commented that Meissner's method assumes complete dissociation and should be used with caution when calculating activity coefficients for systems with complexes (Demopoulos et al, 1987). Sulphuric acid, which dissociates into bisulphate, sulphate, and hydronium ions depending on the solution conditions, can be well-modeled with Meissner's method with the q_0 that is a function of ionic strength.

Should speciation of gypsum in solution be the source of different gypsum q_0 values, a few solubility tests with the component ions in the ionic strength of interest may determine if 0.2 or another suitable system calcium sulphate q_0 is required for accurate modeling of the system.

2-4-2 Sulphuric acid q_0 values and gypsum solubility

Sulphuric acid has an interesting effect on gypsum solubility; Calmanovici et al. (1993) reported the effect of sulphuric acid on gypsum solubility and termed it "ambiguous". The authors mention the common (sulphate) ion effect should reduce the solubility of gypsum, however, the increased sulphuric acid concentration may increase the calcium sulphate solubility. At lower pH's, the sulphate ion concentration does not change dramatically, and the bisulphate concentration increases (Appendix A).

Figure 2-11 compares the solubility of gypsum in sulphuric acid solutions at room temperature, as reported in literature, determined experimentally, and calculated by the model developed in this work. The solubility of gypsum is not a strong function of sulphuric acid concentration below concentrations of about 0.10 molar, (pH 1). Gypsum solubility increases in stronger sulphuric acid solutions.

The model results represent an exaggerated version of the gypsum solubility trend as a function of sulphuric acid concentration. If the q_0 value as a function of ionic strength is a measure of the effect of speciation, then the speciation of calcium sulphate may further complicate the acid system, resulting in inaccurate gypsum solubility predictions.

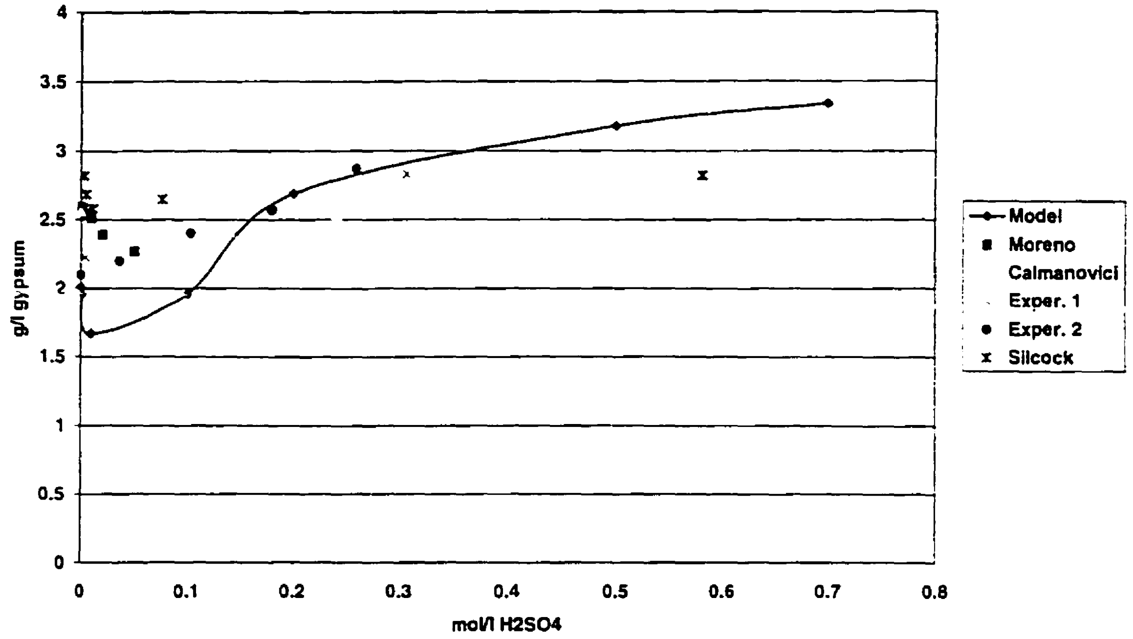

Figure 2-11: Solubility of gypsum in sulphuric acid solutions, $q^{o}_{gypsum} = 0.2$

2-4-3 Uncertainty in the thermodynamic solubility product of gypsum

The solubility of gypsum is derived from the molality of calcium that is calculated by the model, based on a thermodynamic solubility product (K_{sp}) for gypsum that is a function of temperature only.

There is an interesting discrepancy in the literature with regards to the value of K_{sp} for gypsum. Meissner (1980) generates a K_{sp} of 3.69×10^{-5} by calculating the activity of water and the mean activity coefficient of gypsum using the saturated gypsum molality of 0.0156. A letter to the editor in the Journal of Chemical Education (Masterman, 1987, Carpenter, 1987) commented on the often-used and incorrect method of calculating the K_{sp} as the square root of the solubility of gypsum. Carpenter listed five different gypsum K_{sp} values given in different editions of the CRC Handbook. The author quoted four papers that give a "true thermodynamic" solubility product $K_{sp}=(\alpha_{Ca^{2+}})(\alpha_{SO_4^{2-}})$ as 2.5×10^{-5} at 25°C (Meites et al. (1966), Martin (1986), Gardner et al. (1970), and Guenther (1975). Raju (1990) also commented on the disparity of gypsum solubility product values in the literature.

Nakayama et al. (1967) measured the solubility of gypsum using a calcium electrode and the extended Debye-Hückel theory; they reported a K_{sp} 2.67×10^{-5} for a saturated gypsum solution. Moreno (1963) reported a value of 2.45×10^{-5}. The value calculated by the Electric Power Research Institute model at 25°C and used in this work is 2.4×10^{-5} (Banz, 1985).

2-4-6 Modeling gypsum solubility – simulated zinc plant wastewater stream

The ability of Meissner's method to predict gypsum solubility in a multicomponent system was also tested on a synthetic solution representing the average composition of the zinc plant wastewater (Table 2-2)[1]. Meissner's method predicts a solubility of 1.71 g/l for gypsum solubility in the characteristic waste solution, which is within 0.15 g/l first standard deviation of the measured value of 1.83 g/l. This experimental value was determined with the classic dissolution method with a synthetic solution generated in the lab with deionized water. As a comparison, the PHREEQE model calculated a gypsum solubility of 2.32 g/l from the same solution (Appendix C).

Table 2-2: Composition of simulated zinc plant wastewater[1]

Ion/species	H_2SO_4	Zn^{2+}	Fe^{2+}	Mn^{2+}	Mg^{2+}
g/l	5	1	0.03	0.06	0.09

2-5 CONCLUSIONS

The developed model predicts the solubility of gypsum in different sulphate electrolytes using Meissner's method to calculate the mean activity coefficient of gypsum, a gypsum solubility product that is a function of temperature, and the Gibbs equation for calculating the activity of water. The solubility results are dependent on the empirical value of q_o for gypsum; this value should be verified or determined by running solubility tests for the system of interest, as it may be sensitive to ionic interactions. The speciation of calcium sulphate in solution may prevent a singular valid q_o value for gypsum over different ionic strengths.

Calcium finds itself in the middle of the alkali earth element family. The solubility of calcium sulphate salts also lie in the middle of the alkali earth sulphate group solubilities. Calcium sulphate which have solubility values are between the very soluble

---

[1] From CEZinc private communication

beryllium and magnesium sulphates due to the higher solvation of the smaller beryllium and magnesium ions (Lee, 1996) and the insoluble strontium and barium sulphates. The calcium cation tends to form complexes in solution; it also has a diverse portfolio of roles in biology: from structural in bones and shells to functional in muscle contraction and nerve impulses. Its flexible solution chemistry might hint to the potential difficulties of accurately predicting its behaviour in solution.

This gypsum solubility program produces generally good predictive power for the systems tested, up to an ionic strength of 20. As it was written in both FORTRAN77 and as a spreadsheet program, it is a good starting point for future expansions and refinements. Suggested improvements include: incorporating other cations and anions species, generating a gypsum K_{sp} which is valid for temperatures above 65°C, and using a better method of integration in order to solve the Gibbs equation than Simpson's Rule.

The program presented in this section, when combined with some solubility experiments, provides an improved method of predicting gypsum solubility for strong and weak sulphate electrolyte systems.

3 PRECIPITATION OF GYPSUM FROM SOLUTION

The Effect of Supersaturation on Precipitation and Spontaneous Precipitation Study of Gypsum from Sulphuric Acid Solutions.

3-1 INTRODUCTION

This chapter introduces the concepts related to the precipitation of a solid salt phase from an aqueous electrolyte solution. In particular, it outlines the thermodynamic and kinetic driving forces for precipitation from an aqueous phase, and highlights how control over precipitation conditions can result in the production of solids of different qualities. Understanding the effect of process conditions on crystallization thermodynamics and kinetics aids the design of precipitation processes that produce solids with desirable properties.

A waste water neutralization process typical of the zinc industry neutralizes a weak acidic electrolyte with a mixture of sulphate salts to a neutral slurry of gypsum and other solid hydroxide and sulphate salts by reacting the stream with slaked lime. The gypsum solids currently produced by a simple commercial neutralization process[1] are fine, and have a low solids density (<10%). Crystallization theory predicts that this commercial neutralization process design will produce low solids density precipitate, as the gypsum is produced largely by spontaneous precipitation. This chapter explains the crystallization theory related to this prediction, and explains how crystallization theory inspires the design of a novel neutralization process that improves precipitated gypsum solids density.

The novel neutralization process design requires knowledge of spontaneous gypsum precipitation characteristics. Preliminary precipitation tests presented in this chapter support the theory that it is difficult to predict and reproduce spontaneous gypsum precipitation. However, Chapter 4 indicates that, barring normal crystal dispersion, well-grown gypsum crystals can be produced by a process design based on crystallization theory.

---

[1] Private communication with CEZinc

3-2 THEORY

3-2-1 Precipitation Thermodynamics – Equilibrium and Chemical Potential

Equilibrium is a word used in chemistry to denote a static condition, or the absence of change. In thermodynamics, the term equilibrium also describes the absence of a tendency toward change on a macroscopic scale (Smith and van Ness, 1987). For a mixed system of gypsum in aqueous sulphate electrolyte, equilibrium defines a state where the rates of precipitation and dissolution of gypsum solution are equal, and the solution concentration remains constant.

More rigorously, thermodynamic equilibrium may be defined as a state where the change in Gibbs free energy (dG), of a closed system is zero. The Gibbs free energy of the different components and phases of a system can be accounted for with the chemical potential of the different components: μ_i.

A closed system of two phases at constant temperature and pressure is at equilibrium when the difference in chemical potential between the two phases (α and β) is zero, and

$$\mu_i^\alpha = \mu_i^\beta \qquad (3\text{-}1)$$

A closed, two-phase system at the same temperature and pressure, but with different chemical potentials between the two phases is therefore not at equilibrium; the system is expected to change in order to attain equilibrium. A closed solid crystal-aqueous electrolyte system with a difference in chemical potential ($\Delta\mu$) between the fluid and crystal phases has a tendency to precipitate or dissolve. If the chemical potential of the solution is greater than that of the solid phase, the solution is supersaturated and precipitation may be expected. If the chemical potential of the solution is less than the solid phase in contact with the solution, the solution is subsaturated and dissolution is thermodynamically favourable.

The solubility product (Section 2-1-3) is related to the chemical potential through equation 3-2 (μ^*_{ij} is the crystal phase chemical potential, and $\mu^\circ_{i,j}$ are the chemical potentials of the lattice ions):

$$K_{sp} = \exp\left(\frac{-\left(\mu_i^o + \mu_j^o - \mu_{ij}^*\right)}{RT}\right) \qquad (3\text{-}2)$$

3-2-2 Precipitation Thermodynamics – Precipitation Driving Force

The difference in chemical potential between the fluid and crystal phases (α,β) for a species can be defined in terms of the activity of the compound in solution and at equilibrium:

$$\Delta\mu = RT\upsilon \ln\frac{\alpha}{\alpha^*} \qquad (3\text{-}3)$$

Where Λ is the moles of dissociated ions per mole of compound, α is the activity of the compound in solution and α^* is the activity of the compound at equilibrium. This difference in chemical potential is a measure of the departure of the system activity from equilibrium, and is referred to as the kinetic driving force of the precipitation process (Söhnel, 1977). Another term used to express this departure from equilibrium is the supersaturation ratio.

The saturation ratio (S) is the ratio of the activity of a compound in solution and the activity of a compound at equilibrium. This ratio is expressed in many ways (Mullin et al. (1977), Mersmann (1995), p.7):

as a difference in concentration:

$$\Delta C = C - C^* \qquad (3\text{-}4)$$

as relative saturation:

$$S = \frac{C}{C^*} \qquad (3\text{-}5)$$

as a saturation index:

$$\sigma = \frac{\Delta C}{C^*} = S - 1 \qquad (3\text{-}6)$$

Or related to the solubility product:

$$S = \frac{\left(\prod \alpha_i\right)\left(\alpha_w^k\right)}{K_{sp}} \qquad (3\text{-}7)$$

The relative saturation, also known as the saturation ratio (S) is used to represent the degree of gypsum saturation in this work, with a saturated system represented with a supersaturation ratio of one. All precipitation processes require systems with a saturation ratio greater than one; these systems are termed supersaturated. Different methods exist for producing supersaturated solutions from undersaturated solutions.

Supersaturated aqueous systems are generated by cooling, evaporating, or drowning-out an undersaturated system. Supersaturated systems are also produced by chemical reactions that produce a low solubility product such as gypsum. The precipitation method chosen for a particular system depends on the system chemistry and economics. Cooling is used to precipitate a species if its solubility increases strongly with temperature. Evaporative crystallization removes the solvent from solution by boiling, serving to concentrate and supersaturate the solute. Drowning out crystallization involves the reduction of a component's solubility in an aqueous solution by adding an organic solvent such as ethanol. Reaction crystallization is the method by which gypsum is precipitated; a chemical reactant (slaked lime) is added to a reactor, generating supersaturation with respect to a particular solid phase (gypsum).

3-2-3 Precipitation processes

Thermodynamics predicts the tendency for a system to return to equilibrium. A supersaturated solution is predicted with thermodynamics to precipitate a solid phase, but thermodynamics does not describe the rate at which the system will precipitate and return to equilibrium. How rapidly a system will return to equilibrium requires information about the kinetics of precipitation.

The degree of supersaturation of an aqueous system, the presence or absence of solids and the type of solids in solution all affect the manner in which a supersaturated system will nucleate and grow solids. Different types of crystal nucleation are listed in Figure 3-1 and will be briefly described.

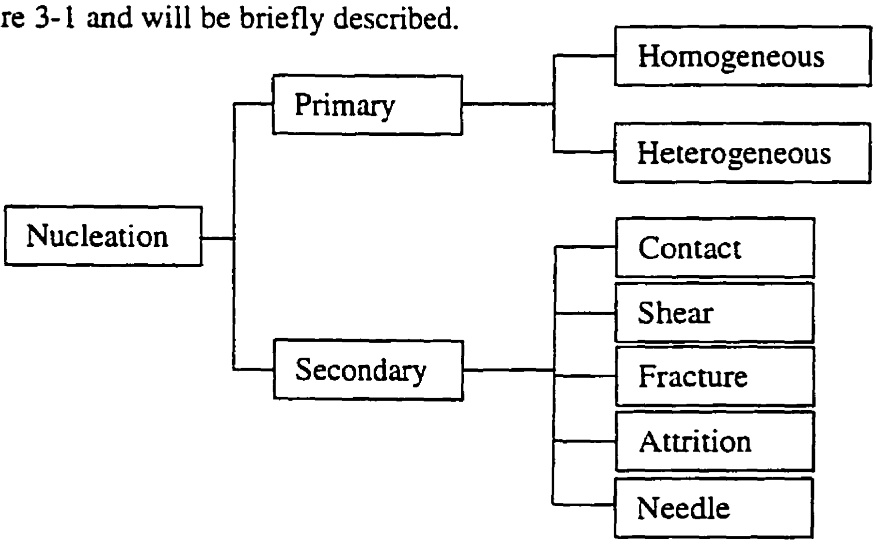

Figure 3-1: Crystal nucleation types (from Mersmann, 1995, p.20)

3-2-4 Precipitation Modes

3-2-4-1 Primary homogeneous nucleation

A supersaturated solution that contains no solid foreign particles or solution-own precipitates will produce a large number of monosized nuclei through primary homogeneous nucleation at a critical supersaturation. This critical supersaturation is the solution activity required for clusters of the solids favored to precipitate from solution to stabilize and develop. This occurs when the free energy released due to generation of a solid volume in solution is greater than the free energy consumed by forming a solid-liquid interface (Figure 3-2, from Mersmann, 1995, p.21). The nucleation rate of solid particles at this critical supersaturation is very rapid, following an exponential relation with supersaturation. The particles produced are often amorphous and very small, ~1um in diameter (Demopoulos et al., 1995), they also have slower settling velocities (Appendix E).

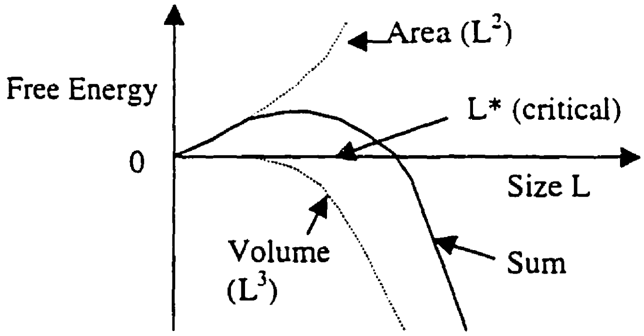

Figure 3-2: Free energy against nucleus size L

3-2-4-2 Primary heterogeneous nucleation

In most industrial crystallization processes, foreign particles are present in precipitating solutions. Precipitation from a supersaturated system on foreign solid surfaces is termed primary heterogeneous nucleation. The rate of primary heterogeneous nucleation is not as rapid as primary homogeneous nucleation, however, the new solids will precipitate at a lower supersaturation than that required for primary homogeneous nucleation as the wetted surface of the foreign particle reduces the nucleation work required by the precipitate (Mersmann, 1995, p.27).

3-2-4-3 Secondary nucleation

If precipitate seed is added or homogeneous nucleation has occurred in a system that is supersaturated, equilibrium will be attained by precipitation of new solids on the solution-own solids at a supersaturation less than that required for either primary homogeneous or primary heterogeneous nucleation. This mode of precipitation is termed true, surface, or needle secondary nucleation, and also proceeds at a slower rate than primary homogeneous nucleation. This type of nucleation is important as crystal growth is favored with this nucleation mode; the seed crystals will increase in size if the growth process is slow enough and there is a large enough surface area for this type of nucleation to predominate. The term secondary nucleation is also used to describe the production of solid fragments by the breakup and motion of larger particles (fracture, attrition, shear) and by the effect of a foreign solid surface in the solution in motion (contact).

A schematic of the rates of nucleation for primary homogeneous and crystal growth as a function of saturation ratio are compared in Figure 3-3 (Demopoulos, 1993). It is clear that the rate of primary homogeneous nucleation is much faster than that for surface growth when the critical supersaturation is exceeded. Well-grown solids are expected to be produced in seeded solutions below the critical supersaturation, and the production of fines through primary nucleation is anticipated above the critical supersaturation.

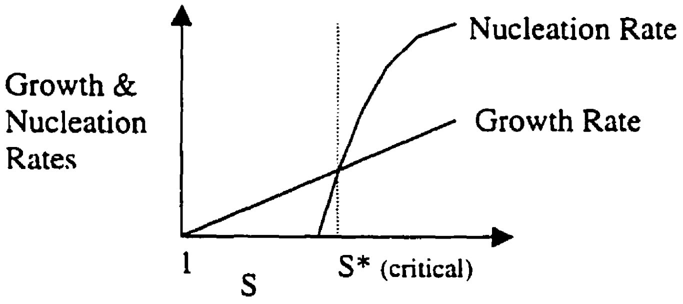

Figure 3-3: Growth and nucleation regimes as a function of nucleation rate and supersaturation ratio (S)

3-2-4-4 Precipitation with different nucleation modes

These different modes of precipitation can be exploited to favor the precipitation of a particular kind of solid under different precipitation conditions. It is logical that a process tailored to produce fines should run under high supersaturation conditions, and the production of large crystalline solids should occur in a low supersaturation environment that favours secondary nucleation on available crystal surfaces. The hydrometallurgy research group at McGill is involved in researching the effect of neutralization process conditions on solid precipitate qualities.

3-2-5 Previous Work

The use of thermodynamic and kinetic crystallization principles to improve the design of conventional neutralization processes has been successfully applied to the neutralization of ferric sulphate and ferric arsenate solutions. Under the supervision of Demopoulos, Zinck (1993) and Droppert (1995) developed neutralization processes that produce large, well-grown precipitates with improved crystallinity, solids density and settling velocity using the principles of supersaturation control and crystallization theory.

The conventional industrial wastewater neutralization process design is a single stage lime neutralization followed by a solid/liquid separation unit such as a thickener that produces a neutral overflow and semicrystalline sludge bottoms (Figure 3-4). These sludges are often contaminated with carry-over ions, are slow to settle in solid/liquid separation units, and have low solids density. The physical characteristics of these solids are predicted by crystallization theory; single stage neutralization occurs at high supersaturation, and favors precipitation of fines by primary homogeneous nucleation.

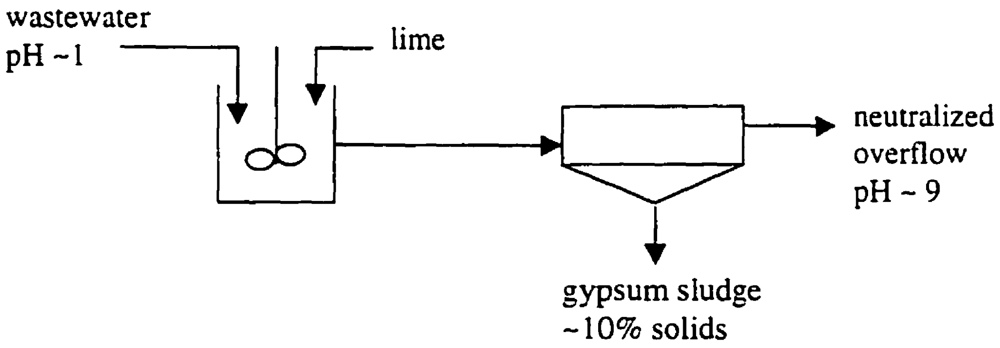

Figure 3-4: Single-stage neutralization schematic

Droppert and Zinck worked with systems whose precipitate solubilities decrease with increasing pH. Figure 3-5 shows a schematic of the solubility of a metal hydroxide as a function of pH, and the critical supersaturation at or above which solids precipitate through primary homogeneous nucleation (S_{cr}). The single-stage neutralization process path is traced on Figure 3-5 with arrow A.

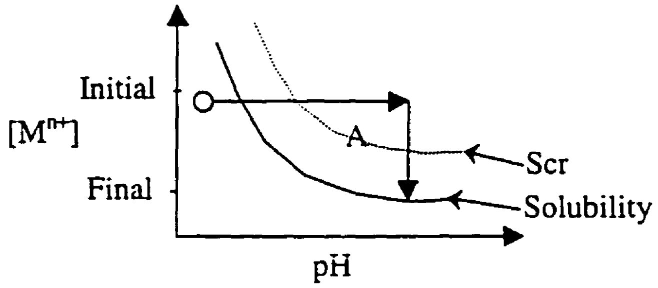

Figure 3-5: Single-stage neutralization process path

3-2-6 The Staged Neutralization Process

Demopoulos et al. (1995a) improved the neutralization process that produces ferric oxy-hydroxide solids from the neutralization of waste acidic ferric sulphate streams. They developed a controlled neutralization process at atmospheric pressure and less than 50°C with recycled ferric oxy-hydroxide seed to produce larger, semi-crystalline ferric hydroxide particles with improved solids density. Demopoulos et al. (1995b) produced large particles of crystalline scorodite at temperatures below the boiling point of water at atmospheric pressure for the first time by controlling the neutralization of acidic ferric chloride arsenate solutions with recycled scorodite seed. Droppert et al. (1996) later successfully applied the same method to the acidic ferric sulphate arsenate solutions.

The results of both of these technologies represent important process improvements, as the product solids have higher solids density and separate rapidly from solution. They are also more stable, as their solubilities are lower than their respective amorphous analogues. It is anticipated that applying a similar controlled neutralization strategy to the treatment of zinc plant wastewater will improve the quality of the precipitated gypsum.

The production of large sized precipitates by these researchers was possible as the critical supersaturation for primary nucleation was avoided while seeded solutions were neutralized. This research pioneered by Demopoulos investigated a novel neutralization path: a staged neutralization in the presence of recycled, solution-own seed (Demopoulos et al., 1995). The new staged neutralization reaction path is illustrated with arrow B in Figure 3-6.

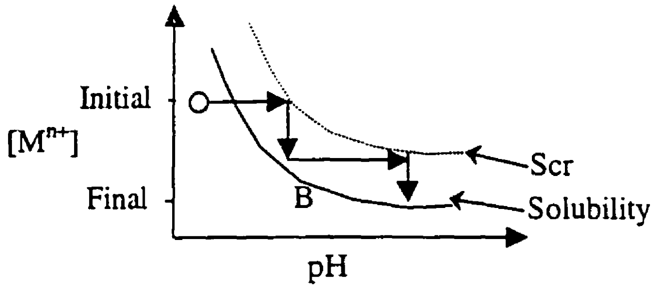

Figure 3-6: Schematic of staged neutralization reaction path

Starting with an acidic undersaturated solution, the same final equilibrium concentration and pH is achieved and primary homogeneous nucleation avoided if the neutralization is staged, as the critical supersaturation is not exceeded, and seed is available for crystal growth between the solubility and critical supersaturation limits. This staging of neutralization with recycled solids can be realized with a cascade of CSTRs (Figure 3-7), each operating at a slightly higher pH. Seed for crystal growth is provided with a recycle stream from the underflow of the solid/liquid separation unit operation.

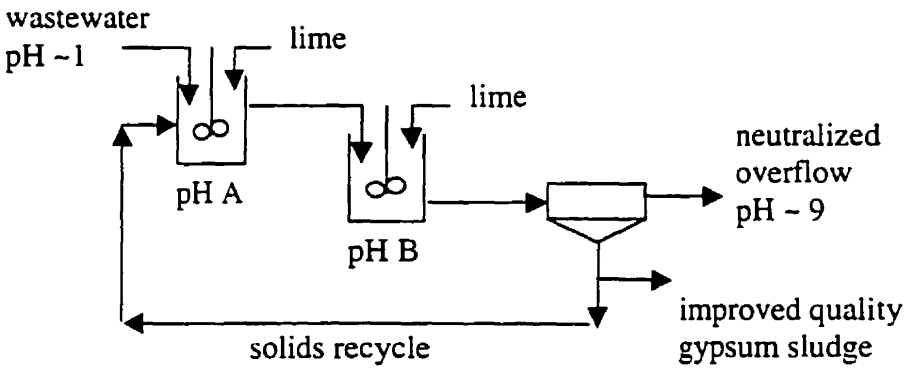

Figure 3-7: Schematic of staged neutralization process

In order to design the number of stages required to maintain a supersaturation lower than the critical supersaturation required for primary homogeneous nucleation, the solubility and critical supersaturation must be determined as a function of pH. The prediction of gypsum solubility in different solutions was addressed in Chapter 2. The critical supersaturation for primary homogeneous nucleation is system-specific, and must be determined experimentally. Determining the critical supersaturation for primary homogeneous nucleation of gypsum is the subject of the rest of this chapter.

3-3 EXPERIMENTAL - Determination of Critical Supersaturation for Gypsum in Sulphuric Acid Solutions

3-3-1 Previous method – Dropwise addition of neutralizing agent

3-3-1-1 Introduction

Zinck (1993) and Droppert (1995) determined the critical supersaturation concentrations for ferric hydroxide and ferric arsenate by slowly neutralizing acidic, undersaturated, solid-free solutions by a dropwise addition of an aqueous base. As the solubility of their target compounds decreased with increasing pH, the supersaturation increased until primary homogeneous nucleation was induced, and a stable cloud of fine precipitates was observed. The solution pH and initial component ion concentration were noted and the point marked on the solubility diagram. This point represents the pH at which primary homogeneous nuclei are stable and can grow to a size that is visible with the human eye. Similar tests were conducted for the precipitation of gypsum from pure sulphuric acid solutions at different concentrations.

3-3-1-2 Materials

Sulphuric acid solutions were produced with deionized water (Section 2-2-2) and concentrated sulphuric acid (Fisher Scientific Reagent, 98%). The slaked lime neutralization agent was prepared with dry calcium oxide (Sigma, 97%) and deionized water to produce a 150 g/l slurry. A magnetic stirrer was used to maintain the slurry in suspension. An Eppendorf micropipette was used to measure solution volumes. The pH was measured with an Orion Model 720A pH meter with Fisher AccupHast combination pH probe.

3-3-1-3 Method

The method used by Zinck and Droppert to determine the supersaturation required to induce homogeneous nucleation in their systems was applied to the precipitation of gypsum from sulphuric acid systems.

Pure 100 ml solutions of a given concentration of sulphuric acid were agitated with a magnetic stirrer in Pyrex flasks. Drops of slaked lime were slowly added to the agitated sulphuric acid. At the moment a “cloud” was seen, the solution was filtered, a 1 ml aliquote was diluted immediately and the pH change was noted. The calcium content of the solution was determined with atomic adsorption (Section 2-2-3).

3-3-1-4 Results

Unlike scorodite and ferric hydroxide, the solubility of gypsum is not a strong function of pH from pH 0.5-7 (Figure 2-11). An aqueous base such as sodium hydroxide or magnesium hydroxide alone will not induce gypsum precipitation from the wastewater system. It is the calcium addition from the slaked lime neutralization agent that supersaturates the system with respect to gypsum, inducing its reactive crystallization. The use of slaked lime as a calcium and hydroxide source adds an interesting complication to this test.

During the dropwise neutralization, the dissolution of slaked lime was observed, but was never observed to be complete. Vestigial solids were present in the acidic solution; it is postulated that these solids were undissolved calcium oxide. These solids could act as seed for gypsum growth, surfaces to induce nucleation in solution (Appendix B), or delayed sources of calcium release as they slowly dissolve during the experiment. For true homogeneous nucleation to be induced, the system must be free of particles; the presence of undissolved lime violates this condition. A new method of determining the concentration of calcium that induces homogeneous gypsum precipitation for a given initial sulphuric acid concentration was developed and tested.

3-3-2 Alternate method – Instantaneous addition of neutralizing agent

3-3-2-1 Method

The slow addition of slaked lime to the acid solution was replaced with an “instantaneous” method of base addition, in order to better detect the critical supersaturation required to induce primary homogeneous nucleation of gypsum in pure acid solutions with slaked lime.

100 ml sulphuric acid solutions of the same concentration were prepared in pyrex flasks. No magnetic stirrer was used to agitate the acid solution in order to remove any

magnetic effect on the homogeneous nucleation process (Appendix D). A measured amount of slaked lime was injected into an acid solution. If no "cloud" of fine precipitates was observed, a second larger measured volume of slaked lime was added to the next pure acid solution. This continued until a stable "cloud" of precipitate was observed. An intermediate amount of slaked lime was injected into the next acid sample to better pinpoint the amount of slaked lime required to induce primary homogeneous nucleation. Calcium concentration was determined for all tests as described in Section 2-2-3.

3-3-2-2 Results

For each instantaneous base addition test, the theoretical calcium concentration in solution was calculated with the measured volume of slaked lime slurry, slurry concentration, and total solution volume, assuming 100% calcium oxide dissolution. A difference value was calculated by subtracting the calcium concentration measured by atomic adsorption from the theoretical added value. This difference value is expected to indicate the onset of precipitation, as gypsum precipitation will remove calcium from solution, resulting in a large positive difference value.

At supersaturations less than the critical supersaturation for primary homogeneous nucleation, the difference value may be negative if there was incomplete calcium oxide dissolution, or the slaked lime slurry was not completely homogeneous so that less calcium was delivered than expected. The supersaturation at which this difference value becomes positive is extrapolated to represent the critical supersaturation value that, if exceeded, will induce primary homogeneous nucleation. Some precipitation may occur on the undissolved calcium oxide particles at low supersaturation, resulting in a small positive difference value at lower supersaturations that do not indicate the onset of primary nucleation.

Figures 3-8 to 3-11 plot the calculated difference in calcium concentration values of different slaked lime addition volumes vs. initial theoretical supersaturation for different initial sulphuric acid concentrations (8, 15, 18 and 36 g/l sulphuric acid). The difference in calcium concentration is plotted as g/l dissolved gypsum. The initial theoretical supersaturation ratio represents the individual doses of slaked lime added to the acid solutions. This was calculated with equation 3-8:

$$S = \frac{[Ca^{2+}]}{[Ca^{2+}]^*} \qquad (3\text{-}8)$$

$[Ca^{2+}]$ represents the calculated calcium concentration in solution and $[Ca^{2+*}]$ represents the saturated calcium concentration. The calculated saturated calcium concentration assumes that the sulphate concentration and activity of water are the same at the same conditions, and makes use of the average values from the solubility data presented in Figure 2-11 to determine the dissolved calcium concentration at equilibrium. The tests that produced observable stable precipitate clouds are starred (*). Sources of error include error in calcium analysis, solution preparation and the errors in the values used to calculate the supersaturation.

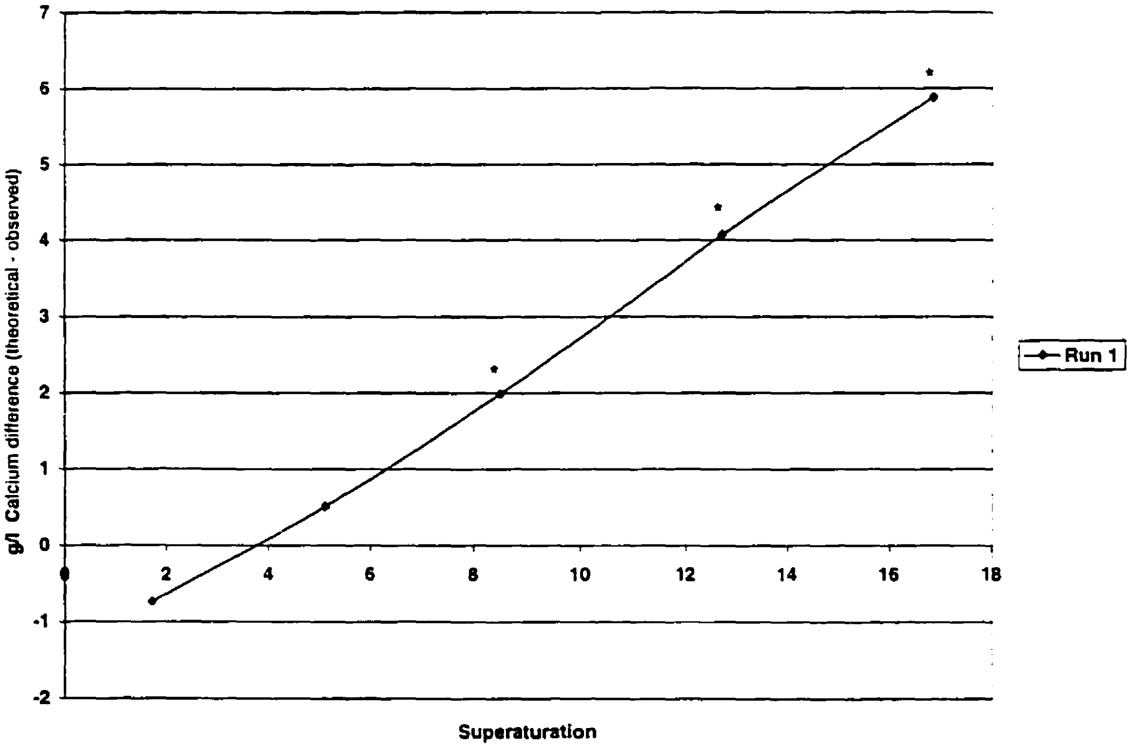

Figure 3-8: Difference between calculated and measured calcium concentration (as dissolved gypsum) vs. initial theoretical supersaturation – 8 g/l sulphuric acid

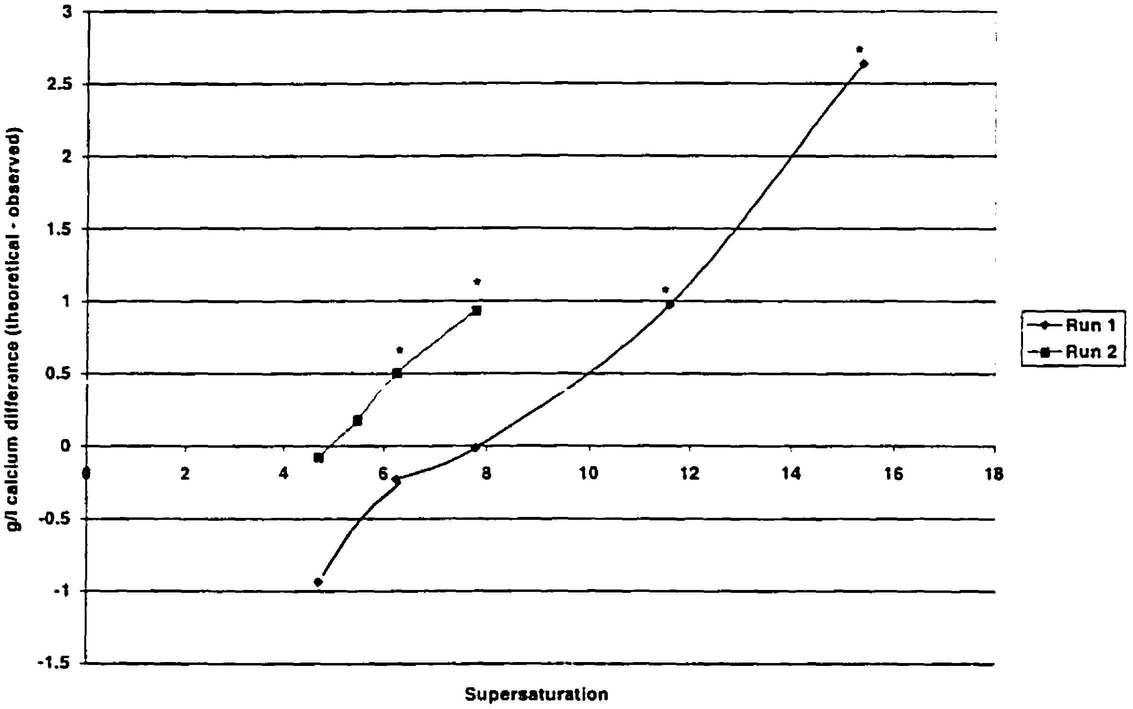

Figure 3-9: Difference between the calculated and measured calcium concentration (as dissolved gypsum) vs. initial theoretical supersaturation – 15 g/l sulphuric acid

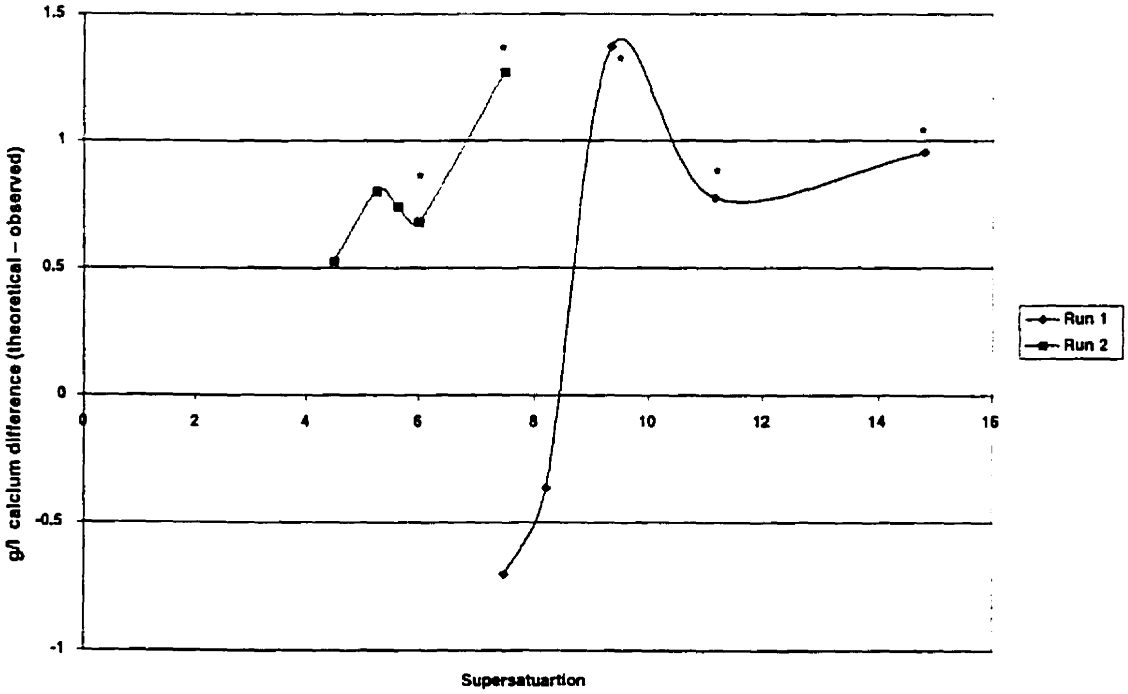

Figure 3-10: Difference between the calculated and measured calcium concentration (as dissolved gypsum) vs. initial theoretical supersaturation – 18 g/l sulphuric acid

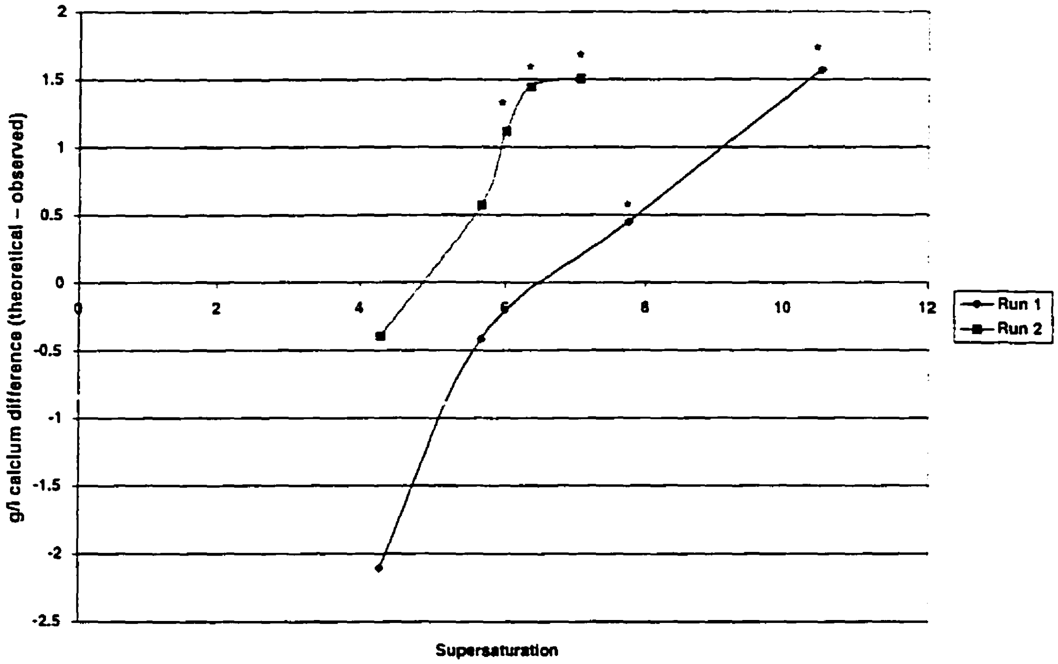

Figure 3-11: Difference between the calculated and measured calcium concentration (as dissolved gypsum) vs. initial theoretical supersaturation – 36 g/l sulphuric acid

In general, all starred points lie at the highest positive calculated difference values between the calcium added and the calcium measured in solution. Except for the low acid tests and the second run results, the starred points correspond to all test points that lie above the zero calcium concentration difference value.

Repeat tests were run for 15, 18, 36 g/l sulphuric acid concentrations. The supersaturation at which the stable precipitate cloud was observed was different for all second runs at the same initial acid concentration. This is not surprising, given that the solutions are inevitably contaminated with dust and possibly other foreign solid bodies, such as different amounts and sizes of undissolved calcium oxide, much like the industrial wastewater solutions.

The lowest supersaturation ratio that was observed to induce homogeneous nucleation in sulphuric acid solutions was 6. The interpolated line crossed the x-axis at an average supersaturation value that increased with increased acid concentration. This could reflect the decrease in free sulphate concentration at higher pH, requiring more calcium for the critical supersaturation to be reached. However, before any conclusions may be drawn about the "homogeneous" nucleation of gypsum from sulphuric acid solutions, literature that reviewed the spontaneous precipitation of gypsum indicated that other published results on this subject may not represent the simple phenomenon of truly instantaneous primary homogeneous gypsum nucleation.

3-4 DISCUSSION

3-4-1 Primary homogenous nucleation and induction times

Early gypsum spontaneous nucleation studies by Schierholtz (1958) indicated that close control of primary homogeneous nucleation experiments was difficult to achieve, and that primary homogeneous nucleation was often preceded by an induction period. The induction period is defined as the time period between the mixing of solutions containing the lattice ions and the appearance of the first solid phase.

The induction period for gypsum was further investigated by Liu and Nancollas (1973). They determined that induction period decreases with increasing temperature and increased concentration of lattice ions. They also fit an equation to describe the induction time as a function of solution concentration. Packter (1974) performed kinetic studies of the spontaneous precipitation of gypsum to determine the induction periods, crystal size and numbers. Packter also reported that induction time decreased with increasing concentration of lattice ions, with induction times ranging from 3 to over 10,000 seconds. Packter noted the decrease in induction period with increased metal salt concentration, referring to Neilsen (1961) who proposed that spontaneous precipitation of sparingly soluble metal salts in solution occurred through a heterogeneous nucleation on dust particles. Consequently, the observation of a stable "cloud" of gypsum fines after mixing of lime with sulphuric acid does not necessarily indicate the critical supersaturation at which primary homogeneous nucleation will occur, but it does indicate a condition where induction time for primary homogeneous nucleation of gypsum is negligible.

3-4-3 Competing growth rates

Another problem with experiments that investigate primary homogeneous nucleation phenomena has been indicated by other researchers. Nancollas (1968 and Nancollas et al., 1979) noted that it is not possible to determine whether crystal nucleation and growth occur simultaneously or consecutively, which presents a problem for spontaneous precipitation studies. A system may precipitate a combination of homogeneously nucleated solids and solids formed on or facilitated by the presence of foreign solids. It is also not clear that one is observing the instantaneous moment of formation of the nuclei when one observes a fine "cloud" of precipitate, or the result of the growth of nuclei to a size one can observe with the naked eye. Verdoes et al. (1992) analyzed the nucleation and growth rates of calcium carbonate and determined that the two rates can not be uncoupled. Consequently, it is not possible to separately evaluate the nucleation and growth rates of unseeded precipitation tests.

More recently, Franke and Mersmann (1995) showed that the primary homogeneous nucleation of amorphous calcium carbonate produced an opaque cloud. Subsequent calcium carbonate growth reduced the supersaturation, and either transformed or newly built crystalline solids grew at this lower supersaturation. This decrease in supersaturation continued until it fell below the solubility of the amorphous phase; remaining amorphous particles dissolve, clearing the solution and slightly increasing the supersaturation. In some of the primary homogeneous tests performed in this work, this cloud formation and dissolution was observed, but was not recorded as the onset of homogeneous nucleation as the dissolution was fairly rapid, and it was assumed that the cloud was not stable.

To conclude that a given supersaturation at a given temperature will induce primary homogeneous nucleation is an oversimplification of a complex process. The experiments do not elucidate the critical gypsum supersaturation above which primary homogeneous nucleation of gypsum will occur, but they indicate that there is a supersaturation above which gypsum will concurrently produce stable homogeneously nucleated fines and other particles. Presumably a neutralization process that exceeds this critical supersaturation will rapidly produce a large number of primary homogeneous nucleated solids. However, van der Leeden et al. (1993) studied the effect of additives on nucleation rate, crystal growth rate and induction time; they determined that primary nucleation of barium sulphate was only heterogeneous in unseeded systems. They concluded that microscopic particles act as more active heterogeneous nucleation centers. Regardless of whether the fine gypsum cloud particles are produced through primary heterogeneous or homogeneous nucleation, the production of these fines does occur over a given supersaturation, and it is expected that they will not exist below that critical supersaturation.

3-4-4 Effect of impurities

The main motivation of these experiments was determining the critical supersaturation, brought about by lime addition, that induces primary homogeneous nucleation of gypsum in an acidic sulphate system. The preliminary experiments were conducted with pure sulphuric acid-lime systems; the presence of other sulphate salts in acidic sulphate wastewater might have an effect on the primary homogeneous nucleation of gypsum. There is evidence in the literature that not-lattice ions in solution can affect primary homogeneous nucleation, meaning this information should not be extrapolated to the mixed electrolyte system.

The tendency for calcium to form compounds in nature is well-known; pure calcium metal is found nowhere on the earth, and its complexing powers are exploited in biological processes. It is possible that its ability to form complexes affects its speciation in solution and its role in the primary homogeneous nucleation of gypsum. Glasner and Weiss (1980) studied the effect of zinc and magnesium ions on the spontaneous precipitation of calcium carbonate from solution. They reviewed the evidence that non-lattice cations influence the nucleation and control the epitaxial growth of crystalline calcium carbonate precipitates. Barium, strontium, zinc, and magnesium at low concentrations have been shown to affect the precipitation of calcium carbonate. Some non-lattice cations induce the precipitation of thermodynamically unfavorable calcium carbonate phases such as vaterite or aragonite. They postulate that the formation of a carbonato-complex $[Zn(CO_3)_2]^{2-}$ ion may serve as a center of nucleation in a supersaturated calcium carbonate solution with zinc; other workers have suggested that $MgCO_3$-$3H_2O$ may be the nucleus responsible for aragonite formation in calcium carbonate solutions doped with magnesium ions.

Reddy and Nancollas (1976) reported the effect of the magnesium cation on spontaneous precipitation of calcium carbonate; they summarized that the dehydration energy of magnesium may inhibit the precipitation of calcium carbonate. It has been proposed that magnesium reduces the nucleation rate of calcite (Bishoff, 1968) and/or destablizes the calcite critical nuclei (Möller, 1974). It is possible that the precipitation behavior of gypsum may also change in the presence of other ion-complexes that are present in a mixed acidic electrolyte solution typical of wastewater influent. It is interesting to note that a controlled precipitation study of Nancollas (1968) reported the crystallization behavior of the bivalent metal sulphates lead, strontium, and barium sulphate salts, but did not include calcium.

Edinger (1973) commented that sodium-calcium complexes were formed in some of the gypsum precipitates that were spontaneously precipitated from different supersaturated electrolytes. Edinger also reported that either nucleation and/or the growth of existing gypsum nuclei were exceedingly slow processes. Schierholtz (1958) also reported a curious accelerating effect of sodium chloride on gypsum crystallization rates from spontaneous precipitation tests, although the induction time was not affected.

3-5 CONCLUSIONS

Single stage, unseeded neutralization processes that exceed the critical supersaturation of primary homogeneous nucleation favor the production of numerous fine solids with low solids density (Section 3-1) and settling velocity (Appendix E).

Precipitating gypsum solids with slaked lime and sulphuric acid solely by primary homogeneous nucleation is not a simple endeavor. Predicting the homogeneous precipitation of gypsum from a mixed acidic electrolyte may be even more difficult. Glasner and Weiss (1980) claim that "no one can disagree with the conclusion, that "thermodynamics fails to predict many of the observed assemblages, suggesting that kinetic mechanisms are more important for these quasi-metastable occurrences", referring to the complexes that may exist in mixed electrolytes and effect the homogeneous nucleation process. In pure and mixed acidic sulphate electrolyte, gypsum may precipitate through a cloud of fines by primary homogeneous, if not primary heterogeneous nucleation above a critical supersaturation, albeit concurrently with other nucleation processes.

It is the goal of the next chapter to design an improved neutralization process that promotes the secondary epitaxial growth of gypsum seed, inhibiting or reducing gypsum precipitation due to primary homogeneous or primary heterogeneous nucleation. Maintaining the process conditions below the critical supersaturation for homogeneous nucleation in the presence of gypsum seed is expected to result in gypsum crystal growth (Demopoulos, 1993 and Mersmann et al., 1994).

4 SEMI-BATCH, SEEDED, CONTROLLED NEUTRALIZATION AND GYPSUM PRECIPITATION

4-1 INTRODUCTION

After the solubility and the critical supersaturation that induces homogeneous nucleation of the precipitation system of interest have been investigated (Chapters 2 and 3), it is useful to test the benefits of seeding and controlled neutralization within the flexible operating conditions of a semi-batch reactor. The results from these tests may then be applied to the design of a new continuous precipitation process (Chapter 5). The goal of this chapter is the investigation of the growth of large gypsum crystals in a simplified semi-batch neutralization process, under different controlled neutralization conditions with seeding. The most desirable gypsum quality to be improved by these tests is solids density, as high solids density gypsum will take up less tailings pond volume, increasing tailings pond life. Other benefits of increased size gypsum precipitate include a decreased surface area to volume ratio, and a more rapid solid-liquid separation. The lower surface area of solids will entrain less cations that adsorb to the solid surface and report to the tailings pond. An easier solid-liquid separation also requires a smaller, and therefore less expensive unit operation.

A literature review revealed only a few studies of gypsum growth from sulphuric acid solutions with lime, (Franke et al. (1995), Macek et al. (1993), Schierholtz (1958)) and even fewer studies on the effect of recycling gypsum solids in a neutralization process (Lockely et al.., 1993). The results of these studies, as well as published theories of reaction crystallization and crystal growth were used to develop and interpret a semi-batch process design that minimizes the factors that produce fines, and maximizes those that promote gypsum crystal growth.

4-2 LITERATURE REVIEW

4-2-1 The effect of growth and nucleation rates on precipitated gypsum product size

The variety of previous work on gypsum growth from solution is summarized in Appendix B. In general, supersaturation and seeding affect the rates of gypsum crystal growth, nucleation rate and nucleation mode. The rates of nucleation and growth play a role in the precipitated crystal size distribution and average size; at high supersaturations, primary nucleation is favoured and fines are precipitated from solution. Under seeded conditions and low supersaturation, the precipitation of large solids by crystal growth is enhanced.

The published effects of supersaturation on these rates have generally been tested in carefully controlled environments, with system supersaturation usually assessed by means of analytical chemistry or atomic absorption of an aliquot of solution. Unless one presumes that there is perfect mixing within the reaction vessel, reported supersaturation values represent only a local value if the system is not at equilibrium. Fluctuations about this local value could also affect the population number and size of crystals grown from a precipitation reactor, as they would affect the different growth and nucleation rates. These fluctuations in supersaturation can be attributed to a number of reactor design parameters.

4-2-2 The effect of reactor design on the size of precipitated particles

As the rates of nucleation and growth determine the size distribution and median size of crystals grown in batch or continuously operated crystallizers, and the mean supersaturation favours different nucleation rates, control of mean supersaturation can lead to the control of product crystal size (Mersmann et al., 1994). A low mean supersaturation favours secondary and surface nucleation and seed growth (Section 3-2-4-4), however, the assumption of low uniform reactant concentrations throughout a precipitation reactor can rarely be met in practice. Variations in the mean supersaturation give rise to different local supersaturation values.

Mersmann and Rennie (1995, p.266) have noted that the local supersaturation in a particular volume of the reactor is dependent on: 1) the concentration and stoichiometry of the reactants, 2) the manner of feed, 3) the location of feed, 4) the fluid dynamics, 5) the presence of seed or recirculated slurry. The reactor micro and macro mixing properties, chemical reaction and crystal growth rates as well as the reactor design can affect the dispersion of reactants throughout the reactor volume, generating local regions of supersaturation that deviate from the mean reactor value. Local pockets of high supersaturation within the reactor could produce undesirable fines through homogeneous nucleation, if the growth of seeds is the preferred mode of crystallization. The reactor design should minimize the probability of these regions in order to produce gypsum crystals with a large mean particle size.

Klein and David (1995, p.377) argued that crystallization CSTR's can not be successfully modeled as perfect reactors. They delineate three different zones: one near the reactant feed point, where local levels of high supersaturation may develop, one near the stirrer, where the energy dissipation is highest, and one characterizing the average volume of the reactor. It is the balance between the chemical reaction, crystallization, and macro/micro mixing rates that determine local supersaturation. This section discusses the effect of reactor design and reactor chemistry on local supersaturation, and consequently, on final particle size. Some of the effects can decrease mean particle size, others can increase mean particle size.

4-2-3 Processes that decrease mean particle size

4-2-3-1 Chemical reaction rates are linked to mixing rates and solids loading

Mersmann and Rennie (1995, p. 266) comment that the rate constant of chemical reactions involving ions is very high compared to crystal growth rates. The progress of quick ionic reactions is usually controlled by the mixing process (Mersmann, et al., 1994). The process of crystal growth is noted to be one of the slowest of the crystallization rates, taking minutes instead of the milliseconds that are necessary for primary nucleation. The precipitate production rate by crystal growth can be favoured with higher seed loading as it provides more nucleation sites for crystal growth. A higher crystal surface area for precipitation provides more crystal growth sites to remove more lattice ions from solution, rapidly reducing system supersaturation. The chemical reaction rate of wastewater neutralization is accordingly assumed to be faster than the crystal growth rate of the gypsum, and is therefore affected by processes that affect supersaturation, such as the mixing process.

4-2-3-2 Reactor mixing rates affect local supersaturation and particle size

Two modes of mixing are responsible for the dispersion of reactants throughout the reactor volume. Macromixing is used to describe the degree of homogeneity in a stirred reactor, and micromixing describes the mixing of reactants at a molecular level.

Mersmann and Rennie (1995, p.267) discussed the effect of micro and macromixing on supersaturation, which in turn affects the nucleation rate of high reaction rate systems.

Macromixing in batch reactors is affected by the operating mode of the reactor (Figure 4-1, from Mersmann and Rennie, 1995, p.267). The semi-batch experiments conducted in this work are modeled after the first setup in order to minimize macromixing times, and minimize the corresponding supersaturation variations.

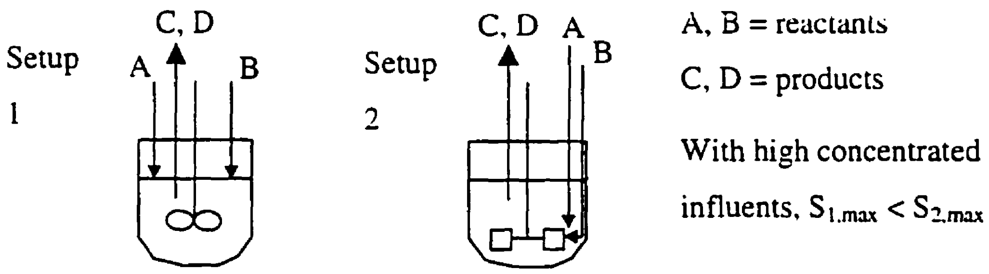

Figure 4-1: Operating modes of semi-batch precipitation crystallizers

Micromixing is affected by solution density, viscosity, and diffusion rates, however, for agitated reactors and fast reaction chemistry systems, agitator power has a predominant effect on micromixing and therefore local supersaturation.

4-2-3-3 Agitator power affects particle size

The specific power input of the agitator can affect the mean crystal size of solids produced by a precipitation reactor. The size of crystals produced by slow chemical reactions are not affected by the specific power input, as the crystal growth is affected by the mean supersaturation, not local supersaturation or local specific power input (Mersmann and Rennie, 1995, p.270). Mersmann and Rennie developed a schematic to represent the median crystal size as a function of specific power input and reactant concentration for different chemical reaction rates. The solids produced from fast ionic reactions are affected differently by mean specific power input than slow chemical reactions. Figure 4-2 (from Mersmann and Rennie, 1995, p.272) presents the effect of mean specific power input on the mean product size of fast ionic reaction products for the two reactor setups.

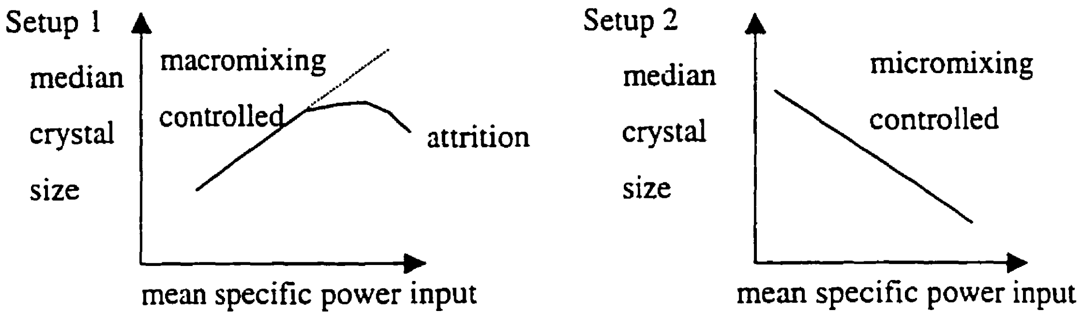

Figure 4-2: Median crystal size against specific power input (fast chemical reaction rate)

Should the reactants of fast ionic reactions be added to the reactor in a similar location and near the agitator, an increase in mean specific power leads to a decrease in mean particle size. This is because the increase in power leads in a decrease in micromixing times. High fluid shear produced by the high agitator power promotes quick mixing across the interface between the volume of liquid containing the added reactants and the reactor contents. This can develop regions of high supersaturation, resulting in the formation of smaller particles by primary homogeneous nucleation. However, if the reactants are added far apart, increased mean specific power input reduces the macromixing time, meaning the reactants are quickly dispersed throughout the reactor volume and the supersaturation is maintained at low levels, encouraging crystal growth and the formation of large particles.

4-2-3-4 Attrition affects particle size

Agitator power also has another effect on crystallization rates. Large particles may also be susceptible to breakage at high specific power inputs; consequently, the median crystal size may decrease past a given power increase. The rate of secondary nucleation, to which attrition contributes via the generation of nuclei by crystal-crystal, crystal-reactor and crystal-agitator collisions, depends on the hardness of the solid and the power input of the agitator. Secondary nucleation is noted by Klein and David as a nucleation mode that arises at low supersaturations and explains the steady-state running of continuous crystallizers (Klein and David, 1995, p.369). The production of these smaller particles generates new nucleation sites for crystal growth, and also contributes to reducing the average particle size of the reactor.

The fractured pieces produced by attrition may be of different sizes and may have different growth potentials/rates. It is not possible to predict the mass abraded per unit time or the number of attrition fragments produced by a given particle size fraction; part of the reason is that it is difficult to know which particles were produced by attrition processes. The stress experienced by the colliding crystals depends on the geometry of the system (size and shape of crystallizer and rotor), operating parameters (rpm of rotor), physical properties of the crystals (density, elastic and shear moduli) and the liquid (density and dynamic viscosity).

4-2-4 Processes that increase mean particle size

Two crystallization processes, other than crystal growth through nucleation on seed surfaces, can increase the mean particle size of solids produced by precipitation processes. They are Ostwald ripening and agglomeration.

Ostwald ripening has an effect on crystal size if fines smaller than 1µm are produced during the reactive crystallization process, and the system attains equilibrium. The solution composition will be in equilibrium with the larger solution-own solids, whose solubility is lower than that of solution-own fines. The system is therefore undersaturated with respect to the fines; consequently, some dissolve while others grow. The increase in solution concentration due to their dissolution promotes the growth of the larger crystals.

Agglomeration will affect crystal size if there is adequate supersaturation; solid particles collide and remain in contact long enough for precipitation to occur that "cements" the particles together. Agglomeration is affected by the system hydrodynamics, solvent properties, crystal habit and size, crystal population density, supersaturation and related growth rate, and the cohesion forces between the solvent, impurities and crystals (Klein and David, 1995, p.372). As it is difficult to study rigorously, agglomeration publications are few.

4-2-5 Temperature

Increased temperature can have a positive effect on crystallization systems, often increasing product size and crystallinity. The high flows of wastewater could not be heated without considerable expense; the neutralization processes tested in this work all operated at room temperature in order to avoid that cost. Appendix L expands on the effect of temperature on gypsum precipitation, and presents the results of some test work.

4-2-6 Summary

The aforementioned mechanisms are all at work during all precipitation processes. They contribute to final particle size distribution and mean particle size. Dispersion, which is the random spread about a mean particle size produced by a crystallizer es expected to various degrees for every crystallization process. The minimization of crystal size dispersion is desirable for production processes that require a target particle size, however, the focus of this research is the improvement of gypsum solids density. This improvement in gypsum solids density is achieved by producing large-sized gypsum crystals through decreasing the rate of fines production, and designing the crystallization reactor and process to favour the growth of large gypsum crystals.

The optimum conditions for growing large-sized particles involve the minimization of the local and mean supersaturation by a combination of : 1) good macromixing of the vessel but poor micromixing of feed streams located close to the feed point, 2) vigorous seeding, especially near the feed point, 3) high circulation of slurry with a high solids density, and 4) low concentration of reactants (Mersmann and Rennie, 1995, p.272). These principles were tested with the following semi-batch neutralization of sulphuric acid with slaked lime and calcium carbonate.

4-3 EXPERIMENTAL

4-3-1 Introduction

The goal of these experiments was the production of large-sized gypsum crystals with high solids density from the repeated neutralization of sulphuric acid solutions seeded with gypsum with a semi-batch crystallization setup through high and low pH ranges. Low supersaturation was maintained via a slow neutralization agent delivery and corresponding slow rise in pH in order to encourage crystal growth and minimize fines production due to homogeneous nucleation. Slaked lime and slurried calcium carbonate neutralization agents were both tested.

4-3-2 Materials

4-3-2-1 Seed

The first neutralization of a recycled series used synthetic gypsum seed (Sigma, ACS Reagent, 99.7%) (Figure 4-3). Succeeding runs were seeded with the dry solids that were recovered from the previous neutralization.

Figure 4-3: SEM image of synthetic gypsum seed

4-3-2-2 Acid solutions

The solutions for pH 0.5-1 neutralization tests were synthesized with deionized water and concentrated reagent sulphuric acid (98%). Solutions for the low acid neutralizations (pH 1-5 or 1-7) were recovered from the final filtered solution of the high acid neutralization tests (pH 0.5-1)or were prepared with deionized water and oncentrated sulphuric acid.

4-3-2-3 Neutralizing Agents

The effects of two common industrial neutralization agents, slaked lime and slaked calcium carbonate, on precipitated gypsum solids density and morphology were compared. Slaked lime is a more rapid neutralization agent, especially at higher pH's, when compared to its less expensive counterpart. In all cases, the base slurries were suspended with a magnetic stirrer. Slaked lime slurries were prepared at 50 g/l, and an equivalent molar calcium concentration (0.89 mol/l) of 89 g/l calcium carbonate was used.

4-3-3 Experimental Design

4-3-3-1 Neutralization tests

The chemistry of gypsum production by reactive crystallization of acidic sulphate solutions was simplified in these tests in order to reduce the number of factors that could affect gypsum nucleation and growth. In two series of tests, 10 g/l sulphuric acid solutions (~pH 1) slurried with gypsum seed were neutralized to a neutral pH with pure slaked lime or calcium carbonate slurries. Dilute neutralization agent concentrations were used to decrease the possibility of generating a region of high supersaturation at the neutralization feed point.

Another two series of tests investigated the semi-batch neutralization of 25 g/l sulphuric acid solutions (~pH 0.5) through to pH 1. This pH range was examined to observe any effect of the bisulphate ion and the lower activity of water on the precipitation of gypsum. The effect of the two neutralizing agents, slaked lime or calcium carbonate slurries on the precipitate quality were compared.

4-3-3-2 Seeding

Reagent-grade gypsum was used to seed the first neutralization run of each test. In order to simulate the effect of recycling solids through a neutralization circuit, the solids produced by a neutralization run were sourced as seed for the succeeding neutralization run. Ten neutralization cycles were performed for each test condition, simulating the effect of recycling solids through a neutralization process ten times.

The solids concentration that would maintain a rate of crystal growth greater than any potential primary nucleation rate at the process conditions was required, so that the production of fines through primary nucleation would not be favoured. Preliminary tests that surveyed the effect of seed concentration on solids density indicated that 50 g/l of seed would provide adequate surface area for the rate of crystal growth the exceed that of fines production through primary nucleation (Appendix F). Therefore 25 g of new or recycled seed was added to each initial 500 ml volume of acid solution.

4-3-3-3 Reactor setup

The semi-batch neutralization reactor was set up to favour the best macro and micro mixing according to Section 4-2-3-2. A schematic of the reactor setup is presented in Figure 4-4.

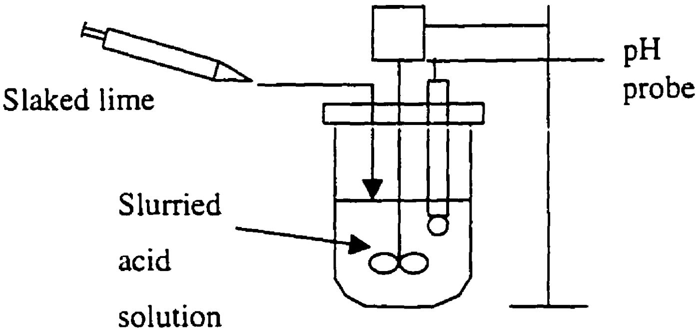

Figure 4-4 – Semi-batch crystallization experimental setup

A 1L pyrex reaction kettle was used as a reaction vessel; a plastic-coated 3-blade marine-type agitator powered by a Cole-Parmer Stir-pak Laboratory mixer (3-250/50-5000 rpm) motor kept the slurry in suspension. The agitator was run at the minimum speed required to keep the solids in suspension to minimize the production of fines due to attrition. The neutralization agent was added manually with an Eppendorf Reference micropipette (100-1000uL), and the pH monitored with a Orion Model 720A pH meter and Fisher Accu-pHast pH probe.

4-3-4 Experimental Method

Each neutralization test began with 500mL of agitated acid solution in the reactor. The pH was recorded, 25g of reagent grade or recycled gypsum seed added, and any change in pH noted. Neutralization agent slurry was added to the reactor at the surface of the solution, midway between the agitator and the reactor wall in 3ml increments every two minutes. The change in pH after each neutralization agent addition was recorded. Once the target pH of the test was reached, the settling velocity of the solids in solution was determined (Appendix E, Section 4-3-5-2). The solids settled under gravity and were tested for solids density (Section 4-2-5-1). The percent fines were determined (Section 4-3-5-5). The rest of the slurry was filtered through Whatman Qualitative 1 filter papers by vacuum filtration (Cole-Parmer Model 7050-00 aspirator pump), and dried in a standard oven at temperatures ranging from room temperature to 40°C. The dried solid product was weighed with a Mettler AE200.

The only difference between the experimental procedures for slaked lime and calcium carbonate neutralization was the final pH at which the high pH tests were stopped. The calcium carbonate neutralizations were stopped at pH 6 as calcium carbonate is not an effective neutralizing agent above this pH. Not only was the rate of pH change very slow from pH 5 to 7, but undissolved calcium carbonate solids present at pH 7 were recycled with the gypsum as seed to the next recycle run. These solids reduced the amount of recycled gypsum seed by an unknown amount. A fraction of the undissolved calcium carbonate solids is expected to have dissolved once carried over as recycled seed for another run, whereas others may be coated by heterogeneous gypsum nucleation. These unwelcome unknowns were reduced by ending the calcium carbonate neutralizations at a lower pH than those of slaked lime, reducing the amount of undissolved calcium carbonate at the end of a neutralization run.

4-3-5 Analysis

4-3-5-1 Solids density

After the slurry was allowed to settle by gravity, three aliquots of the solids were sampled from the settled mass and weighed. They were dried under atmospheric pressure and temperatures ranging from 40°C to 20°C and re-weighed. The classic solids density calculation was performed to check the solids density:

$$Solids\ density\ (\%) = \frac{(dry\ sample\ mass)}{((wet\ sample\ mass)} \times 100 \qquad (4-1)$$

Three aliquots of slurry were taken for each data point so that a measurement error value was determined for each solids density value.

4-3-5-2 Settling velocity

Appendix E discusses the settling velocity tests and the relevance of their results. As the settling velocity is a function of solids content, and not a definitive indication of increased gypsum particle size, the results were not used to evaluate the precipitate for each run. SEM imaging proved to be a better technique to observe the increase in gypsum particle size. However, for an equivalent solids loading, the settling velocities of precipitate grown on recycled gypsum seed were higher than that of precipitates produced without seed.

4-3-5-3 Imaging

Images of selected solid samples were generated by a JSM 840 scanning microscope at 10 kV after the samples were coated with gold and platinum in a Hummer VI plasma sputter coater. The images were used to indicate particle size, qualitative particle size distribution and morphology. As morphology indicates the rate of growth of the crystal faces, these images also provide information about the growth rates of the different faces.

4-3-5-4 Morphology

The gypsum morphologies were compared to the theoretically predicted gypsum morphology and the gypsum morphology usually observed in pure water (Simon et al., 1965) (Figure 4-5) (see Appendix G for more gypsum morphology information).

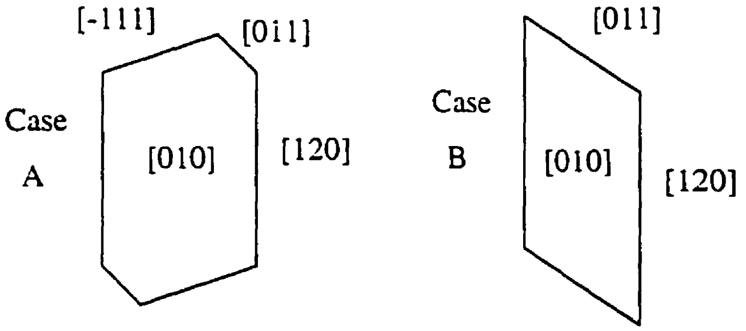

Figure 4-5: Gypsum morphologies predicted theoretically (A) and observed in pure water (B)

4-3-5-5 Percent fines

After the solids density and settling velocity measurements were taken, the slurry was agitated and left to settle with gravity for five minutes. Invariably, a population of fines would still be in suspension; these solids were decanted from the bottoms, filtered with Whatman Qualitative 2 filter papers under vacuum, dried, and weighed. Their mass is presented as a percent fines value, which is the percent value of their mass to the total solid mass in the reactor.

4-4 RESULTS AND DISCUSSION

4-4-1 Introduction

As two pH ranges and two neutralization reagents were tested, the results of the four semi-batch neutralization runs are presented separately. The results for each system consist of the change in pH vs. time, the change in solids density with succeeding recycle runs, and the change in precipitate size and morphology.

Sources of error for these results include loss of mass during handling, inaccurate measurement of seed mass acid volume, and solids density masses, errors in pH measurement (which is amplified at low pH), inconsistencies in solids density sampling, inconsistent delivery of neutralizing agent volume, inconsistent times between neutralization doses, and inhomogeneous slurry concentrations.

4-4-2 Low acid neutralizations: 10 g/l acid starting solution, pH 1-7

4-4-2-1 Slaked lime neutralizing reagent

4-4-2-1-1 Change in pH with time

A typical neutralization curve for this process is presented as Figure 4-6. A point of interest is the rapid pH change after pH 3, to pH 7. The average neutralization run time over the ten recycle runs was 35 minutes.

4-4-2-1-2 Change in solids density with recycle run

Figure 4-7 tracks the change in solids density with neutralization cycle. The first two neutralization cycles indicated an improved solids density to 45%, however, the solids density of the second recycle product dropped to 30%. An overall continuous increase in recycled solids density to 45% was observed after this drop.

The drop in solids density after the second recycle is attributed to an anomalous delivery of slaked lime. The slaked lime slurry agitation had malfunctioned ,and a slurry concentration greater than 50 g/l was used for the second recycle run, generating higher supersaturations. The solids density measurement error ranged from less than 1 to 10% of the average solids density value.

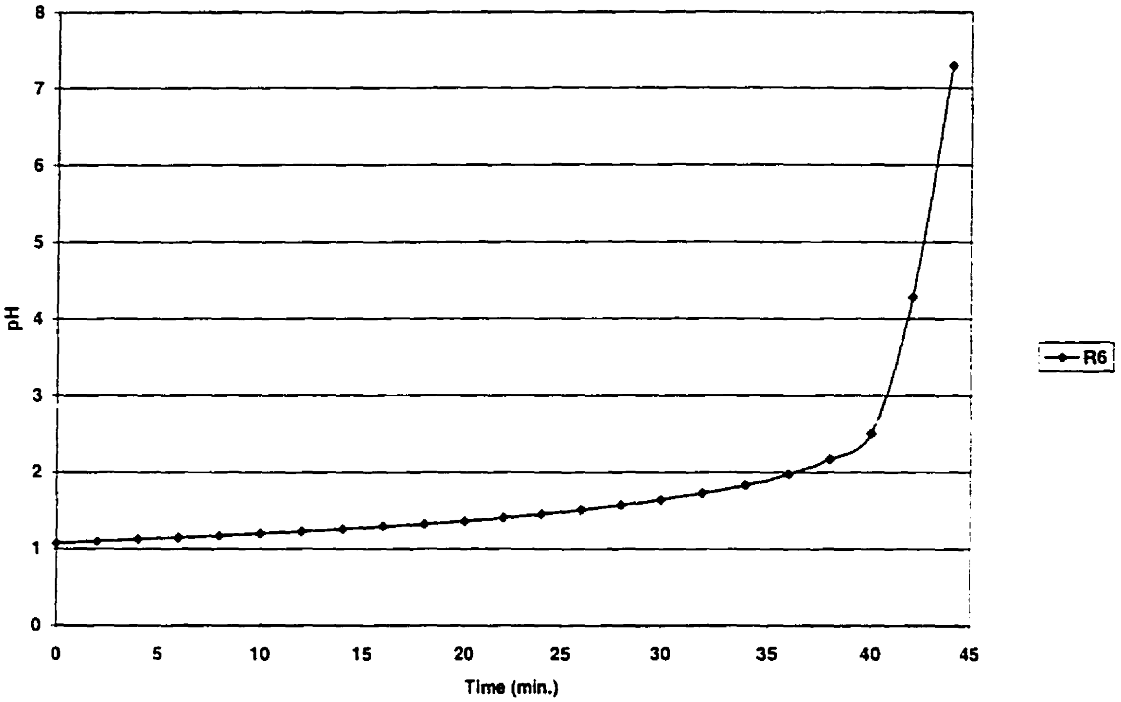

Figure 4-6: Change in pH with time, semi-batch controlled neutralization from pH 1-7 with 50 g/l slaked lime, and 50 g/l seed, 6th recycle

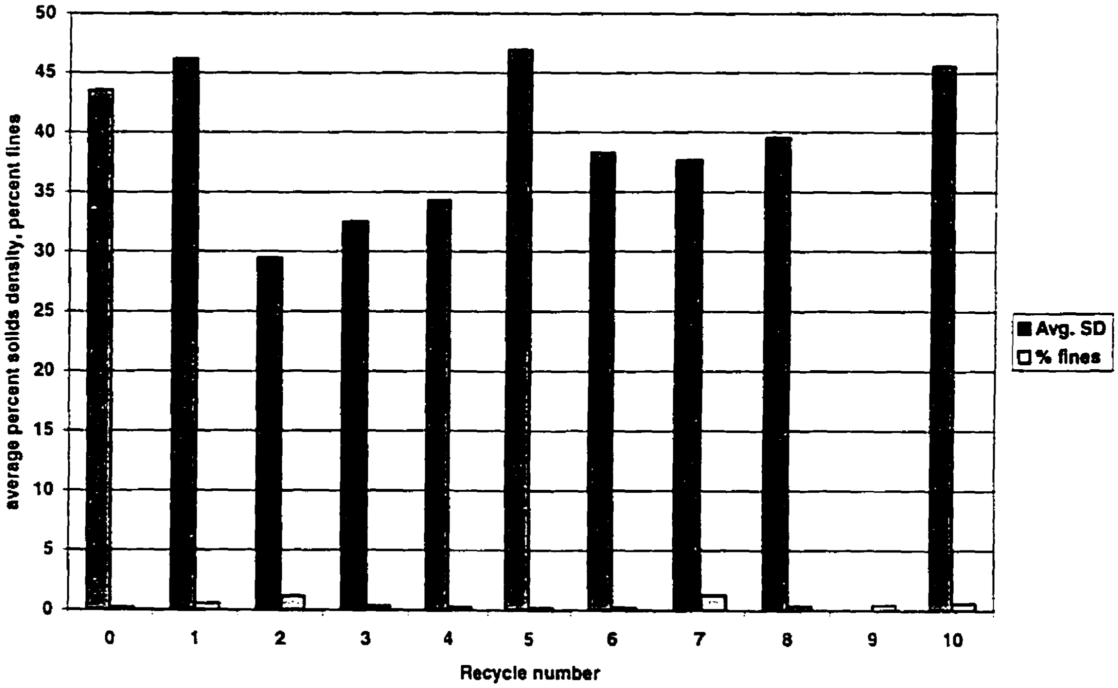

Figure 4-7: Change in solids density and percent fines with recycle run, semi-batch controlled neutralization from pH 1-7 with 50 g/l slaked lime and 50 g/l seed.

This higher supersaturation could have been responsible for the increased percent fines for that run, which may be correlated to the decreased solids density value.

A decrease in product solids density is not evident for the rest of the recycles, however, the trend in increasing solids density with recycle number decreased and stalled at the sixth and seventh recycle. There was also an interesting increase in percent fines to 1.3% for the seventh run from an average of 0.5%. It is possible that the reduction in seed surface area due to the recycling of a constant mass of crystals that are increasing in size and therefore decreasing in surface area to volume ratio reached a critical value. If not enough surface sites for crystal growth were available, primary heterogeneous nucleation may have been favoured. This results in the production of new fines that act as new surface nucleation and growth sites for the rest of the neutralization runs.

An average of 12.6±5.9 g/l gypsum was produced by each neutralization run. A value for the ninth recycle was not available due to experimental error.

4-4-2-1-3 Change in gypsum particle size

The solids produced by the tenth recycle (Figure 4-8) averaged about 100 μm in length, and 20 μm in width. Their depth was less than 10 μm. The fines exhibited a different morphology (Figure 4-9). They ranged in size from 10-50 μm, and tended to exist as clusters (Appendix H). On average, less than 0.51±0.37 % of the total reactor mass was separated as fines.

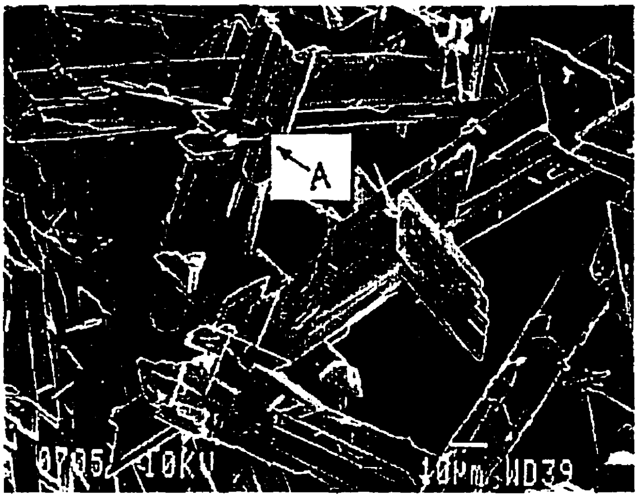

Figure 4-8: SEM Image of 10th recycle gypsum precipitate, semi-batch controlled neutralization from pH 1-7 with 50 g/l slaked lime and 50 g/l seed.

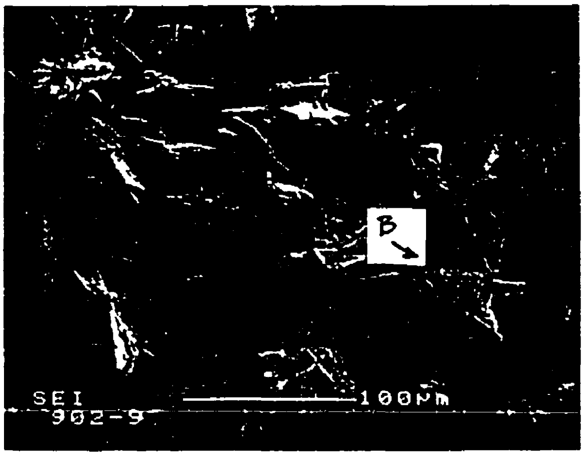

Figure 4-9: SEM Image of 10th recycle gypsum precipitate fines, semi-batch controlled neutralization from pH 1-7 with 50 g/l slaked lime and 50 g/l seed.

4-4-2-1-3 Gypsum crystal morphology

The precipitated product can be grouped into two major morphology types: the classic bladed gypsum morphology (Appendix G) as well as stellate clusters (Appendix H). The two morphologies are depicted in the SEM image of Figures 4-10. These two morphologies were also found amongst the fines.

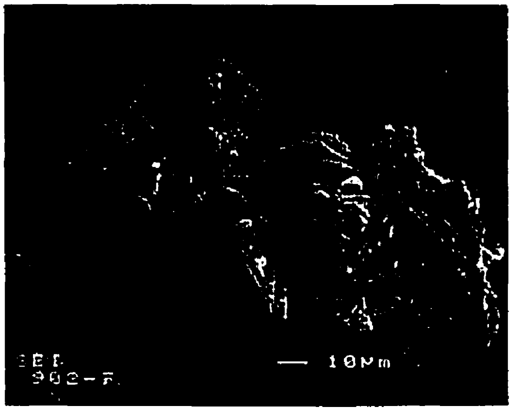

Figure 4-10: SEM Image of 7th recycle gypsum precipitate, semi-batch controlled neutralization from pH 1-7 with 50 g/l slaked lime and 50 g/l seed.

The classic gypsum morphology of the precipitates indicates that the [011] face is the most favoured growth face in these neutralization conditions, as it is extinguished in the numerous bladed crystals. The [-111] face has grown faster than the [120] or [010] faces, as the crystals are longer along that growth axis. The surface roughening on the

[-111] face indicates that growth is continuous on this face. However, the [010] face shows evidence of a polynuclear growth mechanism with the small crystallites nucleated on the [010] face (Söhnel et al., 1992).

Also of interest is the twinning (Appendix I) observed to originate from the nucleation of a growth unit on the [010] face at a 55-65° orientation to the major growth axis (Figure 4-10, pt. A). Some swallow-tail crystals are also present, indicating twinning along the [120] axis. The swallow-tail angle is very close to the angle of the twinned crystallites that nucleated and grew on the [010] face. There is also evidence of this swallow-tail twinning in the fines (Figure 4-9, pt. B).

Based on the morphology of the larger crystals, it is postulated that the relative reactivity of the gypsum faces in this growth environment is: [-111] (extinguished) >>[011]>[010] ≈ [120].

4-4-2 Low acid neutralizations: 10 g/l acid starting solution, pH 1-7

4-4-2-2 Calcium carbonate slurry neutralizing reagent

4-4-2-2-1 Change in pH with time

A typical neutralization curve is presented as Figure 4-11. A rapid change in pH occurs between approximately pH 2.5-4.5, with low calcium carbonate utilization efficiency after pH 5. The neutralizations were terminated at pH 6 instead of pH 7 from recycle 5 through to 10. The average neutralization run time was 50 minutes for a neutralization run to pH 7, and 40 minutes for a neutralization run to pH 6.

4-4-2-2-2 Change in solids density with recycle run

Figure 4-12 shows the interesting trend in solids density with recycle run. An average solids density of 55% over the first recycles steadily declined after the fifth recycle to below 25%. The decrease in solids density at the fifth recycle coincides with an increase in the percent fines to 3% from an average of 0.9%, not including the first neutralization.

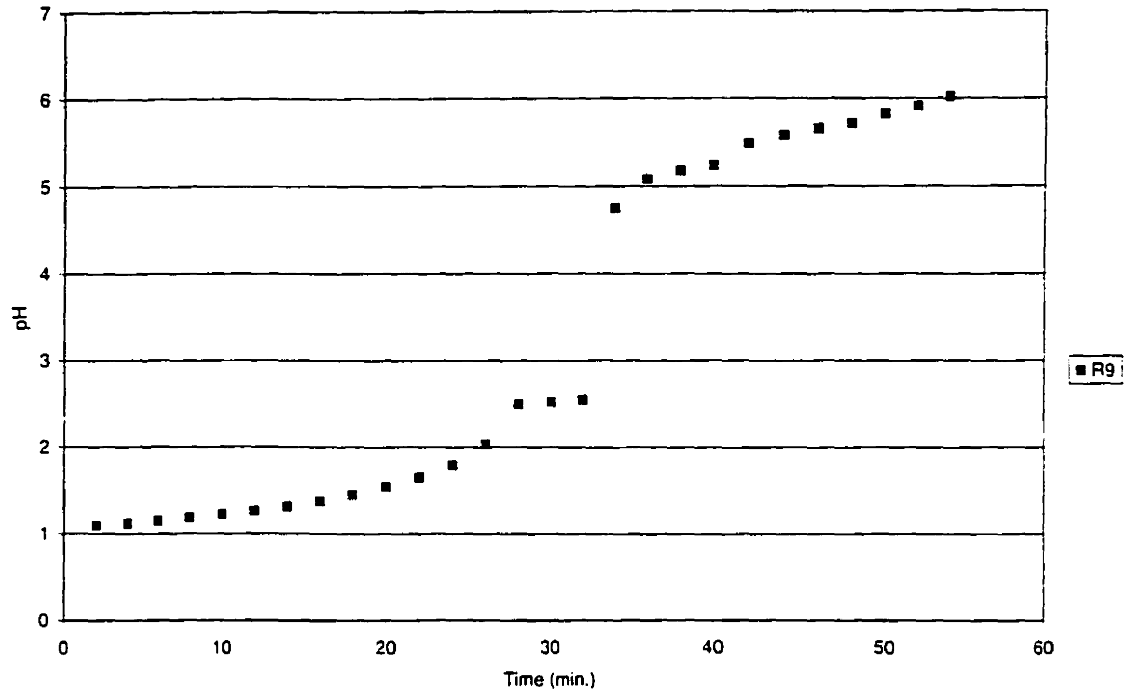

Figure 4-11: Change in pH with time, semi-batch controlled neutralization from pH 1-6 with 86 g/l calcium carbonate slurry and 50 g/l seed, 9th recycle

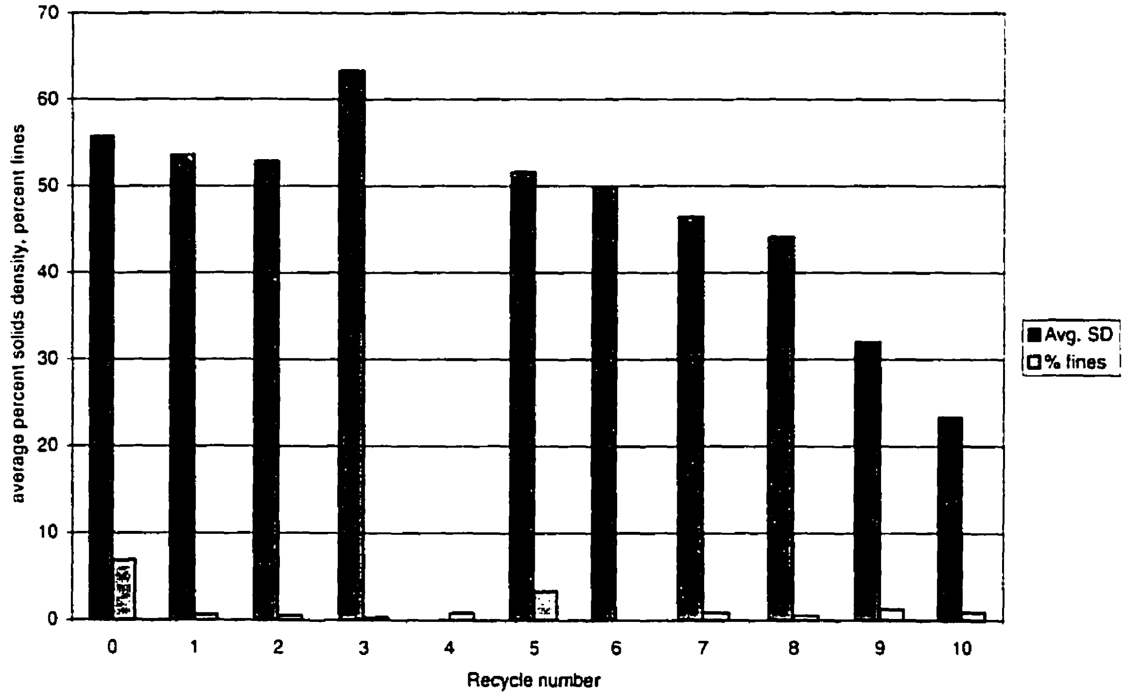

Figure 4-12: Change in solids density and percent fines with recycle run, semi-batch controlled neutralization from pH 1-6 with 86 g/l calcium carbonate slurry, 50 g/l seed.

An average of 15.5±5.6 g/l of precipitate was produced by each neutralization run. The average error in the solids density measurement was 3.7±2.6%. A value for the fourth recycle was not available due to experimental error.

4-4-2-2-3 Change in gypsum particle size

The precipitates with a solids density above 50% (Figure 4-13) are large, not as regular as the precipitate grown with calcium oxide, and are randomly "dusted" with what could be unreacted calcium carbonate solids.

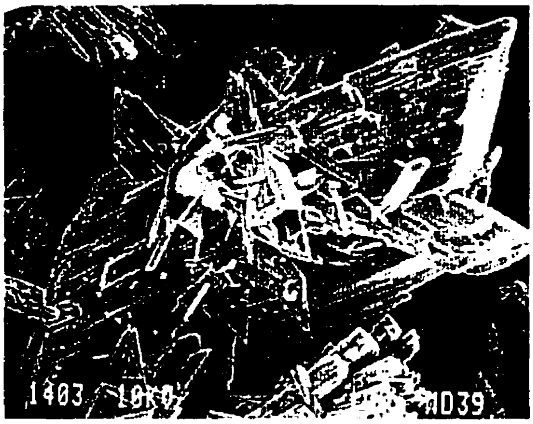

Figure 4-13 SEM Image of 10th recycle gypsum precipitate, semi-batch controlled neutralization from pH 1-6 with 86 g/l calcium carbonate slurry and 50 g/l seed.

The average size of the gypsum particles precipitated by the tenth recycle is 100 um.

The fines produced at the tenth recycle (Figure 4-14) vary in size from 10-50 um; they averaged less than 1% of the total precipitated solid mass.

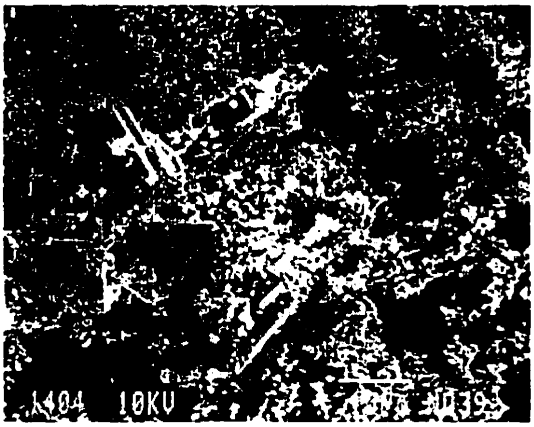

Figure 4-14: SEM Image of 10th recycle gypsum precipitate fines, semi-batch controlled neutralization from pH 1-6 with 86 g/l calcium carbonate slurry and 50 g/l seed.

4-4-2-2-4 Gypsum crystal morphology

Like the gypsum solids produced by lime neutralization, well-grown angular bladed crystals and clusters of gypsum were produced. Unlike the gypsum solids produced by lime neutralization, there was a higher frequency of twinning in the gypsum precipitated with calcium carbonate slurry (Appendix I).

Present amongst the fines were crystals that have twinned on the [010] face at the characteristic 55-65° angle (Figure 4-15), and star-burst clusters (Figure 4-16). Point A on Figure 4-15 shows the nucleation and growth of a crystal that is aligned with another crystal twinned to the parent crystal with the same orientation.

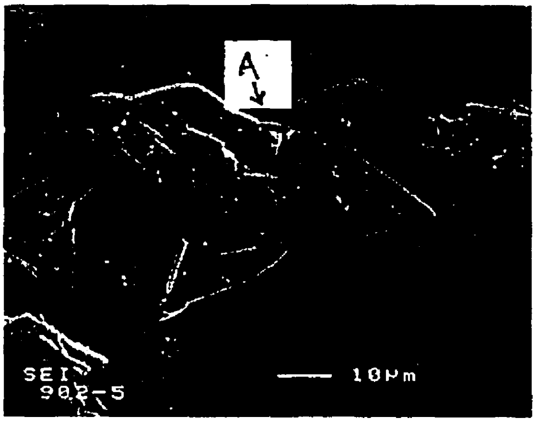

Figure 4-15: SEM Image of 10th recycle gypsum precipitate fines, semi-batch controlled from pH 1-6 with 86 g/l calcium carbonate slurry and 50 g/l seed.

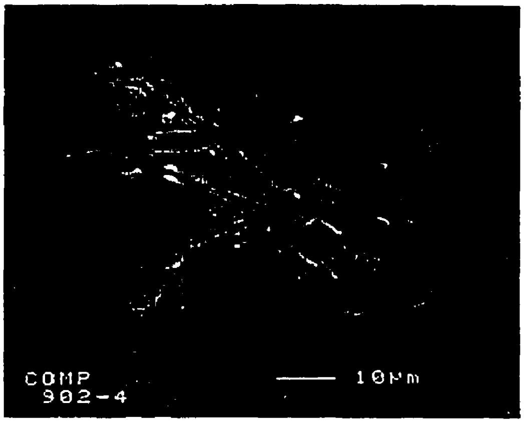

Figure 4-16: SEM Image of 10th recycle gypsum precipitate fines, semi-batch controlled neutralization from pH 1-6 with 86 g/l calcium carbonate slurry and 50 g/l seed.

Crystal growth again was most favoured on the extinguished [011] face, however, the presence of the carbonate ion or the calcium carbonate solid appears to favour growth of the [120] face, as evidenced by the wider shape of the gypsum crystals. There also appears to be extensive polynuclear growth resulting in many layers growing on the [010] face, producing thicker solids with a smaller aspect ratio than the crystals grown with lime neutralization.

All gypsum faces appear to have grown, with a relative rate that decreased from [-111] (extinguished)>>[010] ≈ [011] ≈ [120].

4-4-3 Strong acid neutralizations: 25 g/l acid starting solution, pH 0.5-1

4-4-3-1 Slaked lime neutralizing reagent

4-4-3-1-1 Change in pH with time

The change in pH with time (Figure 4-17) is nearly linear with respect to time. The predominance of the bisulphate ion buffers the pH change throughout this neutralization (Appendix A). The average neutralization run time was 94 minutes.

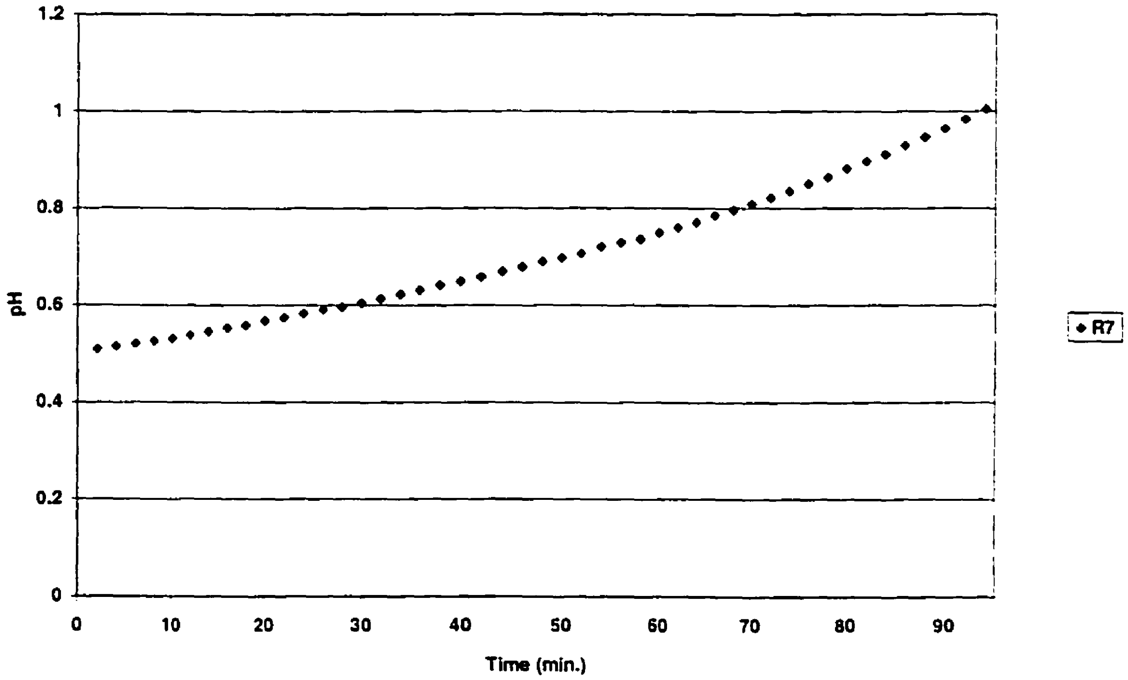

Figure 4-17: Change in pH with time, semi-batch controlled neutralization, from pH 0.5-1 with 50 g/l slaked lime and 50 g/l seed, 7th recycle.

4-4-3-1-2 Change in solids density with recycle run

The solids density of the precipitation products hovers about 26% until the sixth recycle, where it begins to increase, reaching a value over 35% by the tenth recycle (Figure 4-18). An average of 33.6±4.6 g/l of gypsum was produced by each neutralization run. The average error for the solids density measurement was 3.8±3.2%. A value for the second recycle was not available due to experimental error.

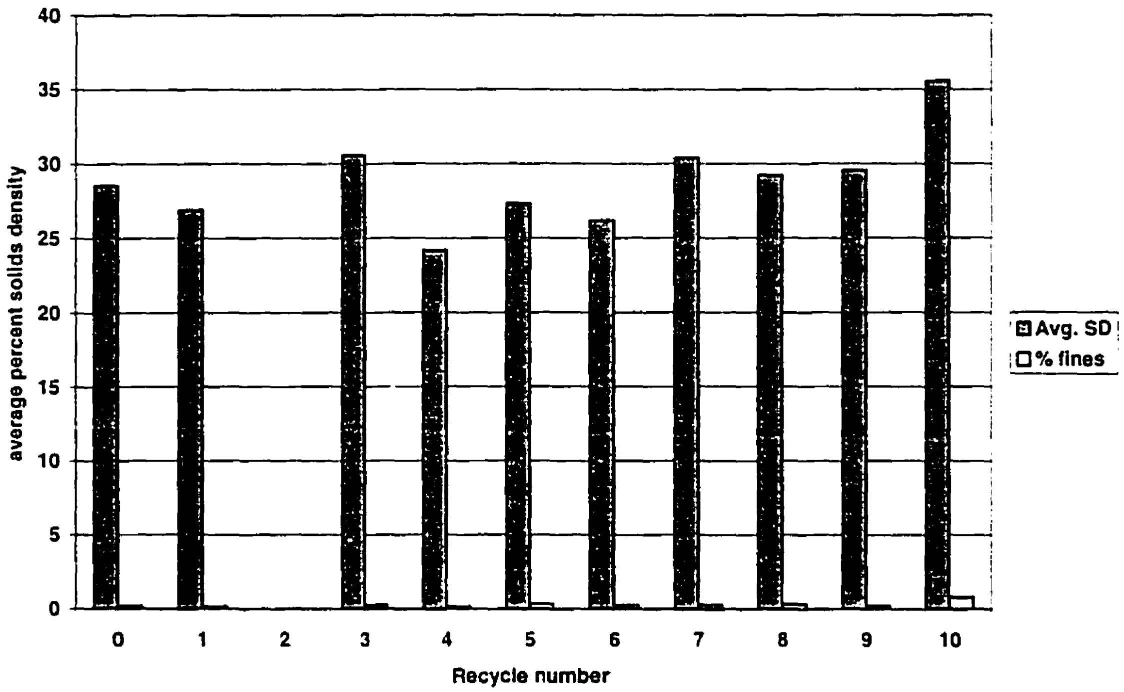

Figure 4-18: Change in solids density and percent fines with recycle run, semi-batch controlled neutralization from pH 0.5-1 with 50 g/l slaked lime and 50 g/l seed.

4-4-3-1-3 Change in gypsum particle size

The acicular, needle-shaped solids produced by the tenth recycle average about 400 µm in length, and 25 µm in width (see Figure 4-19). The depth of the needles is less than 15 µm. Crystallite fines of a continuum of sizes (from 2-50 um) exhibiting similar morphologies are present (Figure 4-20). An average of 0.30±0.18% of the precipitated solids were fines.

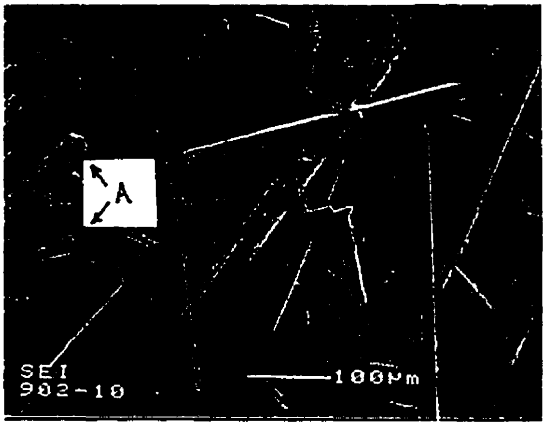

Figure 4-19: SEM Image of 10th recycle gypsum precipitate, semi-batch controlled neutralization from pH 0.5-1 with 50 g/l slaked lime and 50 g/l seed.

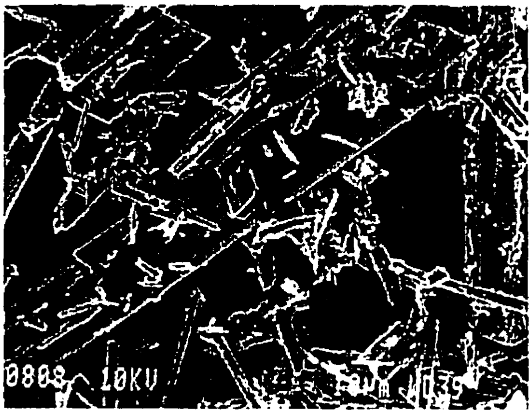

Figure 4-20: SEM Image of 10th recycle gypsum precipitate fines, semi-batch controlled neutralization from pH 0.5-1 with 50 g/l slaked lime and 50 g/l seed.

4-4-3-1-4 Gypsum crystal morphology

The flat gypsum needles produced by this mode of neutralization are strikingly different than the crystals produced at higher pH's with lime neutralization, even though they have both grown from the same seed crystals. The needles have "arrowhead" tips that suggest the growth rate of the [011] face matched the growth rate of the [-111] face in these neutralization conditions (Figure 19, pt. A). These two faces have grown faster than the [120] and [010] faces, resulting in the acicular product crystals. Other bladed crystals are also elongated along the [120] axis. The predominance of the bisulphate ion in solution may be responsible for the accelerated growth rate of these faces (Appendix B).

Closer inspection of a crystal needle tip (Figure 21) shows other interesting growth features. Figure 22 is a schematic of the proposed tip morphology.

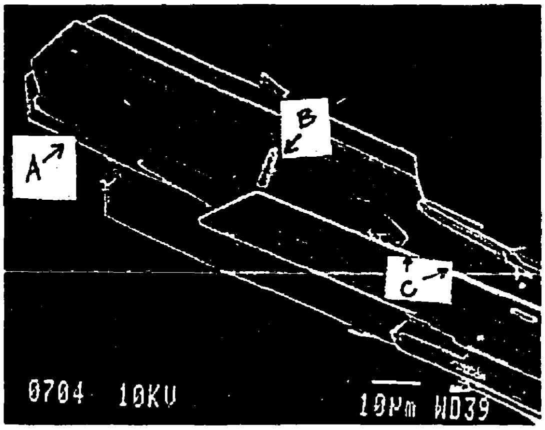

Figure 4-21: SEM Image of 10th recycle gypsum precipitate, semi-batch controlled neutralization from pH 0.5-1 with 50 g/l slaked lime and 50 g/l seed.

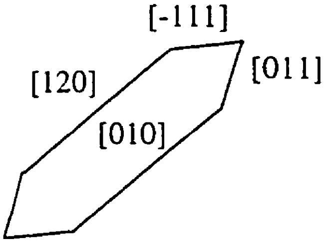

Figure 4-22: Schematic of acicular gypsum crystals faces grown at low pH with slaked lime

A morphological feature of interest is the presence of the smooth arrowhead striations (Figure 21, pt. A) which indicates layered growth of gypsum on the [010] face. These striations also appear to end in arrowheads. The second interesting feature is the presence of pits and nuclei on the [010] surface (Figure 21, pt. C). Pits and nuclei were observed on the same gypsum face in dissolution and precipitation imaging tests by Bosbach et al. (1994) and Hall et al. (1996). It is also interesting to note the layering of three crystallites that have nucleated on the [010] surface at about a 65° angle to the predominant axis of growth, with a fourth crystallite nucleated on the very top with an orientation in line with the parent crystal (Figure 4-21, point B). The precipitated needles were not populated with any large-sized [010] twinned crystals that form "x"-shaped solids. They may have been shorn off, or overgrown.

Crystal growth appears continuous and rapid on the [-111] and [011] faces. The crystallites on the [010] face suggest a polynuclear growth mechanism. Growth along the [120] face seems to be polynuclear as well, based on the stages evident on Figure 4-21, on the [120] edges of the crystal.

The fractal nature of these crystals is interesting, as Figure 4-23, which images the fines from the 10th recycle (magnified 1400x), is similar to the image of the larger solid product, Figure 4-21 (magnified 170x).

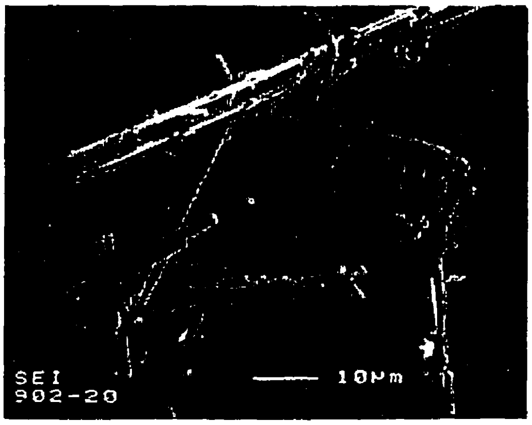

Figure 4-23: SEM Image of 10th recycle gypsum precipitate fines, semi-batch controlled neutralization from pH 0.5-1 with 50 g/l slaked lime and 50 g/l seed.

Very little twinning or clusters are evident in the precipitates by the 10th recycle. It is postulated that the rapid dissolution of the calcium oxide particles at the very low pH does not leave adequate time for epitaxial growth of gypsum on the calcium oxide surface, reducing the probability of agglomerate production. The infrequent evidence of twinned gypsum crystals may result from the non-interfering nature of the bisulphate ion on the growing crystal surfaces. The correct incorporation of the lattice ions or compounds onto the crystal surface is unimpeded, and/or crystallites that nucleate incorrectly on the surface are sheared off or overgrown.

The relative reactivity of the faces appears to decrease from [-111]≈[011]>>[120]>[010].

4-4-3-2 Calcium carbonate slurry neutralizing reagent

4-4-3-2-1 Change in pH with time

The change in pH with time (Figure 4-24) is straightforward and linear. Again, it is assumed that the change in pH is not only affected by the neutralization reaction, but the buffering effect of the bisulphate ($HSO_4^- \leftrightarrow H^+ + SO_4^{2-}$, pK_a= 1.92 (25°C)) and bicarbonate dissociation as well ($HCO_3^- \leftrightarrow H^+ + CO_3^{2-}$, pK_a=10.25 (25°C)).

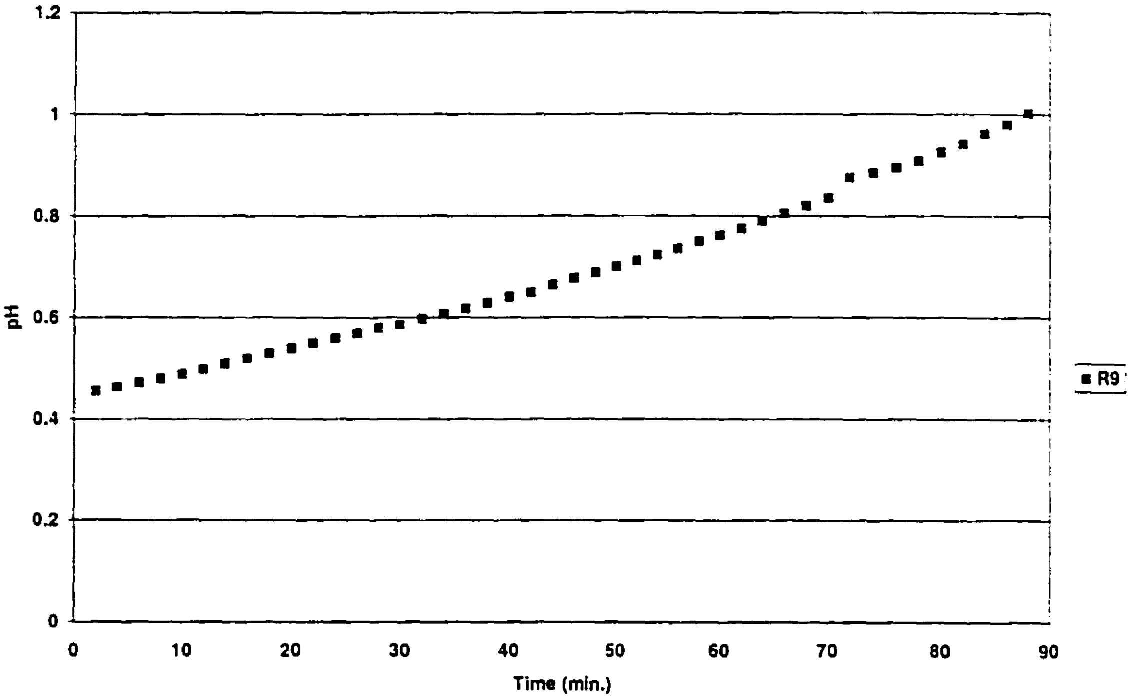

Figure 4-24: Change in pH with time, semi-batch controlled neutralization from pH 0.5-1 with 86 g/l calcium carbonate slurry and 50 g/l seed, 9th recycle

4-4-3-2-2 Change in solids density with recycle run

The solids density increased from an average of 34% to the fourth neutralization recycle, followed by an increase to an average of 53% to the tenth recycle (Figure 4-25). The mass of precipitate produced by these recycles averaged 36.8±7.7 g/l. The error in solids density measurement averaged 3.2±2.8%.

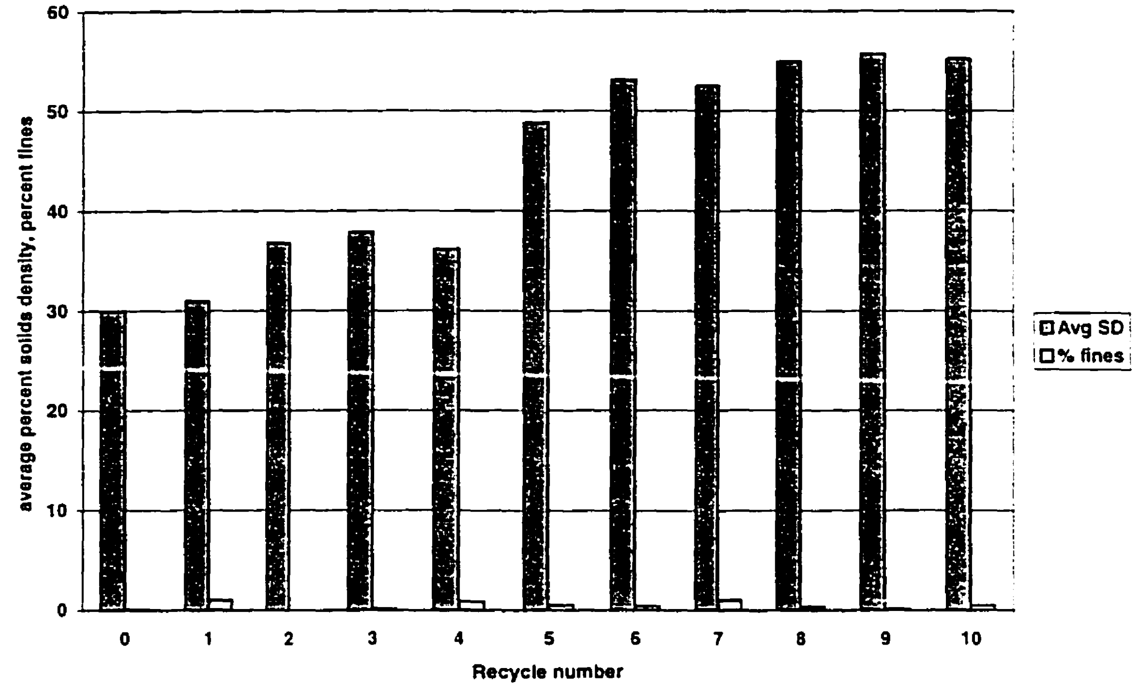

Figure 4-25: Change in solids density and percent fines with recycle run, semi-batch controlled neutralization from pH 0.5-1 with 86 g/l $CaCO_3$ slurry, 50 g/l seed.

4-4-3-2-3 Change in gypsum particle size

The well-grown solids produced by the tenth recycle are approximately 400 μm long, 100 μm wide, and about 10 μm deep (Figure 4-26). There is a smaller population of crystallites (10-25 μm long) that are visible on parent crystal surfaces; some of these appear independently as well (Figure 4-27, pt. A). An average of 0.52±0.33% of the precipitated solids were fines.

4-4-3-2-4 Gypsum crystal morphology

The bladed, long gypsum needles produced by this mode of neutralization were again unique in morphology. The larger well-grown crystals were often swallow-tailed, indicating the characteristic twinning of gypsum along the [120] axis (Figure 4-28, 4-29). There were also a significant number of twinned crystals with an "x" shape that had twinned on the [010] plane.

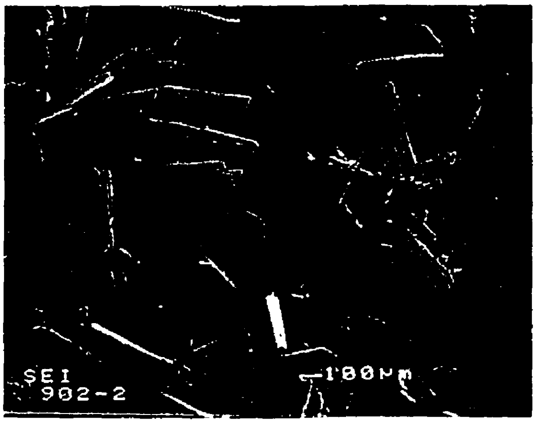

Figure 4-26: SEM Image of 10th recycle gypsum precipitate, semi-batch controlled neutralization from pH 0.5-1 with 86 g/l calcium carbonate slurry and 50 g/l seed.

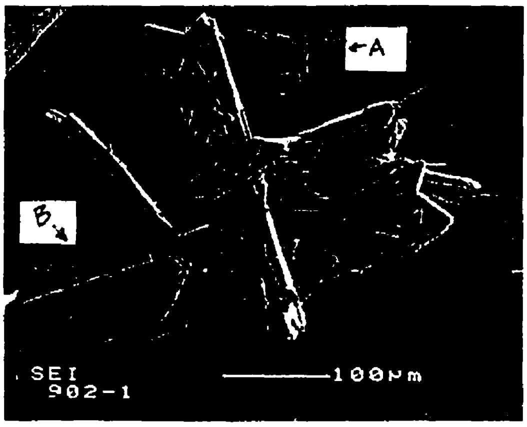

Figure 4-27: SEM Image of 10th recycle gypsum precipitate fines, semi-batch, controlled neutralization from pH 0.5-1 with 86 g/l calcium carbonate slurry, 50 g/l seed.

A photomicrograph taken at the third (Figure 4-28) recycle shows evidence of either a slowed [-111] face growth or an accelerated [011] face growth as the arrowhead (pt A) morphology is present. A smaller [-111] face is also visible on some crystals (pt B). The addition of the carbonate ion may have favoured growth on the [120] face as well, as these crystals are wider than the ones produced by the high acid lime neutralization.

Twining on the [010] face is also visible on Figure 4-27, pt. B, however, the more advanced recycled products do not appear to have many large "x"-shaped crystallites. They may be subject to mechanical attrition in the reactor.

The relative face reactivity seems to decrease from [-111]≈[011]>>[120]>[010].

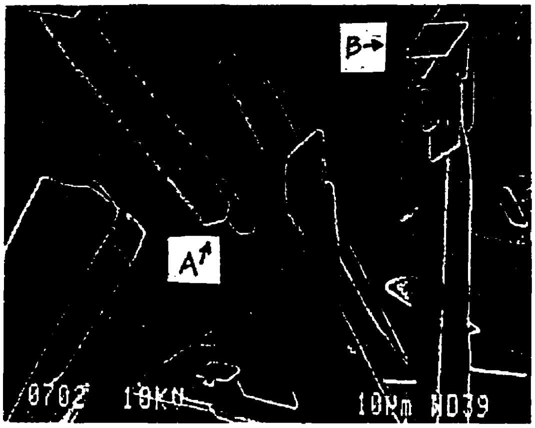

Figure 4-28: SEM Image of 3rd recycle gypsum precipitate, semi-batch controlled neutralization from pH 0.5-1 with 86 g/l calcium carbonate slurry and 50 g/l seed.

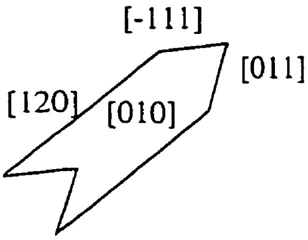

Figure 4-29: Schematic of acicular gypsum crystal faces grown at low pH with calcium carbonate

4-5 CONCLUSIONS

Controlled, seeded neutralization in different sulphuric acid pH ranges produced product gypsum crystals of different morphologies. The use of calcium oxide or calcium carbonate as a neutralizing agent also affected the precipitated gypsum crystal morphology. High acid neutralizations (pH 0.5-1) favoured the production of gypsum needles; calcium carbonate use in this neutralization range favoured wider needle growth and frequent [120] twinning. Long needles with arrowhead tips were the observed products of lime neutralization in strong acid solutions. Low acid neutralization (pH 1-7) with calcium oxide produced bladed gypsum shapes, whereas calcium carbonate neutralized systems produced thicker, sometimes twinned gypsum blades. Many clusters were observed amongst the low pH neutralization products.

All four tests resulted in the production of increased sized gypsum crystals by the tenth recycle. From similar seed used in the first neutralization cycle, crystals grew from 100-400% of their initial size by the tenth discrete recycle. A small percent of the solids neutralizations. Although fines are attributed to decreased product solids density, crystal dispersion is a normal crystallization process phenomenon, and a small amount of fines contribute to the increase of the number of nucleation sites available for crystal growth.

The gypsum precipitate solids density change through the four different neutralization conditions varied. Recycling gypsum solids through lime neutralizations from pH 1-7, the system of interest as it is closest to the zinc plant wastewater neutralization system, resulted in an increase to 45% precipitate solids density. The solids density of the recycled precipitate through pH 0.5-1 with calcium oxide increased slightly with increasing recycle number to 35%. The solids density of the recycled precipitate through pH 0.5-1 with calcium carbonate increased to 55% with increasing recycle number. The use of calcium carbonate to neutralize sulphuric acid solutions through pH 1-7 is not efficient; the solid density of the recycled precipitate decreased with increasing recycle number, and unreacted calcium carbonate was present at the end of each neutralization cycle.

The promising results from the pH 1-7 neutralization tests with calcium oxide were applied to the development and testing of a staged, continuous process with solids recycle that neutralized pure acid, acidic zinc sulphate, and finally simulated zinc plant wastewater.

5 CONTINUOUS NEUTRALIZATION PROCESS DEVELOPMENT AND TESTING

5-0 INTRODUCTION

The positive solids density results of the semi-batch tests of the last chapter provided the incentive to build and test a staged, continuous neutralization process with solids recycle. Previous publications have discussed the effect of recycling solids on both improving the solids density of precipitated gypsum from wastewater neutralization (Lockley et al., 1993) and reducing scaling (Standiford, 1961). To date, no publications exist that report the results of a combined staged neutralization process with solids recycle.

This chapter is divided into three sections. The first investigates the effect of seed loading and neutralization agent concentration on precipitated gypsum solids density in order to elucidate the optimum values for the continuous process. The second reviews the effect of the number of neutralization stages on precipitated gypsum solids density in order to determine the optimum number of stages to maintain low supersaturation for the continuous process. With this information, a continuous wastewater neutralization process was designed and tested. The third section reviews and compares the novel, optimized multi-staged and seeded continuous process results with the results of single-staged with and without seed and solids recycle, as well as multi-staged neutralization without seed and with solids recycle continuous processes.

5-1 ANALYSIS OF EFFECT OF SEED LOADING AND NEUTRALIZATION AGENT CONCENTRATION ON PRECIPITATE SOLIDS DENSITY

5-1-1 Objective

The goal of these experiments was to determine the calcium oxide concentration and minimum gypsum seed loading of a wastewater neutralization process to ensure that the rate of surface growth on gypsum seed is faster than the rate of homogeneous nucleation and gypsum fines production. A concentrated neutralization solution is desirable, as it would minimize the amount of water added to the process. However, a concentrated reagent may increase reactor supersaturation past the critical value for primary nucleation, producing many fines that would reduce the solids density of the product. The additional water of a dilute reagent lowers the supersaturation by diluting the reactor contents, but is undesirable as it increases the size and cost of the process equipment. As the continuous process will operate above pH 1, calcium carbonate will not be used as a neutralizing agent due to its inefficient performance at higher pH neutralizations.

5-1-2 Experimental Plan

A range of seed loading and calcium oxide concentrations were tested to determine the concentration that maximizes precipitate solid density. Slaked lime concentrations of 25, 75, 150 g/l as well as dry calcium oxide were tested for the neutralization of two sulphuric acid solutions from pH 0.5 to 1 and 1 to 7. Seed loadings of 0, 10, 50 and 100 g/l synthetic gypsum seed and 50 g/l (50R) recycled gypsum seeding were tested for all of the above conditions. Gypsum produced by the semi-batch recycle tests of the same pH range with its particular morphology was used as recycled seed. As different morphologies developed during gypsum precipitation in the different pH ranges, and a continuous process will run with recycled solids with a characteristic morphology, these were included in the test to better represent the continuous test results.

Settling velocity information was collected to determine the effect of solids loading and seed type on settling velocity (Appendix E).

5-1-3 Experimental Method

Solution preparation and both pH and mass measurements were taken as outlined in Chapter 4. All tests were performed at room temperature. 250 ml Erlenmeyer flasks were used to contain 100 ml of acid solution or acidic slurry. The solutions were manually agitated during neutralization; magnetic stirrers were not used due to the possibility of a magnetic effect on primary nucleation (Appendix D), and to avoid the crushing of solids under the stirrer. Sources of error for these tests include solution preparation, solids density measurement, and pH readings

5-1-4 Results and Discussion

5-1-4-1 Results Quantification

Three solids density samples were taken at the end of each neutralization run as described in Section 4-3-5-1. SEM images were taken of the gold-platinum coated samples, again with the JSM 840 scanning electron microscope.

5-1-4-2 Effect of slaked lime flowrate and seed loading on precipitate solids density

A low neutralization rate was required to maintain low system supersaturation when testing high neutralization agent concentrations. The highest manageable slaked lime concentration (150 g/l) was used to test two low slaked lime flowrates for the two different pH neutralization ranges. After comparing slaked lime flowrates of 0.1 ml/min for low pH neutralization and 0.5 ml/min with high pH neutralization with a 1 ml/min flowrate, the faster flowrate was chosen to represent a low supersaturation neutralization base case. The results indicated that if 10 g/l of seed was used, the precipitate solids density was affected by the slaked lime flowrate, but for higher seed concentrations, the effect was not as evident. Predictably, the lower seed loading tests produced precipitate with a lower solids density than the higher seed loading tests.

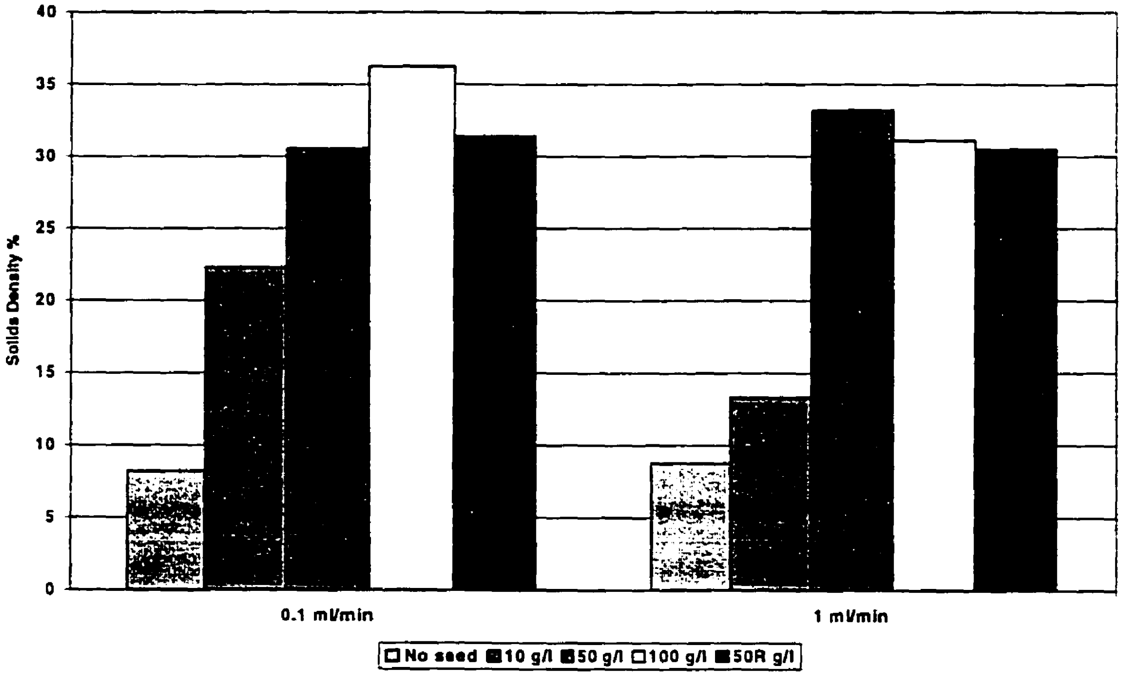

Figure 5-1: The effect of different neutralization flowrates and seed concentration/solids content on precipitated gypsum solids density, 150 g/l slaked lime, pH 0.5-1, 100mL test.

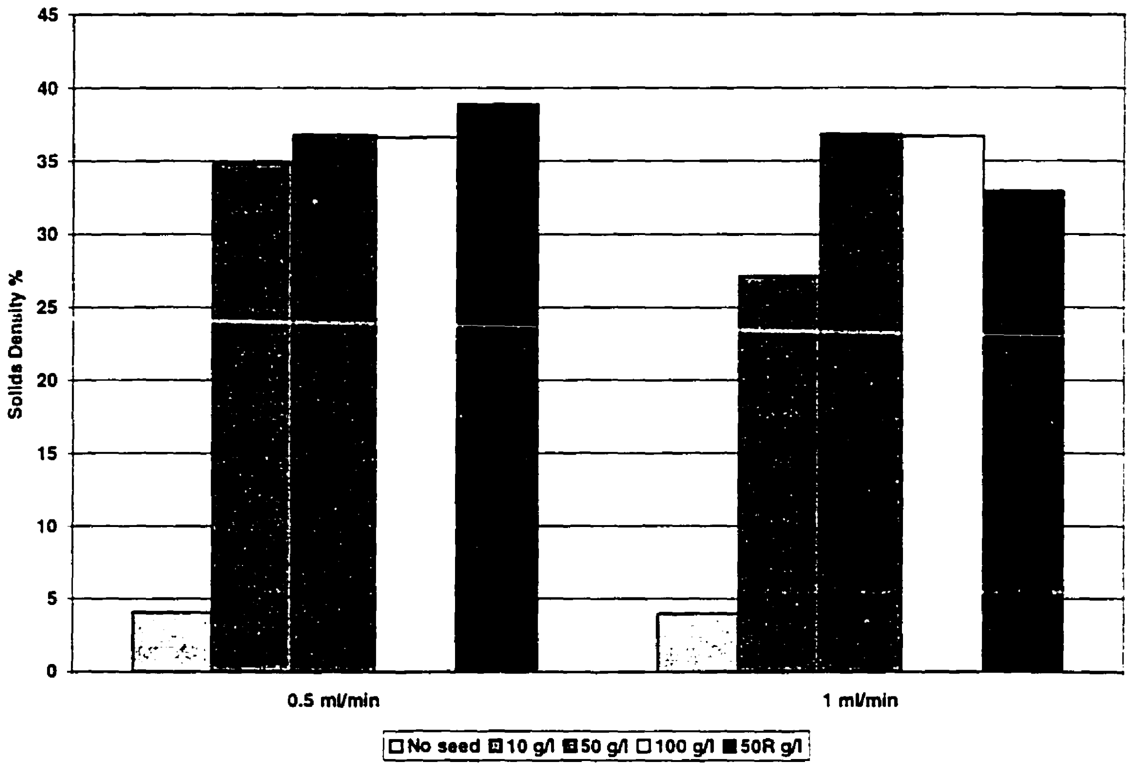

Figure 5-2: The effect of different neutralization flowrates and seed / solids content on precipitated gypsum solids density, 150 g/l slaked lime, pH 1-7, 100 mL solutions.

SEM images (Figures 5-3, 5-4 and 5-5) of the precipitates produced by neutralizing 0, 10 and 50R g/l seed in 0.5 ml/min 150 g/l slaked lime from pH 1-7 show interesting morphological features. The clusters (Figure 5-3) precipitated from solution with no seed are characteristic of gypsum produced on foreign nuclei (Appendix C). Figure 5-4 shows the mix of fines and larger, irregular solids produced with 10 g/l seed. The more uniform solids produced with 50 g/l recycled seed (Figure 5-5) are indicative of a seed growth rate that is larger than the rate of fines production, due to an adequate seed surface area for continuous crystal growth.

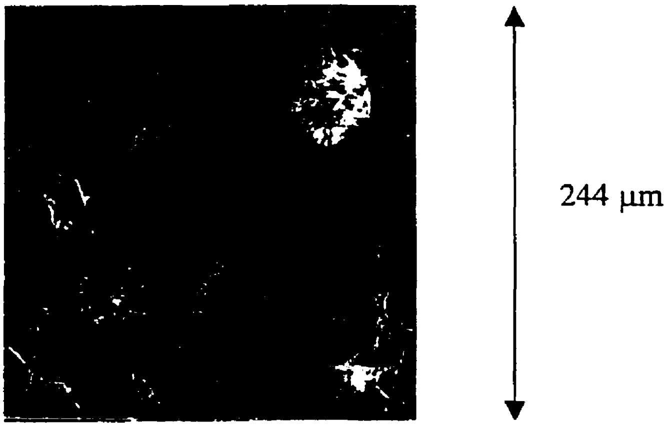

Figure 5-3: SEM image of gypsum precipitate produced by pH 1-7 neutralization with 0.5 ml/min of 150 g/l slaked lime, no seed.

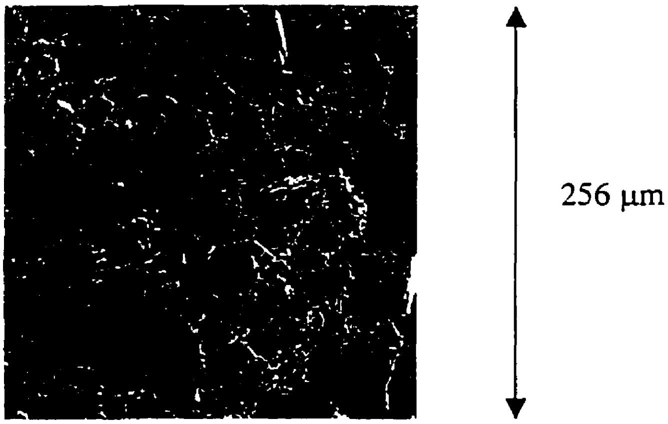

Figure 5-4: SEM image of gypsum precipitate produced by pH 1-7 neutralization with 0.5 ml/min of 150 g/l slaked lime, 10 g/l seed.

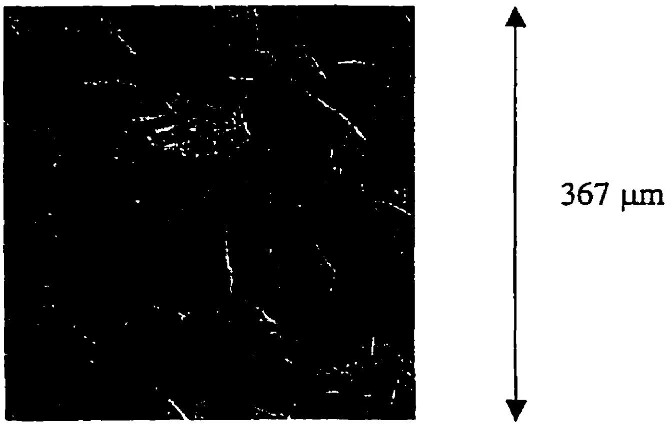

Figure 5-5: SEM image of gypsum precipitate produced by pH 1-7 neutralization with 0.5 ml/min of 150 g/l slaked lime, 50 g/l recycled seed.

5-1-4-3 Effect of slaked lime concentration and seed loading on precipitate solids density

Figures 5-6 and 5-7 present the solids density of the precipitated gypsum with different slaked lime concentrations for the two pH range neutralizations at 1ml/min flow. The error in solids density measurement was below 2.5% for all but two measurements.

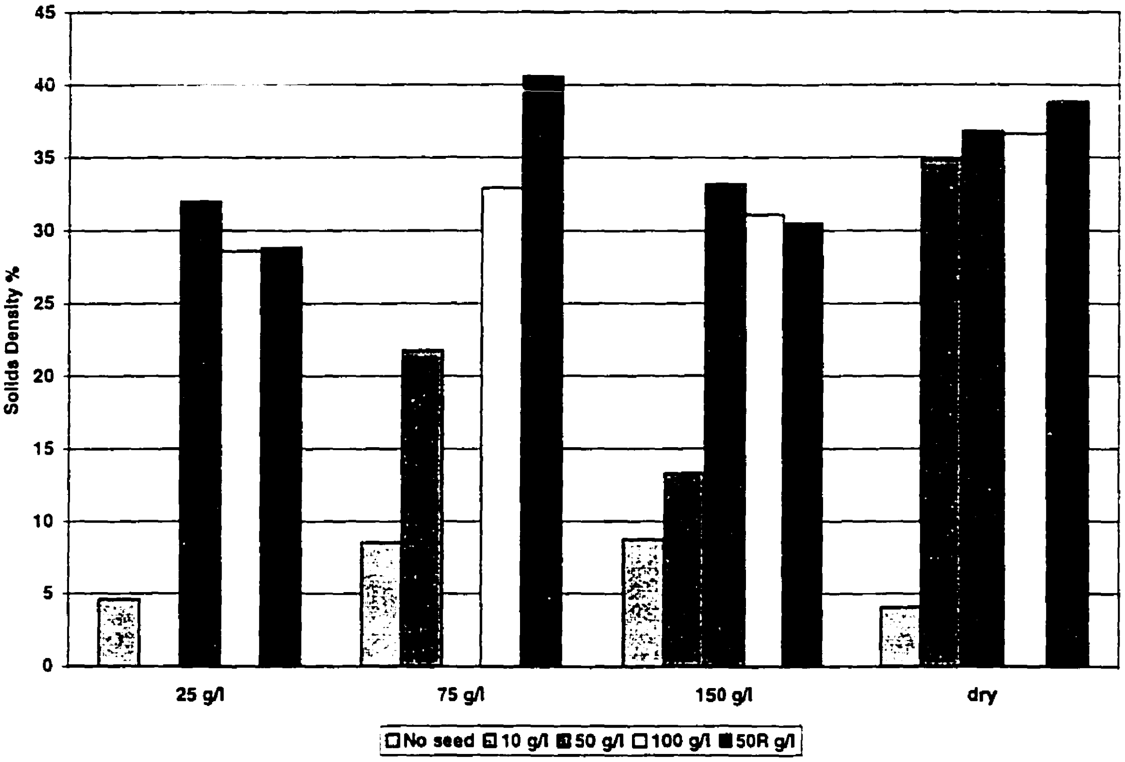

Figure 5-6: Effect of slaked lime concentration and seed loading on precipitate solids density, pH 0.5-1, 1ml/min slaked lime flow, 100 mL solutions.

As predicted by theory, neutralized solutions with a higher seed loading produced precipitate with a higher solids density. At a slaked lime flow of 1 ml/min, the slaked lime concentration did not have a great effect on the precipitate solids density if the seed loading was 50 g/l or higher. It can be concluded that in all neutralization agent concentration cases, solutions seeded with 10 g/l or less gypsum produce precipitate with a lower solids density than solutions with 50 or 100 g/l seed. Except for the two pH 1-7 tests with dry neutralizing agents, the difference between the final solids density of a 50 g/l or 100 g/l slurry is close to or less than the first standard deviation of the results.

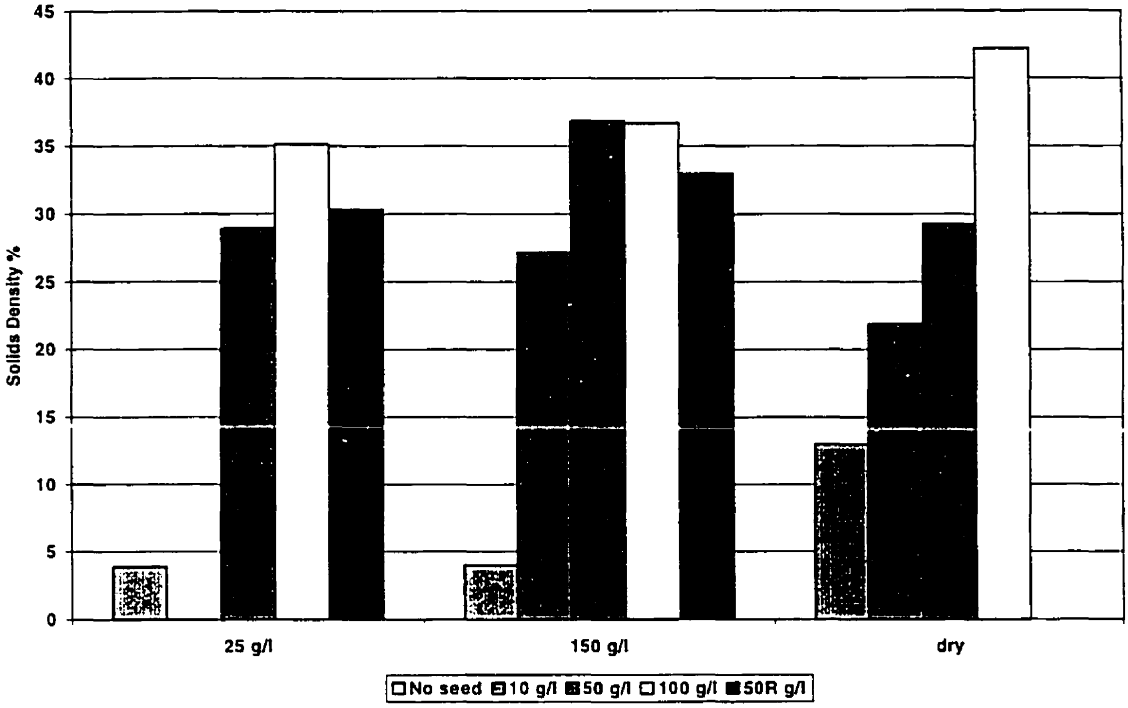

Figure 5-7: Effect of slaked lime concentration and seed loading on precipitate solids density, pH 0.5-1, pH 1-7, 1ml/min slaked lime flow, 100 mL tests.

Although the dry neutralizing agent solids density results were impressive, the use of dry neutralization agents produced many clusters, and not many well-grown crystals as the undissolved calcium oxide solids can act as foreign nuclei (Appendix H). Even in the presence of seed, continuous seed growth is not guaranteed, as depicted in Figure 5-8. Dry lime is also undesirable, as it is difficult to pump and handle.

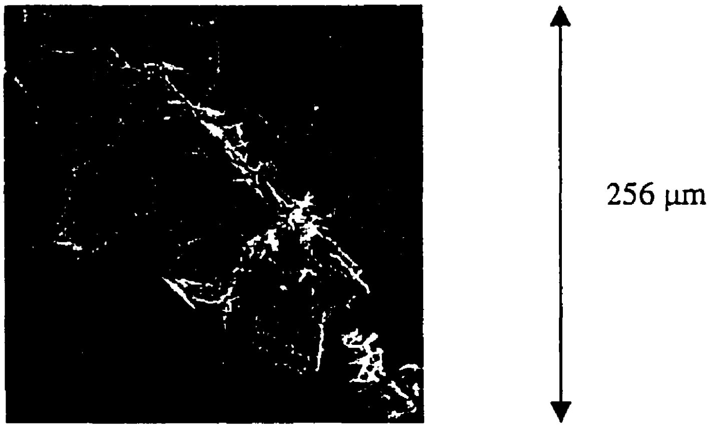

Figure 5-8: SEM image of gypsum precipitate produced by neutralization through pH 0.5-1, 10 g/l seed loading, dry CaO neutralizing agent.

5-1-5 Conclusions

The neutralization case of interest, neutralization through pH 1-7 with slaked lime, behaves as theory predicts. The highest workable slaked lime concentration (150 g/l) generated a high solids density product in when used in conjunction with an adequate seed loading at a 1 ml/min slaked lime flowrate to 100ml of acid solution. The precipitated solids density produced with 50 g/l recycled or fresh seed loading was close to that produced by 100 g/l seed loading; as it is easier to handle a lower solids content slurry, 50 g/l was chosen as the solids content for further testing. The most concentrated slaked lime slurry (150 g/l) does not decrease product solids density if delivered at low enough flowrates.

5-2 THE EFFECT OF NEUTRALIZATION STAGES ON PRECIPITATE SOLIDS DENSITY

5-2-1 Objective

With the process conditions of 50 g/l gypsum seed loading and the use of 150 g/l slaked lime as a neutralizing agent, the precipitate solids density produced by the semi-batch neutralization of seeded, acidic solutions from pH 1 to 7 in one, two, and three equal stages, and a controlled neutralization agent flowrate (1 ml/min) were compared. The results were compared to determine the minimum number of stages for the continuous circuit that could achieve a solids density comparable to that produced with a slow neutralization rate of a semi-batch process.

The neutralization of seeded acidic solutions with 268 g/l calcium carbonate slurry (an equivalent calcium concentration and neutralizing power to 150 g/l slaked lime) from pH 1-5, as well as the neutralization from pH 0.5-1 with either slaked lime (150 g/l) or calcium carbonate slurry (268 g/l) were also tested for interest.

5-2-3 Experimental method

All tests were performed at room temperature. A 250mL Erlenmeyer flask was filled with 100ml of 10 g/l (pH 1) or 25 g/l (pH 0.5) sulphuric acid solution slurried with 50 g/l gypsum seed. For a single stage test, a calculated volume of neutralizing agent was mixed rapidly into the solution, which was agitated without a magnetic stirrer by manually swirling the flask. Agitation continued until a steady pH was reached. For the two and three stage tests, one-half or one-third of the one-stage slaked lime volume was mixed into the acid solution; the next dose(s) of neutralization agent was/were added after the pH reading stabilized. A neutralization run with a 1ml/min neutralization agent addition rate was also performed for each case to represent the best case of a low supersaturation test. The solids density values were obtained as outlined in the previous chapter.

In order to determine the volume of slaked lime delivered to a one, two, or three-stage test, the neutralizing power of the neutralizing agent had to be resolved. This neutralizing power was calculated in two ways. First, an empirical method of determining the neutralizing power of the neutralizing agent in sulphuric acid solutions was used. A 1ml aliquot of 150 g/l lime measured by the Eppendorf micropipette was injected into 10 and 25 g sulphuric acid/l solutions, and the pH change noted. This change in pH was used to determine the volume of neutralization agent required to complete the 1, 2 and 3 stage neutralizations. Secondly, 1 ml aliquots of base were injected into known volumes of HCl solutions. The change in pH was noted if the dissolution of the lime was complete, and the moles of OH- molecules delivered with each ml was calculated. These values were used to determine a more accurate neutralization effectiveness. Errors in solutions preparation, pH reading and calculations could contribute to the sources of error for these tests.

5-2-4 Results and discussion

5-2-4-1 Neutralizing power of 1 ml of neutralizing agent

The theoretical and measured moles of neutralizing agent per ml of 150 g/l CaO slurry or 268 g/l $CaCO_3$ slurry are listed in Table 5-1.

These results indicate that the mol of OH^-/ml or CO_3^{2-}/ml delivered by the pipette is on average less than the calculated value that assumes a homogeneous slurry with 100% conversion. This is not surprising, given that a homogeneous slurry is difficult to maintain, and 100% conversion is not guaranteed. The discrepancy between the neutralizing power in sulphuric acid and hydrochloric acid measured with the pH meter can be related to the bisulphate-sulphate equilibrium.

Table 5-1: Moles of neutralizing power as moles (OH^-) per ml of slurry:

Neutralizing agent	Calculated (mol/ml)	Measured in H_2SO4 solution (mol/ml)	Measured in HCl solution (mol/ml)
150 g/l CaO	0.0054	0.0015 (pH 0.5-1) 0.0022 (pH 1-7)	0.0034
268 g/l $CaCO_3$	0.0054	0.0019 (pH 0.5-1) 0.0019 (pH 1-5)	0.0039

5-2-4-2 Effect of staged neutralization on solids density

The major effect of staging on the neutralization process is the change in the maximum supersaturation in a reaction vessel. The calculated maximum supersaturations (Equation 5-1) for each neutralization case were calculated with equation 2-1 and are presented in Table 5-2. These values were calculated by using the hydrochloric acid dissolution tests to determine the calcium concentration released with each ml of slaked neutralization agent, the volume of neutralization agent added, the total sulphate concentration, and the gypsum mean activity coefficient which was calculated with the program described in Chapter 2. The equilibrium calcium concentration and activity of water were also taken from the program results. The thermodynamic solubility product constant that represents gypsum activity at 25°C ($2.5\text{x}10^{-5}$) was used.

$$S = \frac{\left(\gamma_{\pm}\left(Ca^{2+}\right)^{2}\left(SO_4^{2-}\right)^{2}\right)\left(\alpha_w^{2}\right)}{K_{sp}} \qquad (5-1)$$

Table 5-2: Maximum supersaturation at the start of the staged test runs.

Test run	pH 0.5 150 g/l CaO	pH 0.5 268 g/l $CaCO_3$	pH 1 150 g/l CaO	pH 1 268 g/l $CaCO_3$
1 ml/min	1.1	1.1	1.8	1.5
1 stage	8.6	6.9	6.1	8.5
2 stages	5.0	4.8	1.8	2.1*
3 stages	3.6	2.7	1.3	3.0*

* These values are reversed due to higher pH in stage 2. Results reflect the reversion.

These values are based on the measured acid concentrations at the beginning of the test, and the calcium added with the first added volume of neutralization agent. They assume that the solutions are saturated with gypsum, and that the concentration of calcium in the neutralization agent is represented by the value averaged from the hydrochloric acid dissolution tests. The first volume addition of neutralization agent was assumed to represent the highest supersaturation of the test, as further additions of calcium are constant while the total volume of the solution increases. The sulphate concentration is obtained from the sulphuric acid speciation calculations (Appendix A).

From these graphs and the theory presented in Chapter 3, it is expected that the highest precipitate solids density will be obtained from the tests with the lowest supersaturation, and the highest supersaturation tests will produce precipitate with the lowest solids density. The precipitate solids density produced by the tests are presented in Figure 5-9.

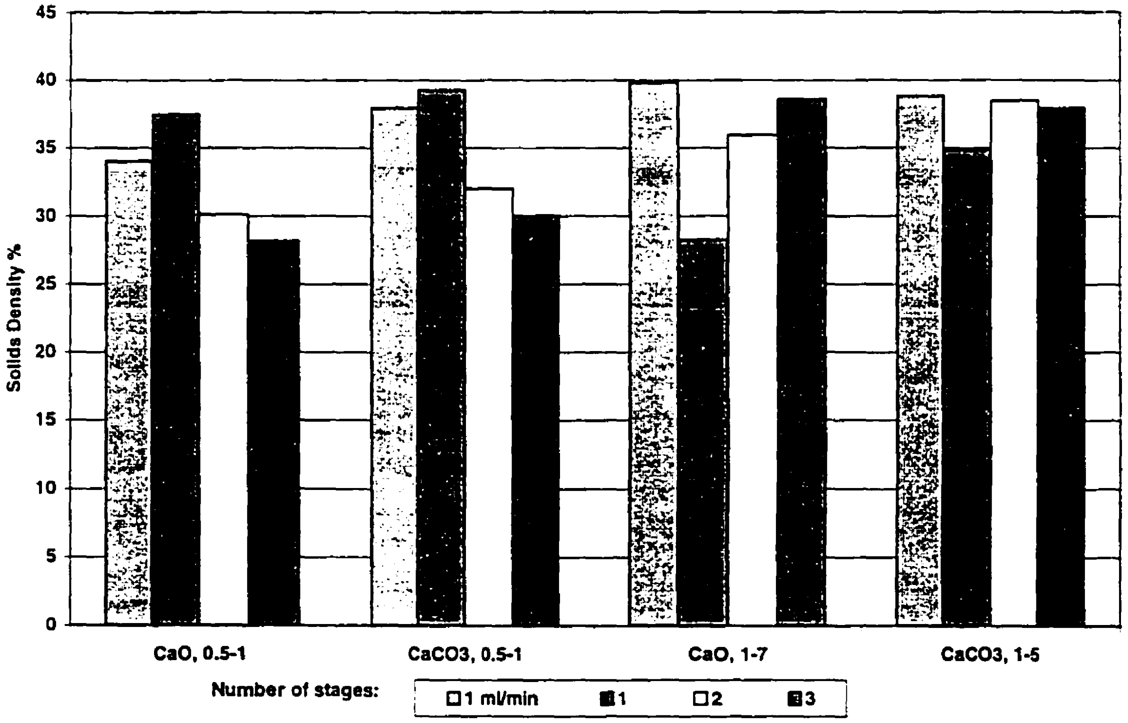

Figure 5-9: Effect of number of neutralization stages on the solids density of gypsum precipitate for pH 0.5-1 and 1-7 neutralizations with 150 g/l slaked lime, and pH 0.5-1 and 1-5 with 268 g/l calcium carbonate, 100mL solutions.

From these tests, it was concluded that the most effective neutralization process from pH 1-7 was the staged neutralization with slaked calcium oxide. It appears that for this case, neutralization in three stages produces a product with similar solids density as the slow, controlled (1 ml/min) neutralization case. The calcium carbonate test from pH 1 to 5 showed similar results consistent with crystallization theory. The low pH neutralization results indicate the reverse trend; an increase in neutralization stages resulted in a decrease in precipitate solids density. The results are not discussed or investigated further here as they do not relate to the main objective of this work.

SEM images of the products produced by controlled (1 ml/min, Figure 5-10), 1 stage (Figure 5-11), and 3 stage (Figure 5-12) pH 1-7 neutralization processes with 150 g/l slaked lime show differences in crystal quality. The 1-stage products do not have the same sharp edges as the continuous and 3 step solids. This roughening is evidence of the more rapid growth process, which occurs at higher supersaturation that also favours the production of fines, and a corresponding decrease in product solids density.

Figure 5-10: SEM image of gypsum precipitate produced by controlled pH 1-7 neutralization with 1 ml/min of 150 g/l slaked lime, 50 g/l seed.

5-2-5 Conclusion

Three-stage neutralization (pH 1-2-5-7) of a sulphuric acid solution slurried with 50 g/l gypsum seed generated the highest solids density precipitate (38%) with a 150 g/l slaked lime slurry. The lower supersaturations of the three-stage process are presumed responsible for this solids density result. From these results, a continuous neutralization process was constructed and tested.

Figure 5-11: SEM image of gypsum precipitate produced by 1-stage pH 1-7 neutralization with 150 g/l slaked lime, 50 g/l seed.

Figure 5-12: SEM image of gypsum precipitate produced by 3 stage pH 1-7 neutralization with 150 g/l slaked lime, 50 g/l seed.

5-3 CONTINUOUS NEUTRALIZATION

5-3-1 Objective

This section outlines the building and testing of a staged continuous neutralization process with solids recycle that neutralizes synthetic acidic wastewater. The precipitate quality of this process was compared with other continuous neutralization processes.

5-3-2 Experimental plan

A continuous setup was built to test one of the stages of the proposed seeded, recycled, staged neutralization process. A pure acid solution influent and an acidic zinc sulphate solution were tested with the single stage. The setup was then expanded to two stages to test the proposed process with simulated zinc plant wastewater from pH 1-5. The composition of the simulated wastewater is listed in Table 5-3.

Table 5-3: Composition of simulated zinc plant wastewater

Ion/species	H_2SO_4	Zn^{2+}	Fe^{2+}	Mn^{2+}	Mg^{2+}
g/l	5	1	0.03	0.06	0.09

Control cases were run to compare the steady state solids density of their precipitates with the proposed neutralization process. The other test cases were:

a) 1 stage neutralization (pH 1-5), no seeding, no solids recycle
b) 1 stage neutralization (pH 1-5), seeding, solids recycle
c) 2-stage neutralization (pH 1- 2- 5), no seeding, solids recycle

The individual ion concentrations and solids density in each reactor as a function of time were also measured.

5-3-3 Experimental Setup

The semi-batch setup used in Chapter 4 (Section 4-3-3-3) was modified and expanded to include another neutralization tank and a thickener (Figure 5-13). Only two stages of the proposed three-stage process were built due to equipment constraints.

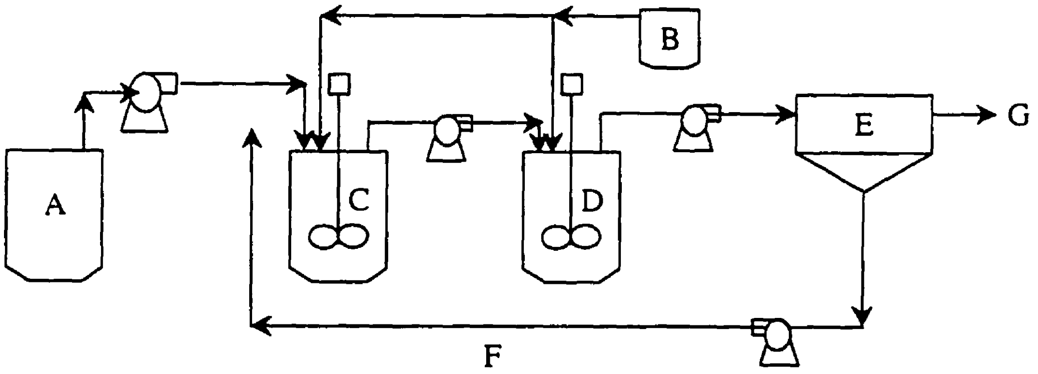

Figure 5-13: Schematic of Continuous Experimental Setup

A: Acidic influent reservoir	E: Thickener, pH 5
B: Agitated slaked lime reservoir	F: Thickener underflow recycle
C: Reactor 1, pH 2	G: Thickener overflow
D: Reactor 2, pH 5	

New process additions from the semi-batch setup include Cole-Parmer peristaltic pumps for transporting process fluids through rubber Masterflex tubing. The flow rate of 150 g/l slaked lime pumped to the first reactor was manually controlled to maintain pH 2 in the first reactor. Manual addition of slaked lime to the second reactor was required due to the slow flowrate required to maintain a pH of 5. The flow of process fluids was set for a minimum reactor residence time of 25 minutes, as 15 minutes was calculated to be the minimum residence time required to provide adequate macromixing in the reactors (Appendix J).

The process flows were manually fine-tuned to maintain approximately 500 ml in the reaction vessels. The solids recycle was calculated to be 25% of the acid flow to the first reactor in order to maintain a reactor solids content of 50 g/l, based on the steady state value of the underflow solids density obtained with the first seeded tests. Test results indicate that a constant reactor solids content was difficult to maintain; the solids content measured at the end of a test varied from 10 g/l for the unseeded tests to 50±10 g/l for the seeded tests. A change in the solids recycle flow was often coupled to a change in the slaked lime flow, as the recycled solution was at a higher pH and some recycled hydroxide solids dissolved in the first reactor. The thickener was suspended to access the underflow for solids recycle. The thickener was manually raked every few minutes to homogenize the settled solids.

5-3-4 Experimental method

Two start-up methods were used to start up seeded and unseeded test runs. Seeded tests with solids recycle began with the reactor(s) that were filled with 500ml of feed acid and 50 g/l synthetic gypsum seed. The process vessels were agitated and slowly neutralized until the continuous pH target steady-stage value was reached. The thickener was filled with the same neutralized slurry as the final reactor. Once all vessels and tubing were full and at the correct pH, the continuous process started up.

Continuous, unseeded tests began with reactors filled with acidic solution feed. The continuous process flows were run with an accelerated slaked lime flows until the target pH(es) were reached; the slaked lime flows were then modified to maintain the target pH in each reactor at steady state operating conditions.

Acid flows varied from 30-40 ml/min during continuous operation. In order to take solids density samples, all flows and agitators were shut down and the solids allowed to settle. Solid samples were removed from the reactors and the thickener. The reactors were agitated for a few minutes before re-starting process flows. The system ran until the solids density values stabilized, steady state was assumed to have been reached at that point.

Aliquots of process solutions from the reactors and thickener were taken at the end of each test for cation concentration analysis.

5-3-5 Result quantification

Samples for solids density measurements were taken from the settled contents of the reactor(s) and the thickener, and analyzed as described in section 4-3-5-1. SEM images of the dried precipitates were obtained as described earlier. EDS analysis was used to determine a qualitative elemental analysis of the solids. X-ray diffraction measurements of the precipitates were taken with a Phillips Power X-Ray Diffraction system, model PW-1710 to identify the precipitate crystal structure and compare relative grain sizes and degrees of crystallinity. An Instrumentation Laboratory aa/ae Spectrophotometer, Model 357 measured cation concentrations of the diluted vessel solutions.

5-3-6 Results and discussion

A discussion of the solids density results for the continuous tests will be followed by a discussion of the simulated wastewater cation concentration results.

5-3-6-1 Solids density results

5-3-6-1-1 Acid and zinc solution tests: single stage, pH 1-2 neutralization, seeded, recycled solids

The first continuous test with 10 g/l pure sulphuric acid solution generated precipitate solids density in the thickener of about 50%, which is higher than that achieved with the semi-batch tests (Figure 5-14). The error bars indicate the first standard deviation in solids density measurement. The solids settled well; a significant fraction of fines was not observed. 5 g/l zinc as zinc sulphate was added to the acidic influent after 110 minutes of continuous run time. The solids density samples taken over the next 180 min. indicated precipitate solids density just under 50%. More continuous tests were then run with the simulated zinc plant wastewater solution.

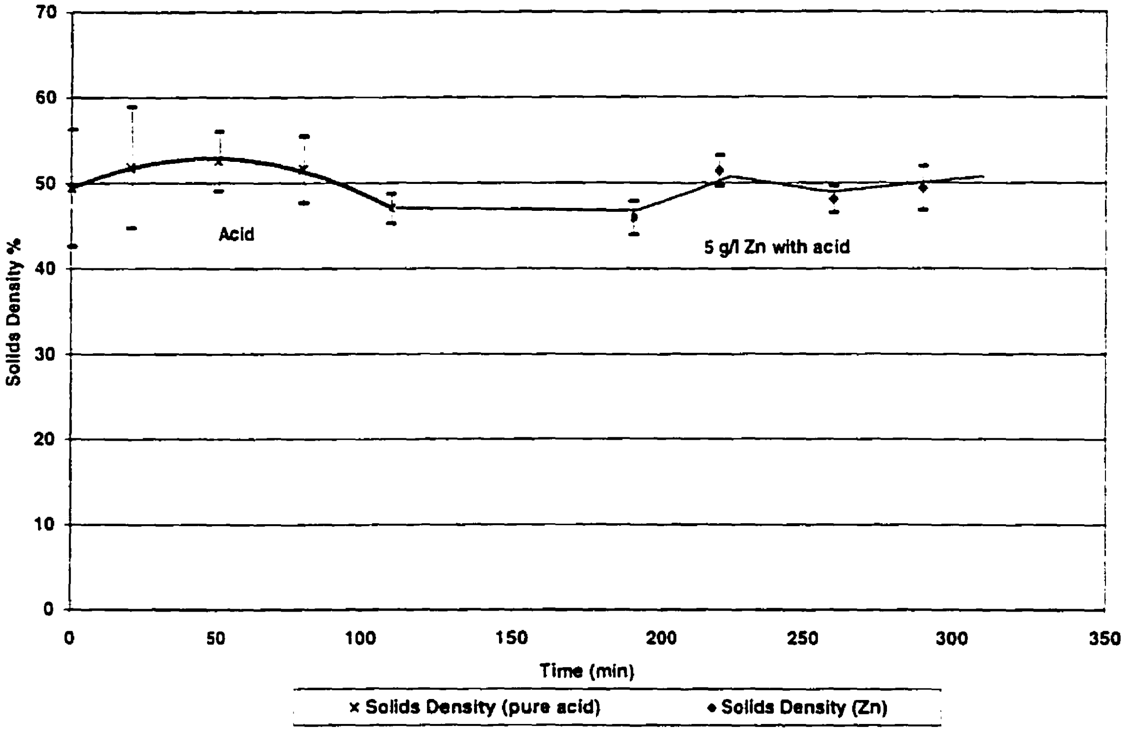

Figure 5-14: Precipitate solids density vs. continuous neutralization process run time, 10 g/l sulphuric acid and acidic 5 g/l zinc sulphate feed solutions, pH 1-2, 150 g/l slaked lime neutralizing agent, 50 g/l seed

5-3-6-1-2 The effect of continuous neutralization process setup on precipitate solids density, with simulated zinc plant influent

The three continuous processes listed in the Experimental Plan, Section 5-3-2, as well as the two-stage, seeded neutralization process were run with simulated zinc plant wastewater until the solids density values from the reactors were considered to be at steady state. Figure 5-15 compares the solids density of the thickener precipitates for the different processes. The solids density measurement error is indicated with the error bars.

The steady-state solids density of the thickener solids produced by both the unseeded, single-stage and the unseeded, two-stage, recycled neutralization tests reached a steady-state value of 10%. These results are far below the values achieved for the seeded and recycled neutralization processes. The single-stage, seeded process with solids recycle produced precipitate in the thickener with a 30% solids density at steady state, and the two-stage, seeded, recycled process produced precipitates with a steady stage solids density value about 50%.

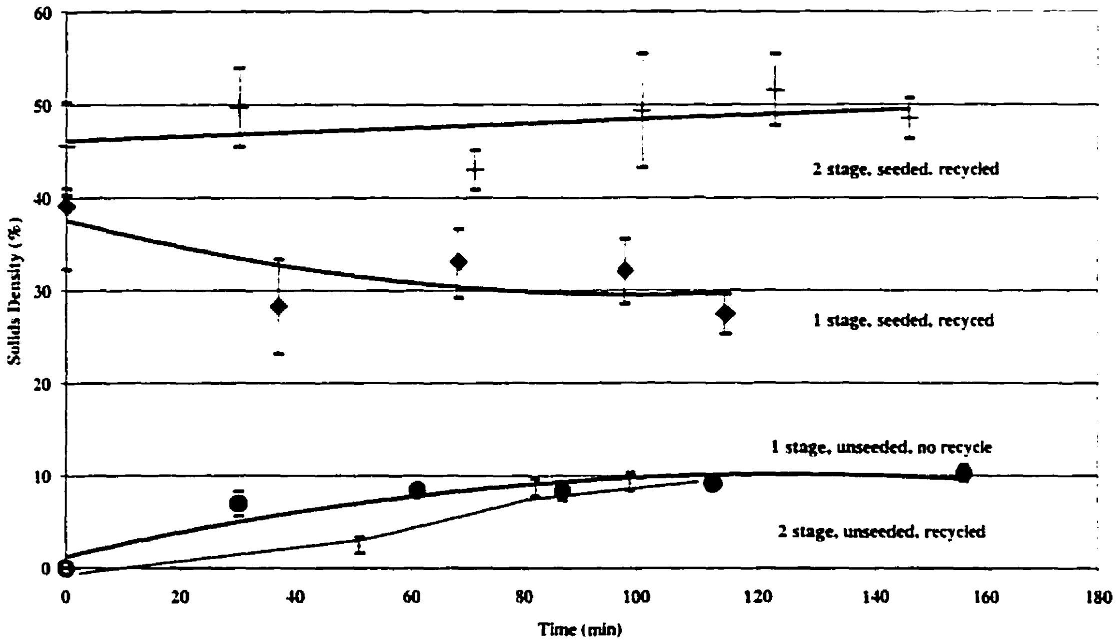

Figure 5-15: The effect of neutralization process staging and seeding on the solids density of the thickener precipitate, pH 1-5, 150 g/l slaked lime neutralizing agent

5-3-6-2 Solids quality results

In order to better understand the solids density results, the quality of the precipitate from each process was examined. SEM images, XRD patterns, and EDS analysis contributed to characterizing the different precipitates.

5-3-6-2-1 Single-stage, pH 1-5, no seed, no solids recycle

The precipitates of this neutralization, which is representative of current industrial practice, are small (~1μm) (Figure 5-16) and beige in colour. The XRD analysis of the dried precipitate indicated gypsum (Figure 5-17).

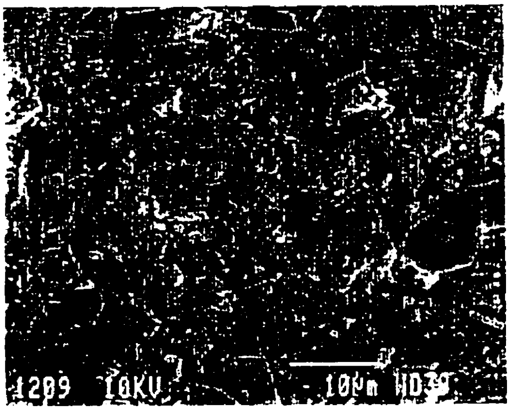

Figure 5-16: SEM image of solids precipitated by single stage, unseeded neutralization with no solids recycle.

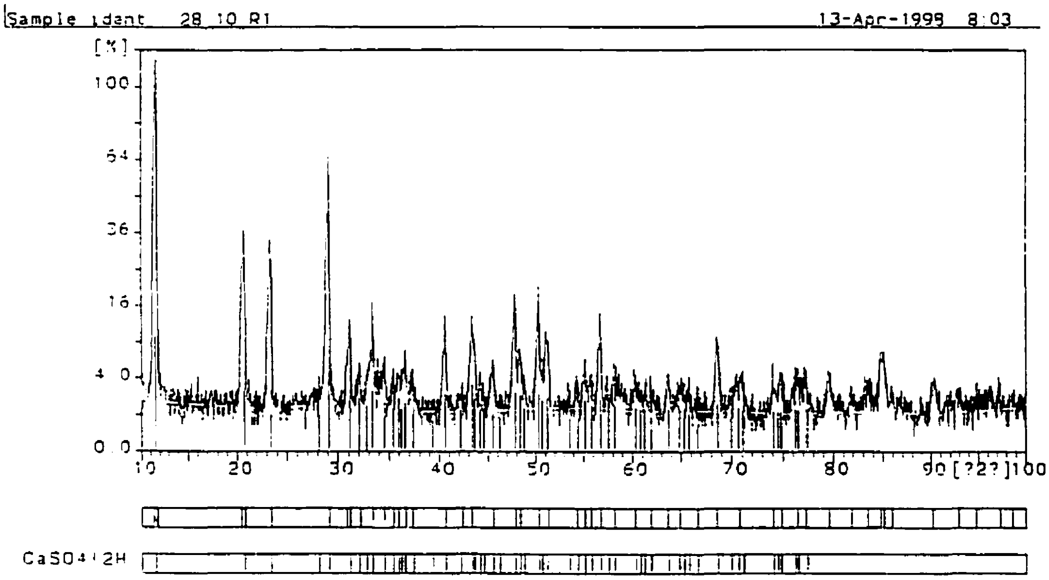

Figure 5-17: XRD results of solids precipitated by single stage, unseeded neutralization with no solids recycle.

5-3-6-2-2 Single-stage, pH 1-5, seeded, solids recycle

As this test was run, the colour of the solids in the first reactor turned from white to beige. The solids in the thickener were also beige in colour. The brown colour is most likely due to the precipitation of ferric hydroxides at pH 5. Amorphous solids can be seen along with the larger gypsum crystals in Figure 5-18. The solids density of the reactor precipitate initially dropped below the solids density of the thickener solids, perhaps as finer metal hydroxides were forming. It is possible that these fines acted as additional nucleation sites when they were recycled through the process, growing in size and presenting a higher solids density with time (Figure 5-19).

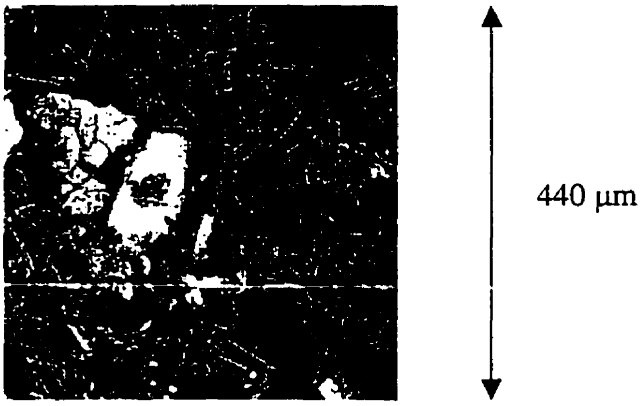

Figure 5-18: SEM image of solids precipitated by single-stage, seeded neutralization with solids recycle.

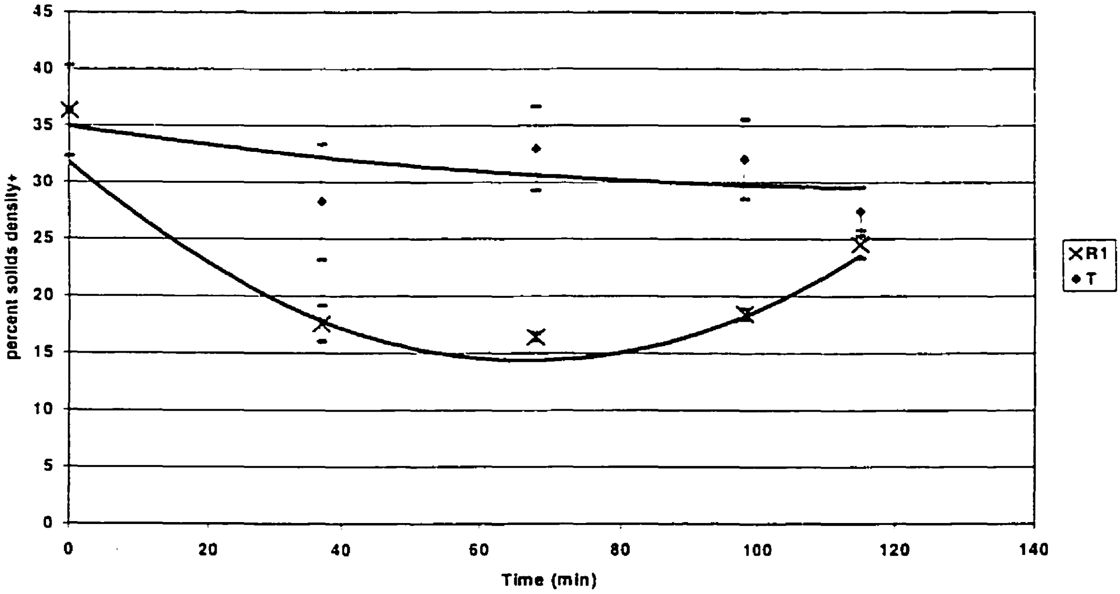

Figure 5-19: Comparison of the solids density of the reactor and thickener precipitates produced by single-stage, seeded neutralization with solids recycle.

EDS analysis over the range of precipitates indicated calcium, iron, manganese, and zinc (Figure 5-20). An EDS analysis of a singular gypsum crystal amongst the amorphous solids (Figure 5-21) showed only calcium and sulphur present; gypsum adsorb or precipitate on a well-grown gypsum crystal at a neutral pH (Appendix K). A further investigation into the effect of impurity cations on gypsum precipitation from solution is presently the subject of the M.Eng. thesis of Niels Verbaan.

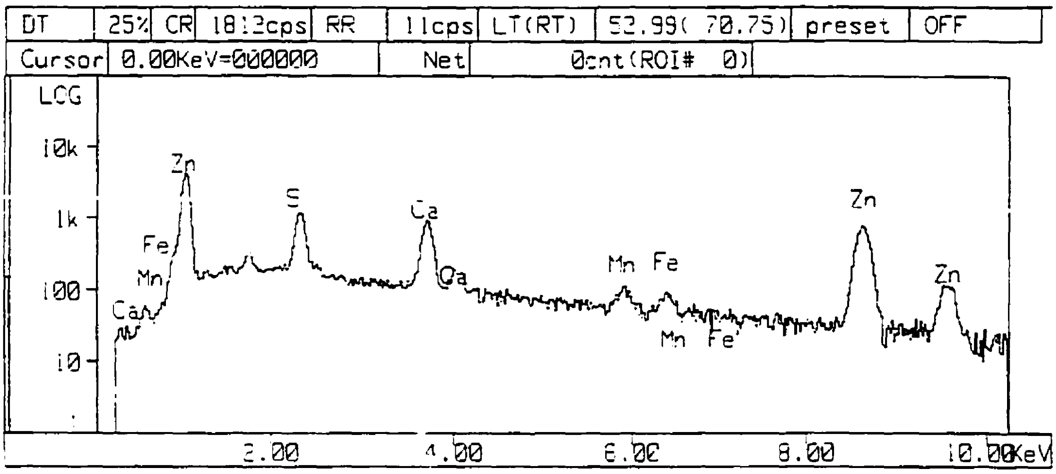

Figure 5-20: EDS analysis of the solids precipitated by single stage, seeded neutralization with solids recycle.

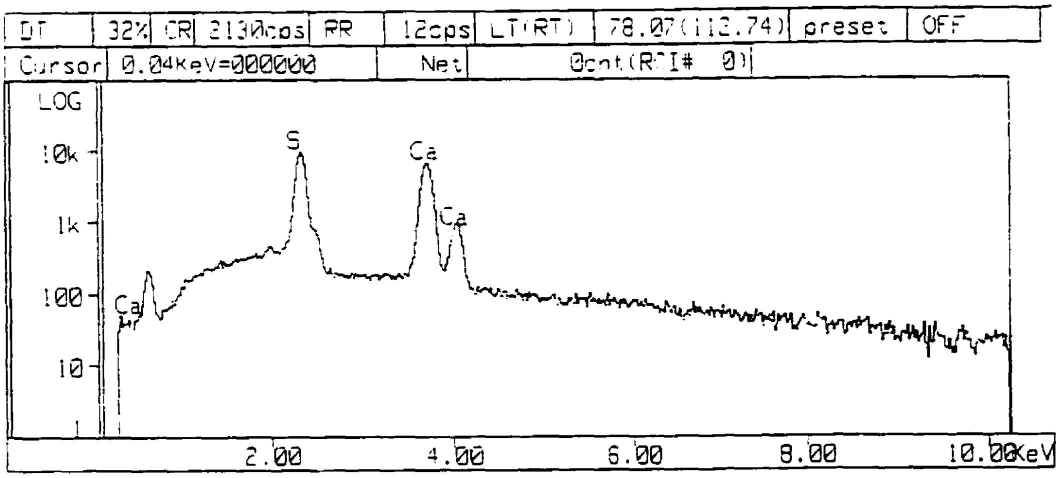

Figure 5-21: EDS analysis of a gypsum crystal precipitated by single stage, seeded neutralization with solids recycle.

5-3-6-2-3 Two-stage, pH 1-2-5, no seed, solids recycle

The solids produced by this test were also brown in colour. The solids present in the thickener were larger, however there was significant size dispersion and the solids were of irregular shape (Figure 5-22). It was presumed that the solids were larger versions of the solids precipitated by the single stage unseeded neutralization process.

Figure 5-22: SEM image of solids precipitated by two stage, unseeded neutralization with solids recycle.

5-3-6-2-4 Two-stage, pH 1-2-5, seeded, solids recycle

The solids in the first reactor of the two-stage solids density test maintained a white colour throughout the test, while the solids in the second reactor and the thickener were beige. The solids in the second reactor turned a darker brown as the test progressed. The solids density of the solids in the second reactor was consistently lower than that of the solids in the first reactor and thickener (Figure 5-23). It is likely that recycled ferric and other hydroxide solids re-dissolve in the low pH conditions of the first reactor, re-precipitating in the second, higher pH reactor. These fines do not grow in size as they are re-dissolved in the first stage and do not act as seed. Their dissolution also released hydroxide ions and consequently reduced the amount of lime required to neutralize the solution. The thickener product solids density may have stayed higher than the solids density of the second reactor precipitate as the fines may have grown slightly larger by Ostwald ripening.

SEM images of the precipitate from the first reactor (Figure 5-24) show clean, large crystals with sharp edges.

The XRD pattern (Figure 5-25) of the same precipitate indicated gypsum, however, the maximum intensity signal was almost twice as great as the single stage, unseeded neutralization product maximum intensity, and the background was almost three times lower. This indicates a larger grain size and a higher precipitate crystallinity compared to the single stage, unseeded with no solids recycle precipitate.

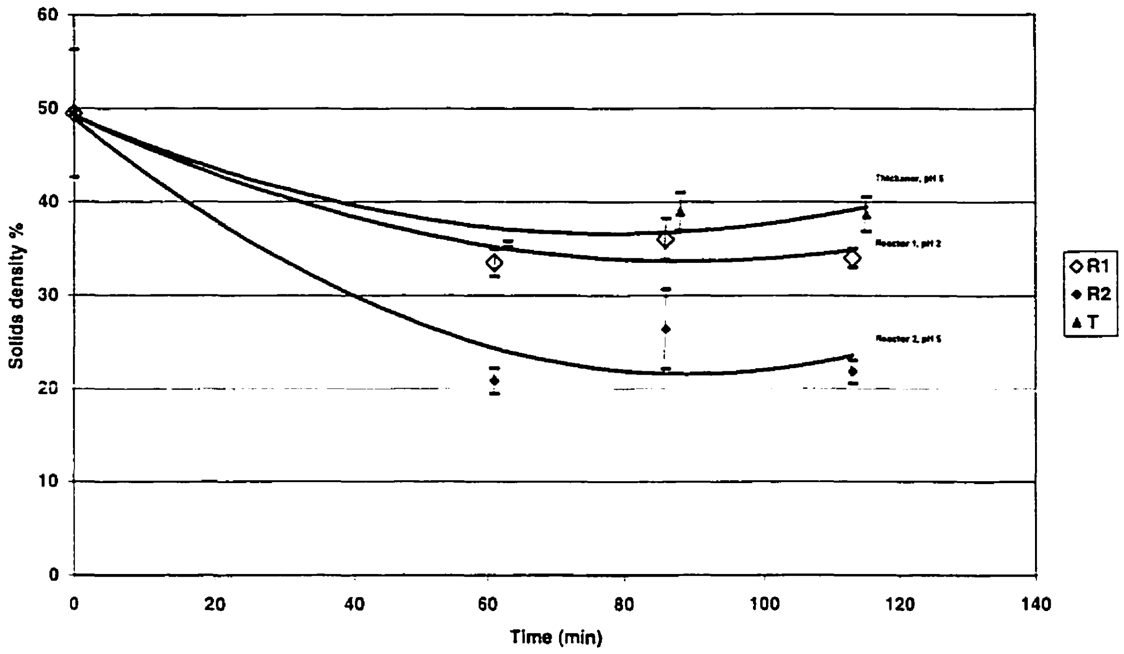

Figure 5-23: Comparison of the solids density of the two reactor and thickener precipitates produced by two-stage, seeded neutralization with solids recycle.

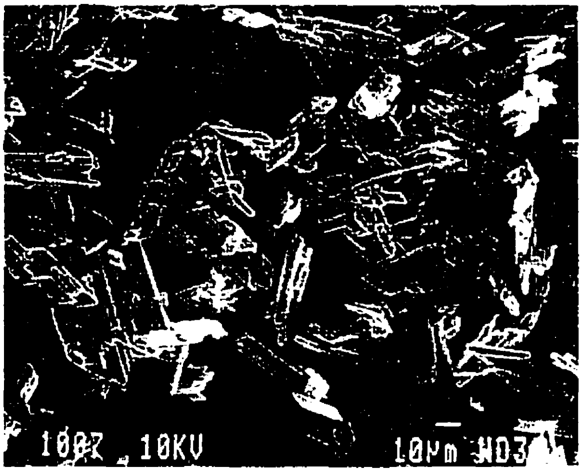

Figure 5-24: SEM image of solids precipitated in the first reactor of the two stage, seeded neutralization with solids recycle process.

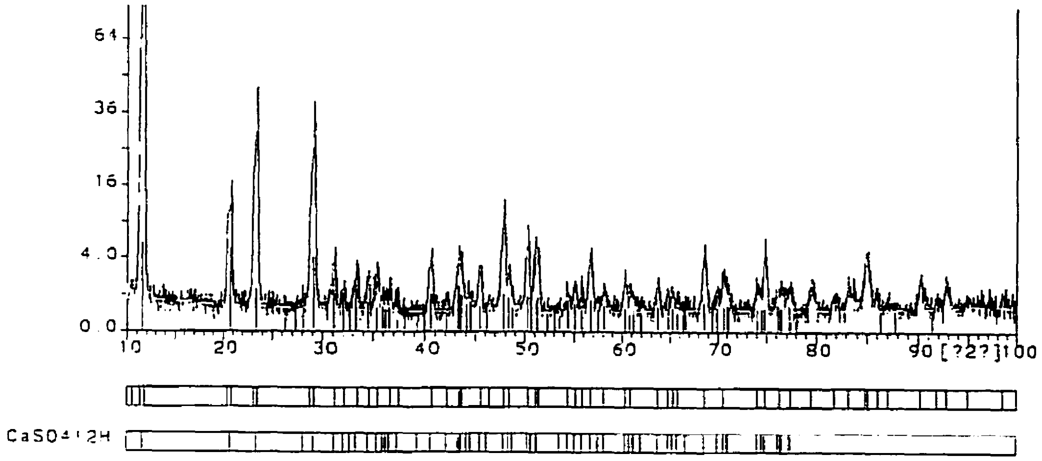

Figure 5-25: XRD pattern of the first reactor precipitates of the two stage, seeded neutralization with solids recycle

Images of the solids in the second reactor show the same crystals that are present in the first reactor along with amorphous solids and an increased fraction of fines (Figure 5-26). Some of the fines are magnified in Figure 5-27.

Figure 5-26: SEM image of solids precipitated in the second reactor of the two stage, seeded neutralization with solids recycle.

The XRD pattern of these precipitates also matches gypsum (Figure 5-28). The maximum intensity was 1.5 times that of the single-stage neutralization precipitate maximum intensity reading, and the background was fifty percent lower. The presence of fines is most likely responsible for this result.

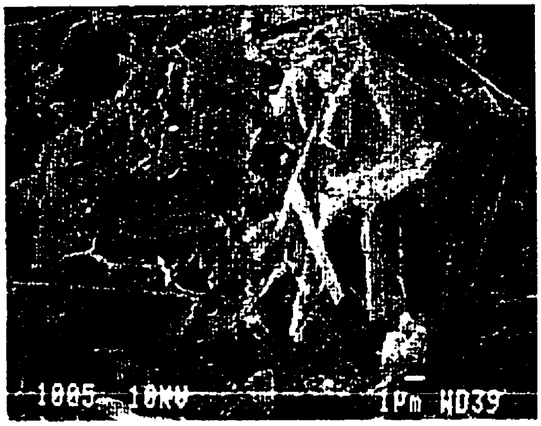

Figure 5-27: SEM image of fines precipitated in the second reactor of the two stage, seeded neutralization with solids recycle.

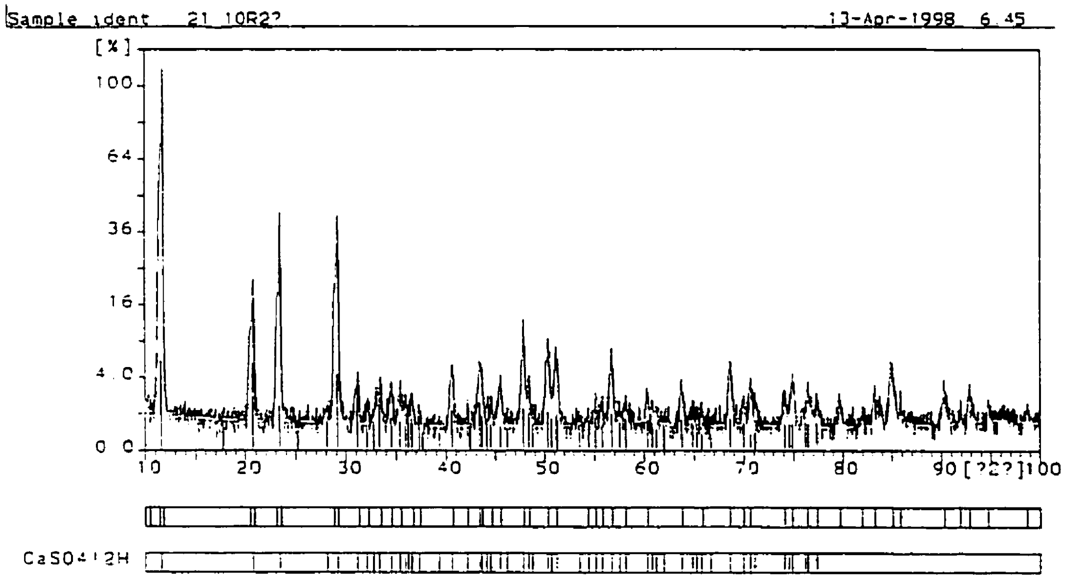

Figure 5-28: XRD results of solids precipitated in the second reactor of the two-stage, seeded neutralization with solids recycle.

EDS analysis of the solids from the second reactor (pH 5) indicated calcium, iron, zinc, and manganese present amongst the precipitates (Figure 5-29). There is less iron and manganese detected in this overall scan than detected in the reading from the single stage, unseeded neutralization products.

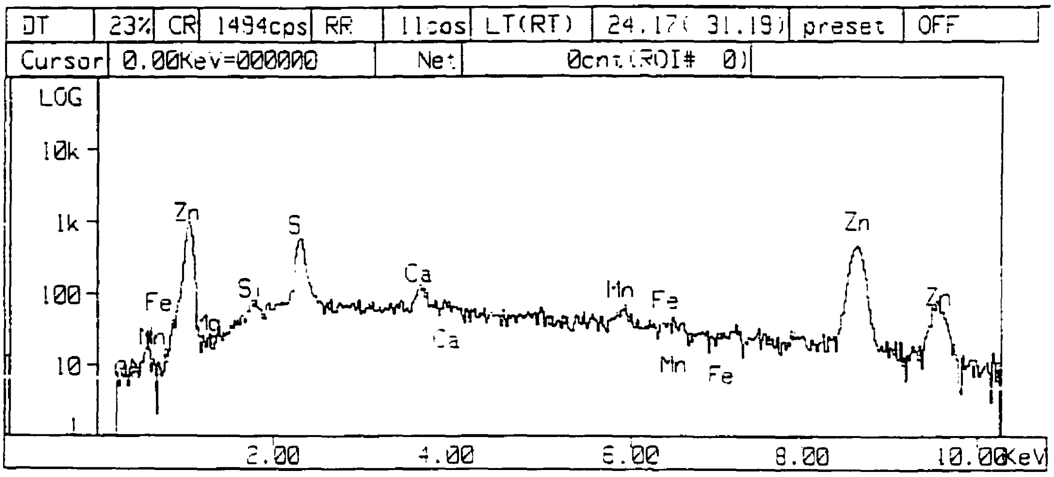

Figure 5-29: EDS analysis of the thickener solids precipitated by two-stage, seeded neutralization with solids recycle.

5-3-6-3 Effect of residence time on thickener precipitate solids density

The two-stage seeded neutralization process with solids recycle was run at three different residence times to test the sensitivity of thickener product solids density to residence time. Figure 5-30 shows that a lower residence time resulted in precipitated solid product with a lower solids density. A longer residence time could contribute to increased individual gypsum crystal size.

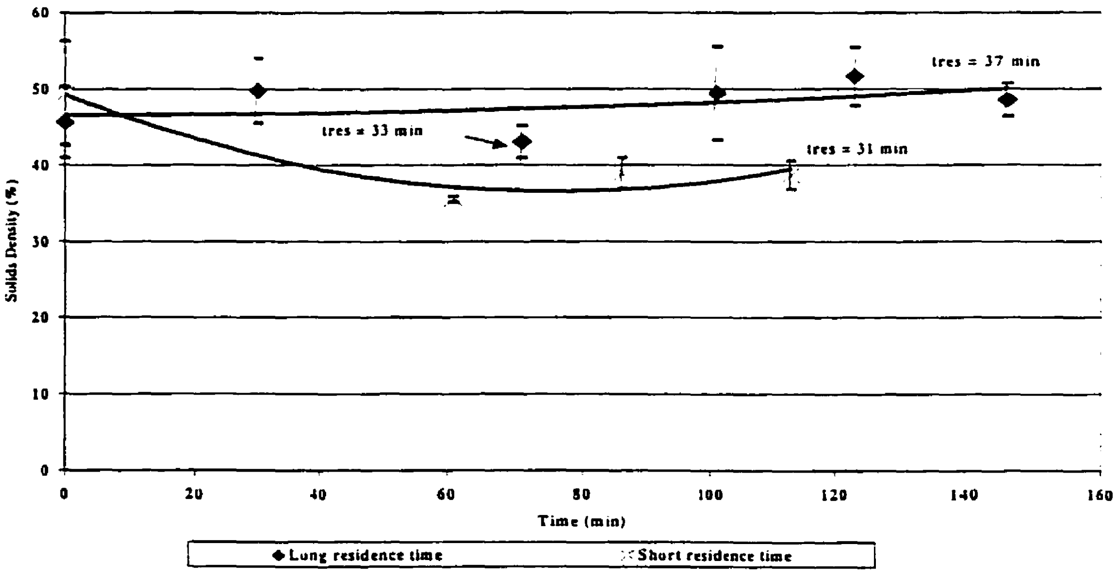

Figure 5-30: Comparison of thickener precipitate solids density with residence time: two-stage, seeded neutralization process with solids recycle

5-3-6-4 Impurity metal ion and calcium concentration results

The concentrations of zinc, iron, magnesium and manganese ions in the inlet, reactor and thickener solutions were recorded at the end of each continuous test. The results of both the single-stage unseeded, and seeded, recycled, as well as both the two-stage, unseeded, recycled and seeded, recycled processes are presented in Figures 5-31 to 5-34. The results of each cation are discussed separately. The process vessels are labeled R1 = first reactor. R2 = second reactor, and T = thickener in the figures.

5-3-6-4-1 Zinc

Reactor and thickener zinc concentrations are compared to the measured simulated waste inlet concentration in Figure 5-31. The single-stage, unseeded and two-stage, unseeded tests show the lowest final zinc concentrations. The seeded, recycled tests show higher final concentrations, and concentrations higher than the inlet concentration in the first reactor. These higher values in the first reactor can be attributed to zinc that is recycled back to the first reactor with the solids recycle stream either in solution or as precipitated solid such as basic zinc sulphate ($Zn_x(OH)_y(SO_4)_z$)that re-dissolves in the acidic first reactor.

The reduced zinc concentrations in the seeded second reactor, unseeded first reactor and thickener may be attributed to zinc co-precipitation with the hydroxide solids at high supersaturation. Zinc incorporation is not favoured in slowly growing gypsum crystal, as it is not chemically adsorbed on the gypsum surface (Appendix K). Less zinc was recycled back with the two-stage, seeded test. This could be attributed to the reduced probability of zinc incorporation in the precipitated solids due to the improved gypsum growth on reagent grade gypsum seed.

5-3-6-4-2 Iron

Iron is absent from thickener overflow in the single-stage, unseeded test (Figure 5-32). This supports the conclusion that ferric hydroxide is precipitated during the single stage neutralization. The concentration of iron in first reactor of the seeded, solids recycle test was higher than the inlet concentration. This supports the theory that the recycled ferric hydroxide solids are re-dissolved in the first reactor. Fine iron hydroxides are re-precipitated in the second reactor run at pH 5, reducing the iron concentration

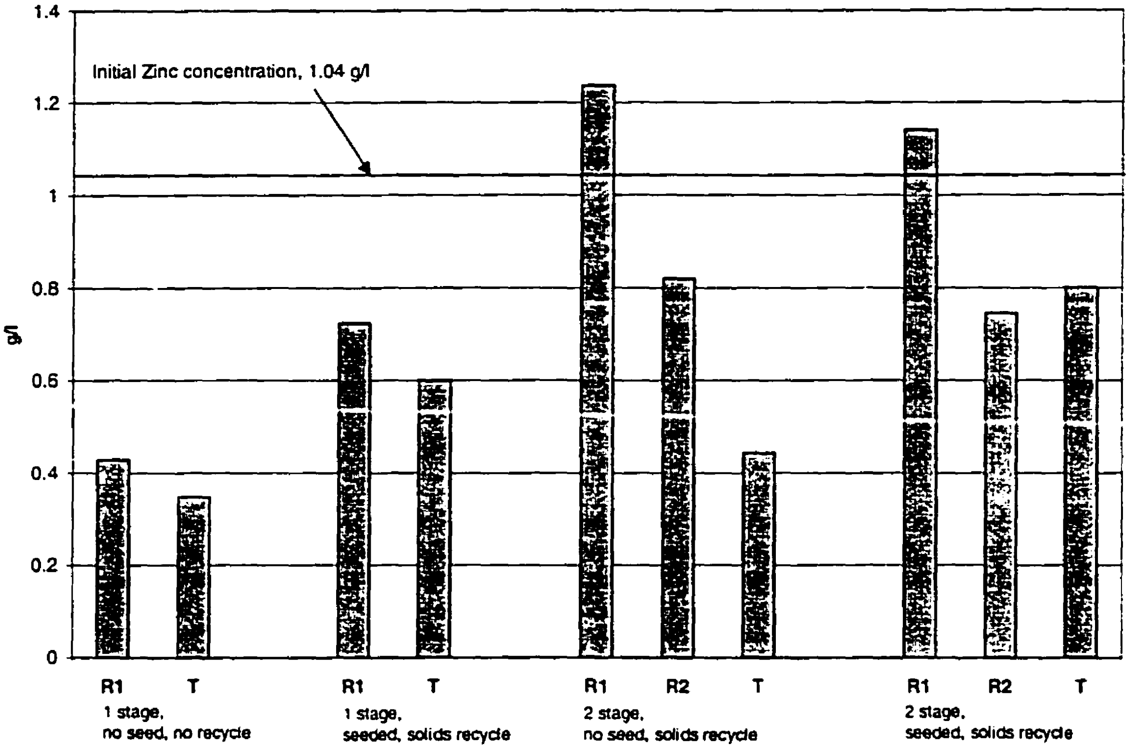

Figure 5-31: Steady-state zinc concentrations in different neutralization process vessels

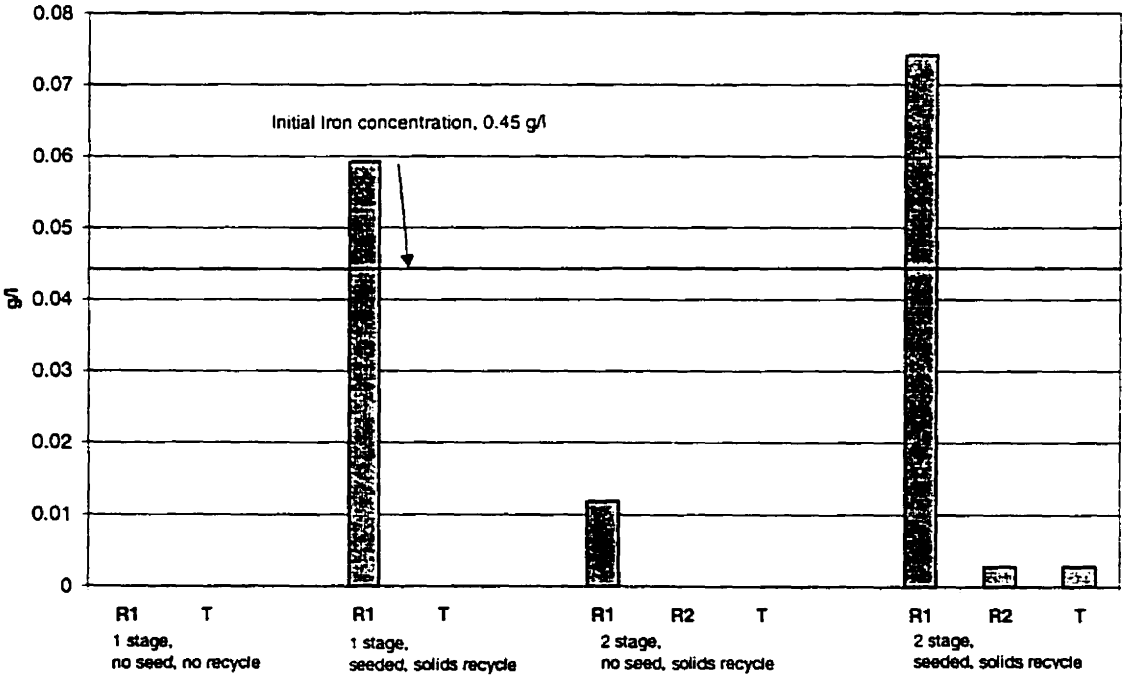

Figure 5-32: Steady-state iron concentrations in different neutralization process vessels

back to below detectable levels. The first reactor of the two-stage, unseeded with solids recycle neutralization process had significantly lower solution iron concentrations than the other tests with solids recycle. It is possible that the initial iron hydroxide solids had the opportunity to grow while being recycled, and these larger solids might not have re-dissolved to the same extent in the first reactor. The possibility of analysis error must not be ruled out as well.

5-3-6-4-3 Magnesium

Magnesium levels are consistently close to or below the inlet concentrations (Figure 5-33). The lower values in the single-stage, unseeded vessels and the staged, seeded second reactor and thickener may be attributed to the co-precipitation and adsorption of magnesium in the colloidal hydroxides with high surface area. The high solubility of magnesium sulphate complements the hypothesis that it is not precipitated, recycled, and re-dissolved in the first acidic reactor.

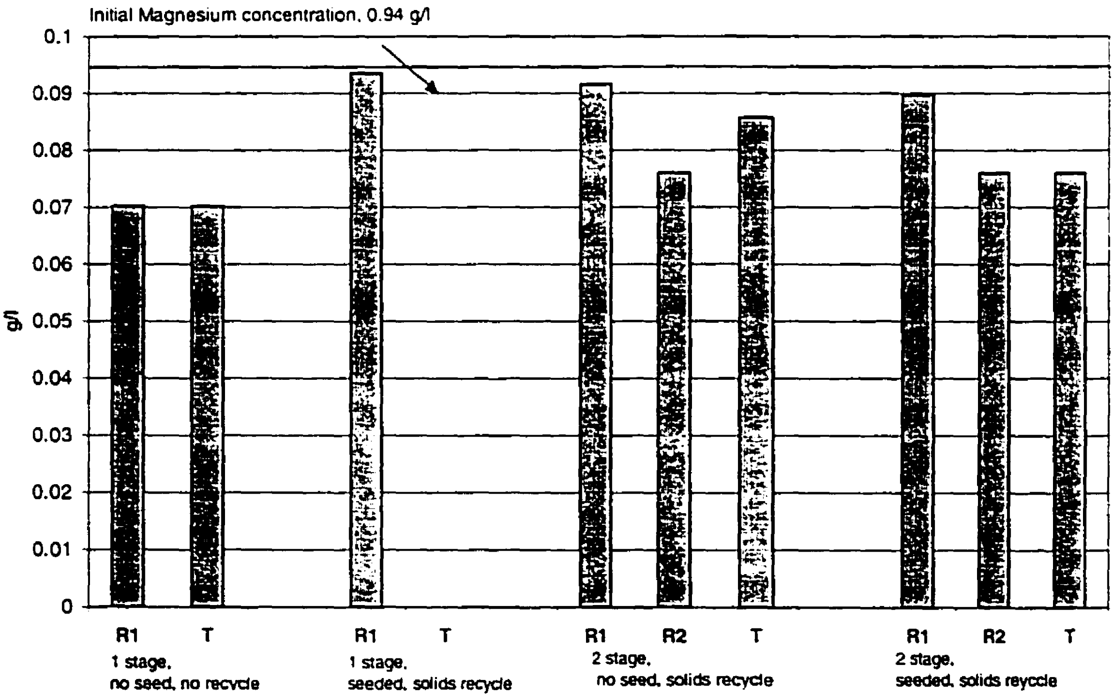

Figure 5-33: Steady-state magnesium concentration in different process vessels

5-3-6-4-4 Manganese

Manganese may have co-precipitated in the higher pH reactor , as its concentrations are lower in all reactors that operated at pH 5. The manganese concentrations in the first reactors run at pH 2 suggest that the co-precipitated manganese is not completely re-dissolved when it is recycled back to the first reactor., as its concentration is not as increased to the same degree as that of zinc.

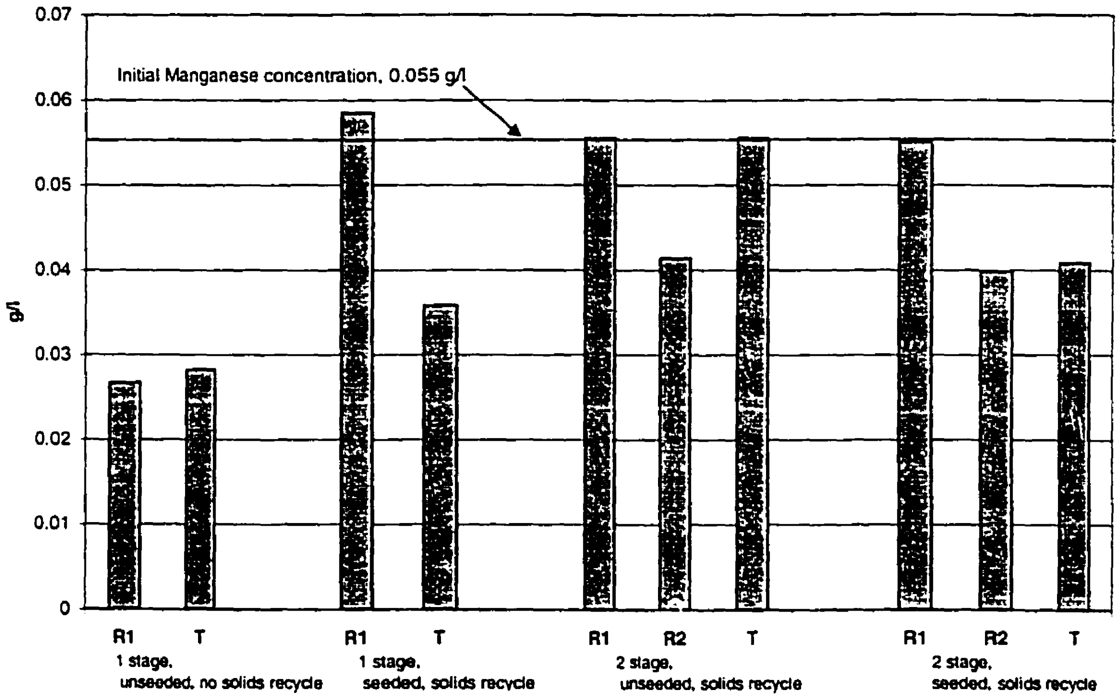

Figure 5-34: Steady-state manganese concentrations in different process reactors

5-4 CONCLUSIONS

The two-stage, pH 1-2-5, 50 g/l seeded continuous neutralization circuit with solids recycle presents many improvements over the single-stage, unseeded process. The precipitated gypsum solids were well-grown and crystalline; the solids density of the precipitate averaged 48%. Less zinc was removed from solution during the neutralization process. This provides potential for returning zinc to the process, as less zinc would report to the tailings pond with the precipitated solids.

The solids density results produced by the seeded, staged process with solids recycle were considerably higher than the 10% average value of the solids density produced by the single-stage, unseeded neutralization process without solids recycle, or the 25% solids density value reported for a zinc plant wastewater neutralization process with solids recycle and flocculant (Lockely et al., 1993) (Figure 5-36).

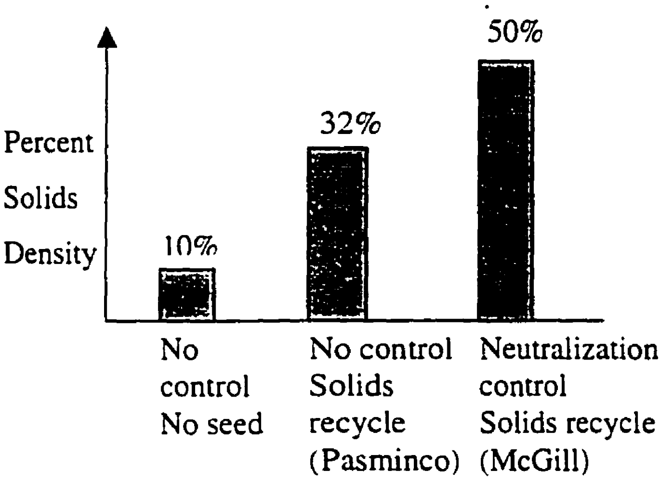

Figure 5-36 Comparison of precipitate solids density produced by three different neutralization processes.

Crystallization theory predicts that solids precipitated at low supersaturation in the presence of suitable seed crystals will be larger and more crystalline than solids produced without seed in a higher supersaturation environment. The results from the gypsum precipitation semi-batch and continuous tests indicated that solutions neutralized at low supersaturation precipitated large gypsum crystals. Gypsum precipitated by this process had a higher solids density and settling velocity than the precipitate produced by an unseeded neutralization at higher supersaturation.

The use of a staged neutralization process with solids recycle that is seeded with gypsum at start-up is recommended to treat zinc plant effluent in order to increase precipitate solids density and decrease the volume of sludge that reports to the tailings pond.

6 FUTURE WORK

The original proposal indicated that the effect of impurities on gypsum precipitation and growth should be investigated after the completion of the controlled neutralization work. Preliminary tests investigating the effect of sodium, ammonium, magnesium and zinc sulphate on gypsum precipitation indicated that gypsum morphology, and perhaps crystal structure are affected by the presence of non-lattice cations. Researchers from the Delft University of Technology in the Netherlands have published numerous works on the effects of phosphoric acid, cadmium, chromium and other impurities (Witkamp (1990), Witkamp (1991), de Vreugd (1994)) on gypsum crystallization. Niels Verbaan, also a DUT graduate, will continue to research the effect of impurities on gypsum crystallization, producing an M. Eng. thesis and concluding the work of the original proposal in the hydrometallurgy laboratory at McGill University.

Also of interest to the impurity work would be determining the threshold concentrations of the different non-lattice electrolytes required to inhibit or significantly alter primary nucleation and the morphology of the spontaneously precipitated crystals. The effect of the different non-lattice ions on the chemistry of the adsorption layer by the crystal surface might further the understanding of why, for example, gypsum grown in acidic sodium or ammonium sulphate solutions with slaked lime exhibits rounded edges.

An investigation of the effect of using either solution-own seed produced through primary nucleation or synthetic gypsum seed in a continuous staged wastewater neutralization process with solids recycle could reduce the operating cost of this process and reveal some other interesting characteristics of the precipitation of gypsum from solution.

The effect of anions on gypsum crystallization would make an interesting and relevant study. Carbonates had a dramatic effect on the morphology of precipitated gypsum; perhaps chloride or other anions would also affect the precipitation characteristics.

Although not critical for the development of the wastewater neutralization process, a study of how the kinetics of gypsum precipitation are affected by seed type, seed concentration, and impurity type and concentration characteristic of wastewater would contribute useful information to the growing body of gypsum precipitation information.

7 REFERENCES

Amatieu, L. and R. Boistelle. *J. Crystal Growth.* 88 (1988): 183-192.

Baltpurvins, K.A., R.C. Burns, G. A. Lawrance and A.D. Stuart. *Wat. Res.* 31.5 (1997): 973-980.

Banz, I. and R.G. Luthy, *J. Env. Eng.* 111.3 (1985): 317-335.

Bloss, F.D., *Crystallography and Crystal Chemistry, An Introduction*. New York: Holt, Reinehart, and Winston Inc, 1971, 335.

Bosbach, D. and W. Rammensee. *Geochim. et Cosmochim. Acta.* 58.2 (1994): 843-849.

Busch, K.W. and M.A. Busch. *Desalination.* 109 (1997): 131-148.

Calmanovici, C.E., N. Gabas and C. Laguérie. *J. Chem. Eng. Data*. 38 (1993): 534-536.

Carpenter, J.H., *J. Chem. Educ*. 64:6 (1987): 184.

Christoffersen, J., M.R. Christoffersen, G.M. van Rosmalen and W.G.J. Marchée. *J. Crystal Growth.* 47 (1979): 607-612.

Christoffersen M.R., J. Christoffersen, M.P.C. Weijnen and G.M. van Rosmalen, *J. Crystal Growth.* 58 (1982): 585-595.

Coburn, A. E. Dudley and R. Spence. *Gypsum Plaster, Its manufacture and use.* London: Intermediate Technology Publications (1989): 8.

Davies, C.W. *J. Chem. Soc.* (1938): 2093.

Davis, R.H., "The Stochastics of Sedimentation" *Sedimentation of Small Particles in a Viscous Fluid, 7, Advances in Fluid Mechanics,* Ed. E.M. Tory, Southampton: Computational Mechanics Publications, 1996.

Demopoulos, G.P. *Processing Materials for Properties.* Hawaii, Nov. 7-10. Warrendale: TMS (1993): 537-540.

Demopoulos, G.P., J. Zinck and P.D. Kondos. *Waste Processing and Recycling in Mineral and Metallurgical Industries II.* Vancouver, Aug. 20-24. Montreal: CIM (1995a) p.401-411.

Demopoulos, G.P., D.J. Droppert, and G. van Weert. *Hydrometallurgy*. 38.3 (1995b): 245-262.

Demopoulos, G.P., P. Kondos and V.G. Papangelakis. *Crystallization and Precipiation* Ed. Strathdee et al.. London: Pergamon Press, 1987. 231-346.

Droppert, D. *The Ambient Pressure Precipitation of Crystalline Scorodite (FeAsO4.2H2O) from Sulphate Solutions*. McGill University. Montreal: McGill, 1995.

Dryden, R. and M. Tsurumi. *J. Young Ad. Club.* 3.1 (1992), 92-93.

Edinger, S.E. *J. Crystal Growth.* 18 (1973): 217-224.

Elliot, M.N. *Desalination.* 8 (1970): 221-236.

Feller, S.E. and D.A. McQuarrie. *J. Phys. Chem.* 96 (1992): 3454-3457.

Filippou, D. and G.P. Demopoulos. JOM, 49.12 (1997): 52-55.

Filippou, D., V.G. Papangelakis and G.P. Demopoulos. *Hydrometallurgy: Fundamentals, Technology, and Innovation.* Ed. J.B. Hiskey and G.W. Warren. Littleton: SME-AIME, 1993. 223-240.

Filippou, D., Internal McGill report (1989)

Finot, E., E. Lesniewska, J-C. Mutin and J-P. Goudonner. *Surface Science.* 384.1(1997): 201-217.

Fogler, H.S. *Elements of Chemical Reaction Engineering.* 2nd Ed. New Jersey: Prentice-Hall, 1992.

Franke, J. and A. Mersmann. *Chem. Eng. Sci.* 50.11 (1995): 1737-1753.

Furby, E., E. Gluekauf and L.A. McDonald. *Desalination.* 4 (1968): 264.

Gardner, A.W. and E. Glueckauf. *Trans. Faraday Soc.* 66 (1970): 1081-1087.

Guenther, W.B. *Chemical Equilibrium*. New York: Plenum, 1975. 172-176.

Glasner, A. and D. Weiss. *J. Inorg. Nucl. Chem.*. 42 (1980): 655-663.

Hall, C. and D.C. Cullen. *AIChE Journal*. 42.1 (1996): 232-238.

Hamdona, S.K., R.B. Nessim and S.M. Hamza. *Desalination*. 94.1 (1994): 69-81.

He, S. and J.W. Morse. *Computers & Geosciences*. 19.1 (1993): 1-22.

Heijnen, W.M.M. and P. Hartman. *J. Crystal Growth* 108 (1991): 290.

Israelachvili, J. *Intermolecular and Surface Forces, 2nd Ed.*. Toronto: Academic Press, 1991.

Jansz, J.J.C. *Hydrometallurgy*. 11 (1983): 13-31.

Klein, J.P. and David, R. "Reaction Crystallization" *Crystallization Technology Handbook*. Ed. A. Mersmann, New York: Marcel Dekker, 1995. 359-400.

Kusik, C.L. and H.P. Meissner. *Ind. Eng. Process Des. Develop.* 12.1 (1973): 112-115.

Kusik, C.L. and H.P. Meissner. *Fundamental Aspects of Hydrometallurgical Processes, AIChE Symposium Series*. 173. 74 (1978): 14-19.

Lee, J.D. Ed., *Concise Inorganic Chemistry, 5th Ed.*. London: Chapman and Hall, 1996.

Liu, S.T. and G.H. Nancollas. *Talanta*. 20 (1973): 211-216.

Liu, S.T and G. H. Nancollas. *J. Inorg. Nucl. Chem.* 33 (1971): 2311-2316.

Lockley, J.V., D.J. Palmer and O.M.G. Newman. *International Symposium – World Zinc '93, October 10-13*, Hobart, Australia (1993): 385-389.

Macek, J., S. Zakrajsek and J. Nyvlt. *Cryst. Res. Technol.* 28 (1993): 847-854.

McCartney, E.R. and A.E. Alexander. *J. Coll. Sci.* 13 (1958): 383-396.

Martin, R.B. *J. Chem. Educ*, 63 (1986): 471-472.

Masterman, D. *J. Chem. Educ.* 64.5 (1987): 408-409.

Meissner, H.P. *Thermodynamics of Aqueous Systems with Industrial Applications.* Ed. S.A. Newman, ACS Symposium Series, 133 (1980): 495-511.

Meissner, H.P. and N.A. Peppas. *AIChE Journal.* 19.4 (1973): 806-809.

Meissner, H.P. and C.L. Kusik. *AIChE Journal.* 18.2 (1972): 294-298.

Meissner, H.P. and J.W. Tester. *Ind. Eng. Process Des. Develop.* 11.1 (1972): 128-133.

Meites, L., J.S.F. Pode and H.C. Thomas. *J. Chem. Educ.* 43 (1966): 667-672.

Mersmann, A. "Fundamentals of Crystallization" *Crystallization Technology Handbook..* Ed. A. Mersmann. New York: Marcel Dekker, 1995. 1-78.

Mersmann, A. "Interaction Between Balances, Processes, and Product Quality" *Crystallization Technology Handbook..* Ed. A. Mersmann. New York: Marcel Dekker, 1995. 79-214.

Mersmann, A. and Rennie, F.W. "Design of Crystallizers and Crystallization Processes" *Crystallization Technology Handbook..* Ed. A. Mersmann. New York: Marcel Dekker, 1995. 215-326.

Mersmann, A., M. Angerhöfer and J. Franke. *Chem. Eng. Technol.* 17 (1994): 1-9.

Mersmann, A. and F.W. Rennie. Chapter 3, *Crystallization Technology Handbook.* Ed. A. Mersmann. New York: Marcel Dekker,, 1994.

Mineralogy, Twinning, 1997, <http://departments.colgate.edu/geology/mineralogy/summaries/twinning.html>

Moreno, E.C. and G. Osborn. *Soil Science Society Proceedings.* (1963): 614-619.

Mullin, J.W. and J. Garside. *Chem. Eng.* (1974): 402-404.

Mullin, J.W. and O. Söhnel. *Chem. Eng. Sci.* 32 (1977): 683-686.

Nakayama, F.S. and B.A. Rasnick. *Anal. Chem.* 39. 8 (1967): 1022-1023.

Nancollas, G. H., W. White, F. Tsai and L. Maslow. *Corrosion.* 35,.7 (1979): 304-308.

Nancollas, G.H., M.M. Reddy and F. Tsai. *J. Crystal Growth.* 20 (1973): 124-132.

Nancollas, G.H., *J. Crystal Growth*, Vol. 3, No. 4 (1968), 335.

Nielsen, A., and J. M. Toft. *J. Crystal Growth*, 67 (1984): 278-288.

Nielsen, A. *J. Crystal Growth*, 67 (1984): 289-310.

Nielsen, A.E. *Acta Chem. Scand.* 15 (1961): 441.

Packter, A. *J. Crystal Growth.* 21 (1974): 191-194.

Parkhurst, D.L., Thorstenson, D.C., Plummer, L.N., 1997 <http://magma.mines.edu/igwmc/software/igwmcsoft/phreeqe.htm>

Pitzer, K. S. *J. Phys. Chem.* 77.2 (1973): 268-277.

Power, W.H., B.M. Fabuss and C.N. Satterfield. *J. Chem. Eng. Data.* 11.2 (1966): 149-154.

Price, C.J. *Chemical Engineering Progress.* 93.9 (1997): 34-43.

Quinn, C.J., T.C. Molden and C.H. Sanderson. *Iron and Steel Engineer.* July, (1997) 47-52.

Raju, K.U. and G. Atkinson. *J. Chem. Eng. Data.* 35 (1990): 361-367.

Reddy, M.M. and G.H. Nancollas. *J. Crystal Growth.* 35 (1976): 33.

Reed-Hill, R.E. and R. Abbaschiam. *Physical Metallurgy Principles, 3rd Ed.*, Boston: PWS-Kent Publishing Company, 1992.

Rinaudo, C. and A. Zarka. *J. Crystal Growth.* 116 (1992): 87-92.

Rinaudo, C., M.C. Robert and F. Lefaucheux. *J. Crystal Growth.* 71 (1985): 803-806.

Seidell, A. and W.F. Linke. *Solubilities of Inorganic and Metal Organic Compounds, 4th Ed.*, Princeton: Van Nostrand & Co., 1958.

Schierholtz, O.J. *Can. J. Chem.* 36 (1958): 1057-1063.

Shriver, D.F., P.W. Atkins and C.H. Langford. *Inorganic Chemistry*. New York: W.H. Freeman and Co., 1990. 150.

Silcock, H., Ed. *Solubilities of Inorganic and Organic Compounds, Vol. 3: Multicomponent Systems of Inorganic Substances.* Toronto: Pergamon Press, 1979.

Simon, B. and M. Bienfait. *Acta Cryst.* 19 (1965): 750-756.

Smith, B.R. and F. Sweett. *J. Coll. Int. Sci.* 37.3 (1971): 612-618.

Smith, J.M. and H.C. van Ness. *Introduction to Chemical Engineering Thermodynamics.* McGraw-Hill, Inc. 1987. 37.

Söhnel, O. and J. Garside. *Precipitation, Basic principles and industrial applications.* Oxford: Butterworth-Heinemann Ltd., 1992. 85-88.

Söhnel, O., J. Garside and S.J Jancic. *J. Crystal Growth.* 39 (1977): 307-314.

Standiford, F.C. and J.R. Sinek. *Chem. Eng. Progress.* 57.1 (1961): 58-63.

Tadros, M. E. and I. Mayes. *J.Coll. Int. Sci.* 72.2 (1979): 245-254.

Tozawa, K. and K. Sasaki. *Iron Control in Hydrometallurgy*. Ed. J.E. Dutrizac and A.J. Monhemius. Chichester: The Metallurgical Society of CIM and Ellis Horwood, Ltd.. (1986): 454-476.

Van der Leeden, M.C., D. Kashchiev, and G.M. van Rosmalen. *J. Crystal Growth.* 130 (1993): 221.

Van Oosterhaut, G.W. and G.M. van Rosmalen. *J. Crystal Growth.* 48 (1980): 464-468.

Van Rosmalen, G., P. J. Daudy and W.G.J., Marchée. *J. Crystal Growth.* 52 (1981): 801-811.

Van der Voort, E. and P. Hartman. *J. Crystal Growth.* 112 (1991): 445-450.

Van Weert, G. and D.J. Droppert. *JOM.* 46.6 (1994): 36-39.

Verdoes, D., D. Kashchiev and G.M. van Rosmalen. *J. Crystal Growth.* 118 (1992): 401.

De Vreugd, C. H. G.J. Witkamp and G.M. van Rosmalen. *J. Cryst. Growth.* 144 (1994): 70-78.

Wang, Y., A.J. Babchin, L.T. Chernyl, R.S. Chow and R.P. Sawatzky. *Chem. Eng. Sci.* (1996): 346.

Weijnen, M.P.C., G.M. van Rosmalen, P. Bennema and J.J.M. Rijpkema, J.J.M. *J.Crystal Growth.* 82 (1987): 509-527.

Weijnen, M.P.C., G.M. van Rosmalen and P. Bennema. *J. Cryst. Growth.* 82 (1987): 528-542.

Weissbuch, I., R. Popovitz-Biro, M. Lahav and L. Leiserowitz. *Acta Cryst.* B51, (1995): 115-148.

Witkamp, G. J., M.M. Seckler, O.S.L. Bruinsma and G.M. van Rosmalen. *J. Cryst. Growth.* 99 (1990): 1117-1123.

Witkamp, G. J. and G.M. van Rosmalen. *J. Cryst. Growth.* 108 (1991): 89-98.

Yadav, S., M.K. Sharma, R.S. Siyag, S.R. Poonia, and R. Pal. *J. Ind. Soc. Soil Sci.* 43.2 (1995): 191-196.

Zinck, J.M. *An Investigation into the Hydrolytic Precipitation of Iron(III) from Sulphate-Bearing Effluents*. McGill University. Montreal: 1993.

Appendix A - Sulphuric acid speciation

The dissociation constants of sulphuric acid at 25°C were used in conjunction with the solubility data of gypsum in sulphuric acid solutions in order to plot the following speciation data.

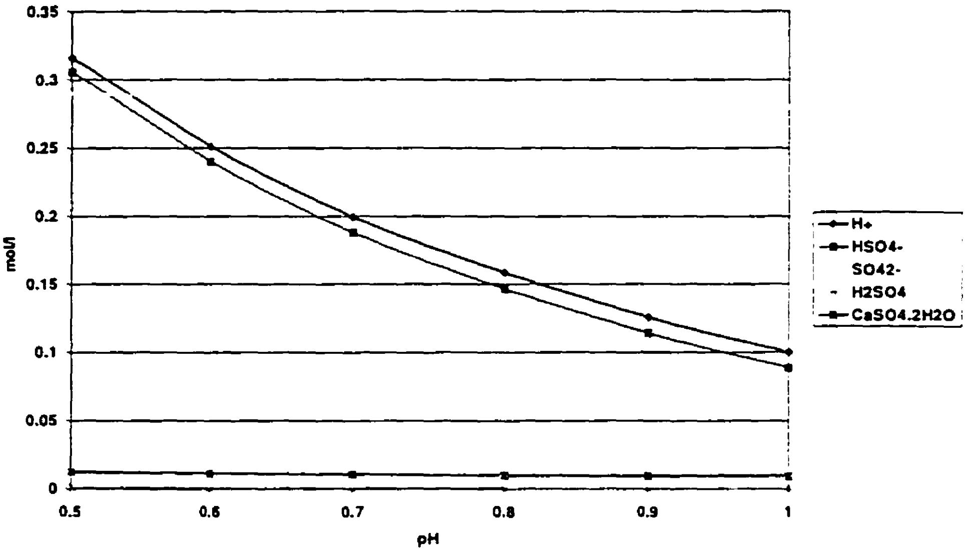

Figure A-1 Speciation of sulphuric acid saturated with gypsum, pH 0.5-1, $CaSO_4.2H_2O$ represents dissolved gypsum, 25°C.

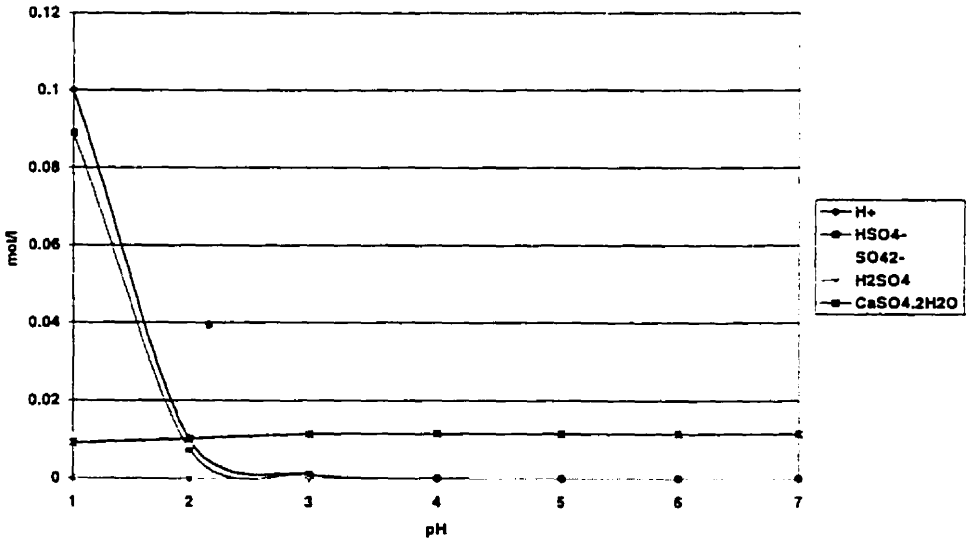

Figure A-2 Speciation of sulphuric acid saturated with gypsum, pH 1-7, $CaSO_4.2H_2O$ represents dissolved gypsum, 25°C.

Appendix B - Gypsum growth rates and mechanisms.

There is a long history of investigation into the growth rates and mechanisms of gypsum crystals. From the early work of Schierholtz (1958), who proposed a first-order rate law, to a second-order growth model proposed by Smith and Sweett (1971), and a fourth-order process described by Packter (1974), different growth rates have been proposed to describe the growth of gypsum from supersaturated solution.

Not only do discrepancies exist amongst the published gypsum growth orders, but also the proposed growth mechanism varies. Tadros and Mayes (1979) argued that the second-order growth kinetics indicate a reaction-controlled mechanism of polynuclear growth. Liu and Nancollas (1973) also concluded a second-order growth rate with respect to supersaturation modelled gypsum crystal growth, but they correlated their results to a screw-dislocation model or surface adsorption model.

Other researchers have attributed responsibility to other crystallization system parameters for changing gypsum growth kinetics. Witkamp et al. (1990), determined that gypsum growth kinetics are second order in pure water solutions, and can vary from 1 at low supersaturations to 4 at high supersaturations in $NaNO_3$ solutions. Weijnen et al. (1987) suggest that the growth mechanism changes with supersaturation, with a high supersaturation favouring a birth and spread mechanism of gypsum growth.

Earlier work by van Rosmalen (1981) suggested that the growth rate is a function of the normalized volume of crystals, and fit their data with a spiral growth model. Christoffersen et al. (1982) published that the overall rate of gypsum growth decreased with increased mass of crystals. They also proposed that a spiral growth mechanism, as well as the growth of cooperating spirals with non-parallel Burgess vectors, growth of grain-boundary spirals and partial outgrowth of concave crystal parts could explain the observed growth rates at low supersaturations.

Amathieu and Boistelle (1988) studied the growth of gypsum at different supersaturations in dense solid suspensions and concluded that a critical supersaturation of 1.6 exists, below which a parabolic growth rate law is satisfied, and above which a linear growth rate is expressed. The rate determining step was concluded to be surface integration, and not volume diffusion.

A more recent paper (Hamdona et al., 1993) echoed a conclusion from an earlier paper (Edinger, 1973), and summarized that the rate of precipitation of calcium sulphate dihydrate depends on the initial degree of supersaturation and the concentration of additive metal ions. This paper also suggested that a surface polynucleation process controls the precipitation reaction. Söhnel and Garside (1992) proposed that crystal growth is controlled by a combination of mechanisms.

No clear explanation can be drawn from the disparity of conclusions. It is proposed that a very complex surface-adsorption layer chemistry may be behind this wide range of results and conclusions. Nielsen and Toft (1984) did not comment on gypsum kinetics but they proposed that the growth rate is controlled by either transport of lattice ions through the solution by convection or diffusion, by a process at the crystal surface, or by a combination of these mechanisms. They related growth rates to surface controlled processes: linear to adsorption, parabolic to spiral integration, and exponential to formation and growth of surface nuclei. Nielsen later commented (Nielsen, 1984) that sparingly soluble electrolytes mostly grow by a parabolic or exponential rate law at smaller supersaturations, changing to a linear rate due to a change to transport control at higher supersaturations. Nielsen correlated the rates of growth to the growth process if it can be assumed that the rate determining mechanism is the dehyrdration and incorporation of cations at kinks in the surface.

Surface chemistry was proposed as a factor that influences gypsum morphology, as it may influence the rate of growth of the different faces. Van Rosmalen's work (1981) commented that the sodium ion may affect the growth rate of the [01 1] face, promoting its development. Bosbach et al. (1994) concluded that growth on the [010] surface of gypsum is a layer-by-layer process, and that local growth is strongly affected by surface topography. More importantly, Weijnen et al. (1987) mentions that the solid phase may have an influence on the structure of the fluid phase in contact with the solid surface.

A wide range of work has been published on the calculation of the population density distribution of ions by charged surfaces. These systems are difficult to model, often requiring Monte Carlo methods of solving the complex interaction equations. Feller and McQuarrie (1992) compare the results produced by a variational hypernetted chain (HNC) / mean sphere approximation (MSA) method and the modified Gouy Chapman

(MGC) method, when applied to the more difficult polyelectrolyte system which reflects the polyelectrolyte situation of calcium and sulphate ions. They calculated surprising nonmonotonic ion density profiles that cannot be found in previous MGC results. They also observed that the potential can change signs in solutions with divalent ions, which is not predicted with MGC theory.

If this is true, then one possible impact of this is an arrangement of not just one kind of ion near a charged surface, but the potential layering of cations and anions near the charged surface. It is proposed that this layering might induce solid nuclei formation at or near the surface. Finot et al. (1997) studied the reactivity of the [010] gypsum face according to relative humidity and noted that a precipitate was formed under the SFM tip within a certain humidity range. The precipitate was strikingly different than the traditional crystal growth from solution, and was postulated to be calcium sulphate anhydride. They noted that the SFM tip may simulate the physical presence of another crystal, possibly extrapolating this SFM situation to include slurried precipitation environments.

It is postulated that the presence of the SMF tip near the gypsum surface enhanced the ordering of the charged Ca^{2+} and SO_4^{2-} species, bringing them into close enough contact that a solid phase coalesced out of solution. The lack of crystal water in the precipitate induced by the SFM tip is curious, and may further the argument that it is the ordering of the charged species that caused the solid phase formation in this situation.

The presence of other charged species will most likely affect the population density of the different species at the gypsum surface, and it is proposed that these changes affect the rate of crystal growth on the different faces as they could change the solution chemistry at the surface of the crystal. For the simulated zinc plant wastewater neutralization system, fairly equant gypsum solids are favoured, which settle and pack well. Therefore, no work was performed to modify the adsorption layer chemistry and favour the growth of different gypsum faces.

Appendix C - PHREEQE in and output

PHREEQE

Order No: FOS 39

PHREEQE is a geochemical reaction model which is based on an ion pairing aqueous model. PHREEQE can determine pH, redox potential, and mass transfer as a function of reaction progress, and also solution composition in equilibrium with multiple phases. The aqueous model, including elements, aqueous species, and mineral phases, is exterior to the computer code, is completely user definable, and has been regularly updated by the authors since its first release. PHREEQE can simulate several types of reactions including addition of reactants to a solution, mixing of two waters, and titrating one solution with another. In each of these case, PHREEQE can simultaneously maintain the reacting solution at equilibrium with multiple phase boundaries. PHREEQE solves the set of non-linear governing equations using a combination of two techniques: 1) a continued fraction approach for mass balance equations, and 2) a modified Newton-Raphson technique for all other equations; the resulting linear equations are solved using Gaussian elimination. Activity coefficients are calculated from either the Debye-Huckel or Davies formulation.

The data base includes the following elements: allumium, barium, borium, bromide, cadmium, calcium, carbon, chloride, copper, fluoride, hydrogen, iron, lead, lithium, magnesium, manganese, nitrogen, oxygen, phosphorus, potassium, silica, sodium, strontium, sulfur and zinc. It also has a database for arsenic, cesium, iodine, nickel, rubium, selenium, silver, and uranium.

The interactive preprocessor PHRQINPT is included with the PHREEQE package to facilitate formulation and editing of the PHREEQE input data. PHRQINPT explains the meaning and significance of each variable when required, and internally checks the validity of entered values.

PHREEQE and PHRQINPT are public domain programs; the IGWMC version is compiled to run in the DOS environment and includes source code, executable image, and example data sets. The documentation consists of installation instruction and the user's manual for both PHREEQE and PHRQINPT.

SYSTEM REQUIREMENTS

Intel 80i86 based computer, 640 Kb RAM, DOS 3.0 or higher; math coprocessor optional.

Authors: D.L. Parkhurst, D.C. Thorstenson, and L.N. Plummer (U.S. Geological Survey).

Output table

```
------------------
Reading data base.
------------------

        SOLUTION_MASTER_SPECIES
        SOLUTION_SPECIES
        PHASES
        EXCHANGE_MASTER_SPECIES
        EXCHANGE_SPECIES
        SURFACE_MASTER_SPECIES
        SURFACE_SPECIES
        END
-------------------------------------
Reading input data for simulation 1.
-------------------------------------

        TITLE CEZ solution
        SOLUTION 1
                pH 1 charge
                temp 25
                pe
                units mmol/L
                Ca 9.7
                Fe 1
                Mg 4
                Mn 1.1
                S 34 as SO4-2
                Zn 15.3
        EQUILIBRIUM_PHASES 1
                O2(g) 0.21
                CO2(g) 0.04
                gypsum
        END
-----
TITLE
-----

 CEZ solution

-------------------------------------------
Beginning of initial solution calculations.
-------------------------------------------

Initial solution 1.

-----------------------------Solution composition------------------------------

        Elements           Molality       Moles

        Ca                 9.748e-03   9.748e-03
        Fe                 1.005e-03   1.005e-03
        Mg                 4.020e-03   4.020e-03
        Mn                 1.105e-03   1.105e-03
        S                  3.417e-02   3.417e-02
        Zn                 1.538e-02   1.538e-02

----------------------------Description of solution----------------------------

                                       pH  =   4.104      Charge balance
                                       pe  =   0.000
                        Activity of water  =   0.999
```

```
------------------------------Saturation indices-------------------------------

        Phase               SI log IAP  log KT

        Anhydrite        -0.22   -4.58   -4.36  CaSO4
        Aragonite        -6.95  -15.29   -8.34  CaCO3
        Calcite          -6.81  -15.29   -8.48  CaCO3
        CH4(g)         -140.84 -184.77  -43.93  CH4
        CO2(g)            0.04  -18.11  -18.15  CO2
        Dolomite        -14.03  -31.12  -17.09  CaMg(CO3)2
        Fe(OH)3(a)       -2.11   15.81   17.91  Fe(OH)3
        FeS(ppt)       -141.52 -179.08  -37.56  FeS
        Goethite          3.79   15.81   12.02  FeOOH
        Gypsum            0.00   -4.58   -4.58  CaSO4:2H2O
        H2(g)           -41.67  -41.67    0.00  H2
        H2S(g)         -132.42 -174.06  -41.64  H2S
        Hausmannite     -14.09   46.94   61.03  Mn3O4
        Hematite          9.58   31.61   22.03  Fe2O3
        Mackinawite    -140.79 -179.08  -38.30  FeS
        Manganite        -2.75   22.59   25.34  MnOOH
        Melanterite     -10.22  -12.43   -2.21  FeSO4:7H2O
        O2(g)             0.21   83.33   83.12  O2
        Pyrite         -225.70 -311.48  -85.78  FeS2
        Pyrochroite     -13.44    1.76   15.20  Mn(OH)2
        Pyrolusite        2.04   43.42   41.38  MnO2
        Rhodochrosite    -5.22  -16.35  -11.13  MnCO3
        Siderite        -12.24  -23.13  -10.89  FeCO3
        Smithsonite      -5.30  -15.30  -10.00  ZnCO3
        Sphalerite     -125.98 -171.25  -45.27  ZnS
        Sulfur          -96.63 -132.39  -35.76  S
        Zn(OH)2(e)       -8.69    2.81   11.50  Zn(OH)2

------------------
End of simulation.
------------------

------------------------------------
Reading input data for simulation 2.
------------------------------------

-----------
End of run.
-----------
```

Appendix D – The effect of magnets on gypsum solubility and precipitation

Efforts to reduce scale formation in industry have included the use of additives and, surprisingly, the use of magnets. It is believed by some that the placement of magnets around inlet pipes to boilers or dishwashers reduces downstream scale formation. Some publications (Quinn et al. (1997), Busch et al. (1997)) investigated this phenomenon; to date, it is not clear what effect magnets might have on gypsum precipitation.

A few solubility experiments both with and without magnets were performed with gypsum in water and sulphate electrolytes in order to investigate any magnetic effect through the use of a magnetic stirrer. Preliminary precipitation tests were also performed.

Effect of magnetic stirrers on gypsum solubility in deionized water

Preliminary results indicate that the solubility of gypsum in water is affected by the presence of a magnetic stirrer. 100ml solutions of deionized water were mixed with reagent-grade gypsum and left to come to equilibrium (at least 2 hours) with or without a magnetic stirrer at room temperature (22°C). The supernatant was analyzed for calcium to determine the gypsum solubility. The solubility of gypsum without a magnetic stirrer was determined to be 2.07 g/l; the solubility with a magnetic stirrer was determined to be 1.57 g/l with a large first standard deviation of 0.37 g/l from repeat tests and analyses. The thermodynamic model and most references quote about 2 g/l gypsum solubility in water at room temperature.

Effect of magnetic stirrers on gypsum solubility in mixed sulphate electrolytes

Mixed sulphate electrolyte tests of gypsum solubility were performed both with and without magnetic stirrers to investigate the magnetic effect[A]. The same electrolyte systems that were used in Section 2-3-4 were used in these tests. Two separate calcium concentration analyses were performed on the supernatants to determine gypsum solubility. They are compared with the thermodynamic model (Chapter 2) predicted values in Figure D-1. As the magnitude of the two different analyses is suspiciously large, (two researchers performed their own dilutions and analyses), an analysis of the difference between the gypsum solubilities in each electrolyte was deemed a better comparison of the results than a comparison of the raw values.

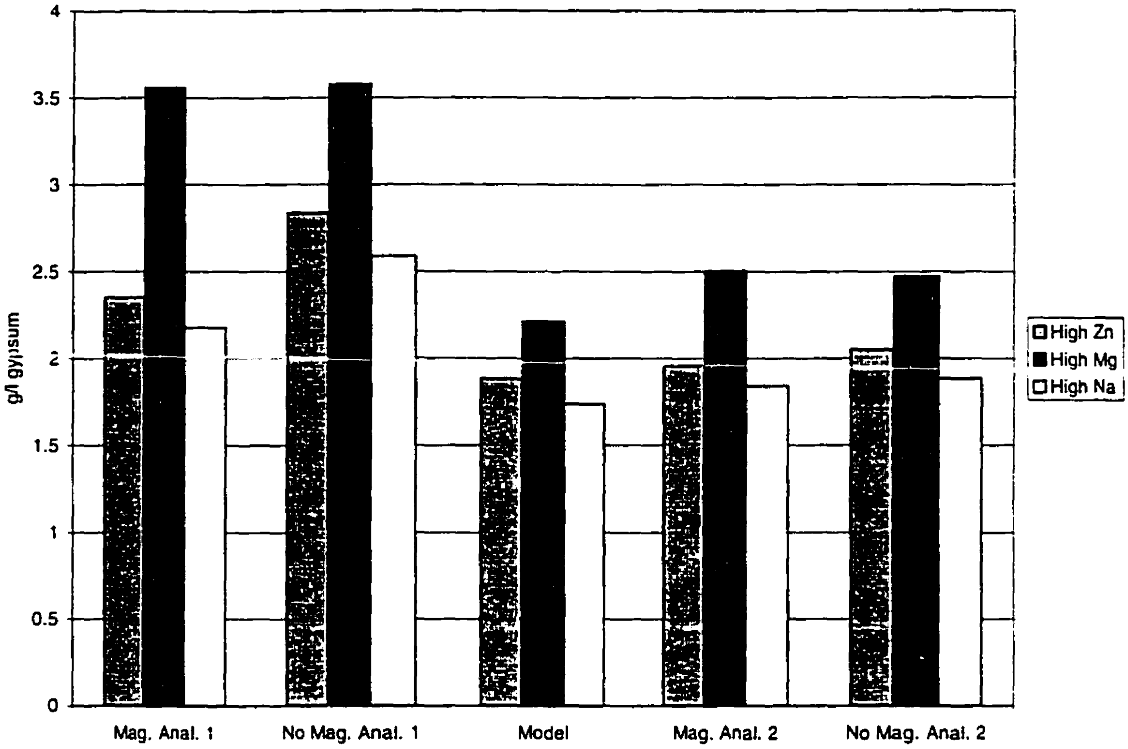

Figure D-1 - Gypsum solubility in mixed sulphate electrolyte, total ionic strength = 1; Comparison of gypsum solubility with and without magnetic stirrers (Mag., No Mag.), predicted model results, and the different calcium analysis results (Anal. 1, Anal. 2).

The difference analysis was made as follows: the solubility of gypsum in the three electrolyte solutions are A (I Zn=0.8), B (I Mg=0.8), and C (I Na=0.8). The B value was always the largest, so the values of A and C were normalized with respect to B. The differences between the normalized values of A and C were compared.

The difference values for the solubility of gypsum without a magnetic stirrer were 0.069 and 0.068 for the two different analyses; the value calculated by the thermodynamic model was 0.066. However, the difference between the normalized solubility values with a magnetic stirrer were 0.0484 and 0.0482 for the two analyses. It appears that the magnetic stirrer may have some effect affect on the solubility of gypsum in mixed sulphate electrolyte solution.

Effect of magnetic stirrers on gypsum precipitation^B

Solutions of saturated gypsum were left to sit in one of two beakers. One beaker included a magnetic stirrer, and one beaker did not. The solutions were left for a few hours at room temperature. Aliquots of the saturated solutions were placed on watch glasses and allowed to precipitate by evaporation at room temperature. The precipitated crystals were imaged by SEM.

In general, the precipitated crystals from the two systems were of the same morphology and size (Figures D-2 and D-3). However, disordered crystal agglomerations were observed in some of the clusters that had precipitated from the solution that was exposed to the magnet (Figure D-4). No such clusters were observed amongst the precipitate that was produced from the solution that was not exposed to the magnetic stirrer. These preliminary tests suggest that the presence of a magnetic field in the electrolyte could affect the crystal growth of gypsum from solution in some way.

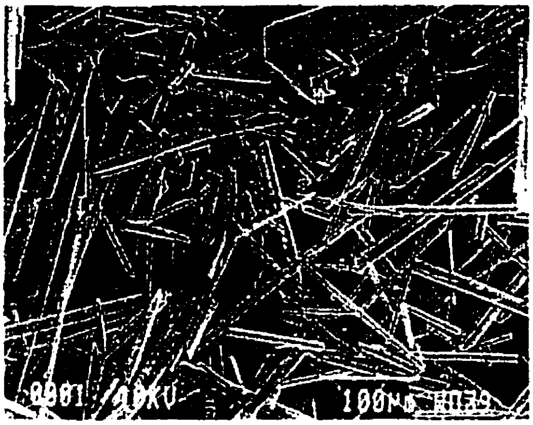

Figure D-2 – SEM Image of gypsum precipitated by evaporation from a saturated gypsum solution not exposed to a magnetic field.

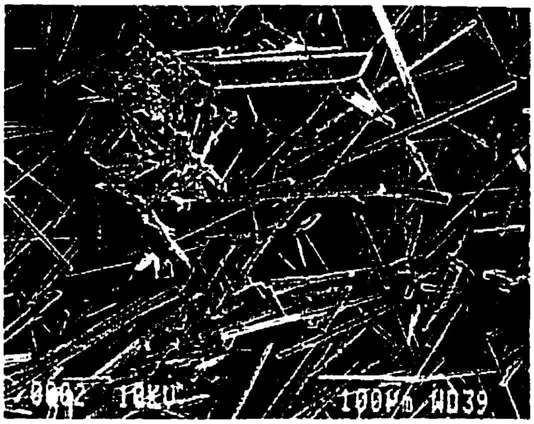

Figure D-3 - SEM Image of gypsum precipitated by evaporation from a saturated gypsum solution that was exposed to a magnetic field (magnetic stirrer).

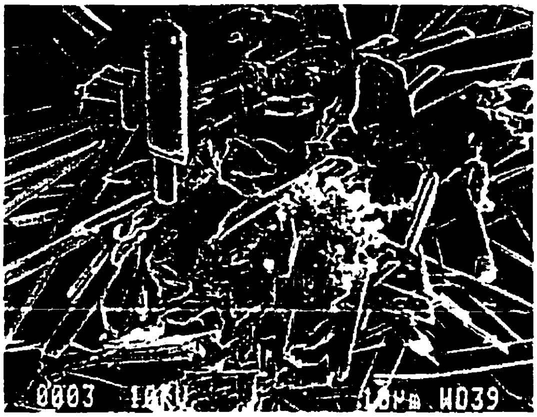

Figure D-4 - SEM Image of gypsum precipitated by evaporation from a saturated gypsum solution that was exposed to a magnetic field (magnetic stirrer).

A - Alex Brassard, an undergraduate student in metallurgical engineering performed these solubility tests as part of an undergraduate research project.

B - An undergraduate student group in chemical engineering (Angel Leung et al.) undertook the study on the effect of magnets on scale prevention as a project for their laboratory research course. They performed the precipitation experiments.

Appendix E - Settling velocity measurements

The settling velocity of the solids in the slurry was taken by measuring the time taken for the solid-liquid front to pass through distances marked on a 250 mL graduated cylinder with a stopwatch. This was often a qualitative judgement, as this test attempted to measure the one of many observed settling velocities during the sedimentation of a mixture of particle sizes. Figure E-1 (taken from Davis, 1996) shows how different regions develop.

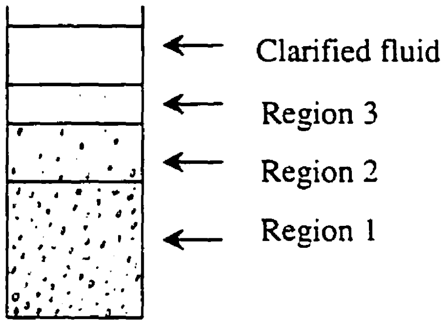

Figure E-1: The regions that develop during the sedimentation of a mixture of three distinct species of particles.

Region 1 contains all three species of particles, region 2 is free of the fastest settling particles, and region 3 is composed of the slowest settling particles (fines)

The wall effects of the 250 mL cylinder were determined to be negligible after the results were compared to those obtained from the larger diameter reaction kettle. In all cases, three readings were taken for each of three samples of slurry volumes, giving a total of nine measurements for each recycle.

The settling velocity values were thought to indicate a change in gypsum particle size, however, the settling velocity is also a strong function of solids content (Davis, 1996) (Figure E-2). For an equivalent solids loading, the settling velocities of precipitate grown on recycled gypsum seed were higher than that of precipitates produced with synthetic seed, which were again higher than the settling velocities of the solids precipitated without seed (Figure E-3). This higher settling velocity of the recycled solids is beneficial for the solid-liquid separation process, as a smaller unit operation may be designed. It was concluded that the settling velocity was not a definitive indication of increased gypsum particle size. Imaging proved to be a better technique of observing the increase in gypsum particle size.

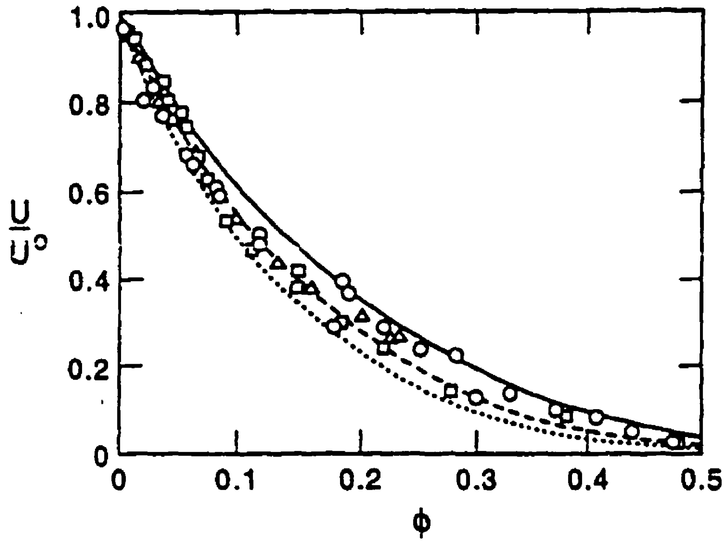

Figure E-2: The dimensionless sedimentation velocity as a function of volume fraction, from Davis et al., 1996

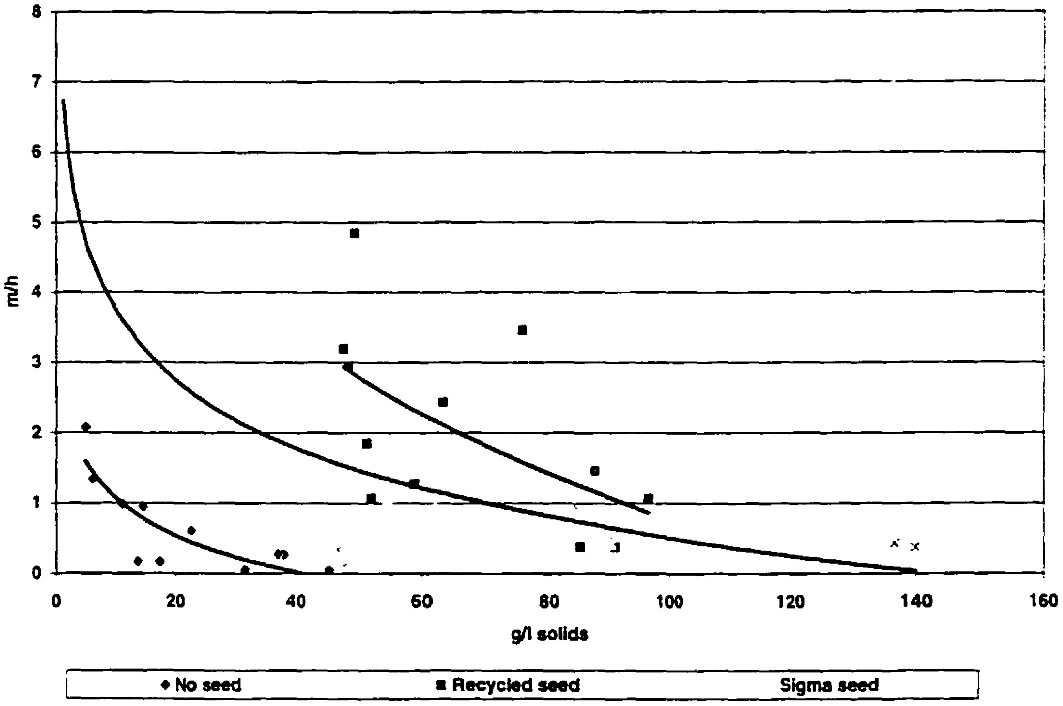

Figure E-3: Settling velocity vs. volume fraction for precipitates produced with no seed, from synthetic (Sigma) seed, and from recycled seed; experimental data.

Appendix F - The effect of gypsum seed concentration on product solids density and percent fines: Determining a suitable solids content for semi-batch neutralization recycle experiments.

Objective

The effect of seed concentration on precipitated product solids density and fines fraction was tested by recycling an initial solids content through repeated neutralizations with either 90% or 50% of the precipitated mass of the previous neutralization run.

Materials

The semi-batch setup described in Section 4-3-3-3 was used for the tests. All chemicals used were reagent grade. Deionized water was used to make the 10 g/l acid solutions. Reagent-grade synthetic gypsum was used as seed for the first neutralization cycle of each test, however, the seed for the next recycle was taken from the seed of the previous neutralization cycle.

Methods

Gypsum was precipitated by neutralizing seeded 500 ml solutions of 10g/l acid (pH 1) to pH 7 with incremental additions of 15 g/l slaked CaO. The neutralization addition rate was approximately 5ml/min (1.3 mmol/min) for all tests. The initial seed concentration for each test varied, depending on the recycle fraction under investigation (Table F-1). Both tests began with a gypsum seed concentration of 30 g/l.

Table F-1 – Recycle run seed concentration (g/l)

% Solids Recycled	1st Neutralization	1st Recycle	2nd Recycle	3rd Recycle	4th Recycle	5th Recycle	6th Recycle
90 %	30	36	39	42	46	50	52
50 %	30	20	15	12	11	10	-

Results

Figure F-1 compares the solids density of each recycle run for the 90% and 50% recycle fractions. A decrease in solids density with decreasing seed concentration can be attributed to the decrease in nucleation sites available for crystal growth, favouring

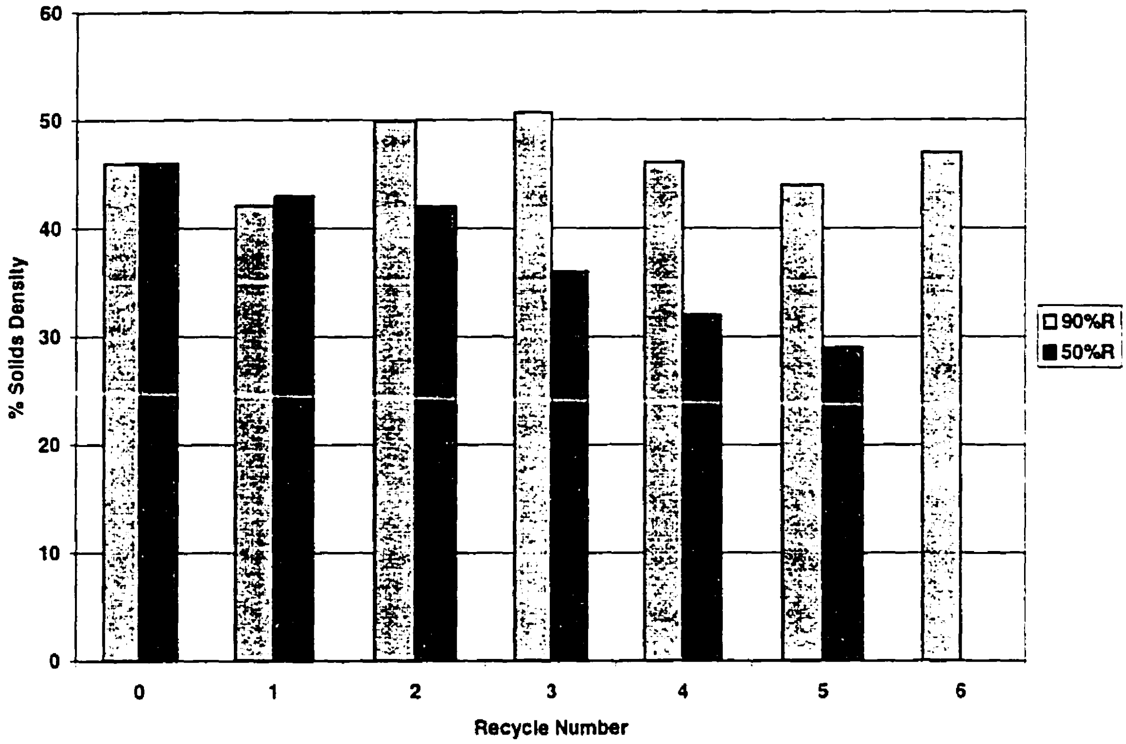

Figure F-1 – Precipitation product solids density vs. recycle number: 90% and 50% recycle fractions

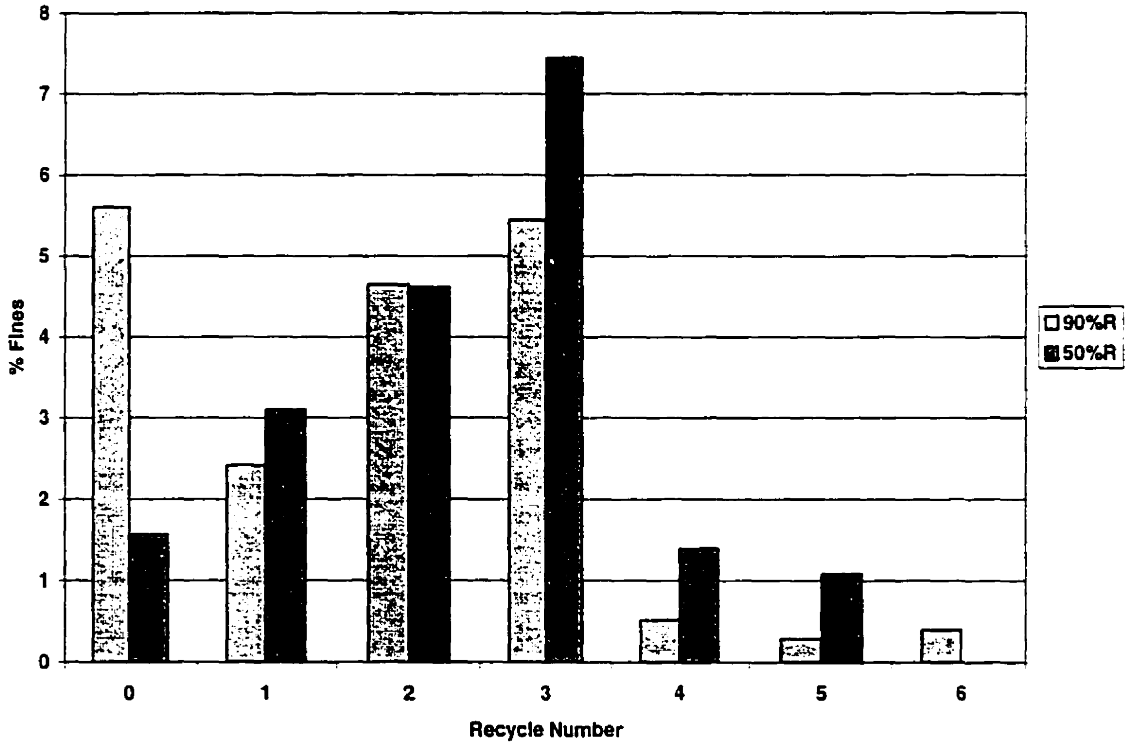

Figure F-2 – Percent fines separated vs. recycle number: 90% and 50% recycle fractions primary nucleation and the production of fines. Figure F-2 presents a "quick-and-dirty" percent fines analysis. Fines are defined as the mass of solids that did not settle within a few minutes after an agitated slurry was allowed to settle, unflocculated, under gravity. The settling time changed from two minutes to five minutes at the fourth recycle, resulting in a dramatic change in the value of percent fines. This change was made as it appeared that what were initially small fines were growing in size as they were recycled, and the amount of newly produced, smaller fines was of interest.

The fines could have been generated by: attrition, primary (homogeneous or heterogeneous) nucleation, and/or the precipitation of contaminating cation (iron) hydroxides, or may be fines that were not separated from the previous run. It is assumed that the mean contribution of attrition and fines carry-over to the fines produced in a succeeding run is equal for each run. For all runs after the second recycle, the fraction of fines increased, and the precipitate solids density decreased with decreasing solids loading, and vice versa. An increase in solids concentration above 40 g/l appeared to produce about a 45% solids density precipitate.

A seed concentration of 50 g/l was chosen to represent a reasonable seed concentration that would not be expected to produce fines due to a lack of seed surface area, and corresponding lack of nucleation sites for seed growth for the semi-batch neutralization recycle tests.

Appendix G – Gypsum morphology

The observed morphology of a crystal grown from solution is the result of the different growth rates of the different crystal faces. The fastest growing faces are either the smallest in size or are extinguished entirely. Figure G-1 (from Bloss, 1971) summarizes how fast-growing faces are extinguished.

Figure G-1: The process of crystal face extinction by different face growth rates. The size of the arrows represents the magnitude of the face growth rate. Face B is the fastest growing face, becoming the smallest face.

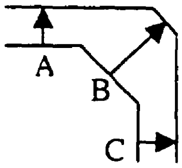

Simon and Bienfait (1965) used the periodic bond chain (PBC) theory to predict the theoretical gypsum crystal morphology (Figure G-2, (A) from Simon et al., 1965). Heijnen and Hartman (1991) also calculated a theoretical gypsum morphology (Figure G-2, (B) from Heijnen et al., 1991), but they both differ from the morphology observed in pure water solutions (Figure G-2, (C) from Heijnen and Hartman (1991)).

Figure G-2: Different calculated and observed habits of gypsum

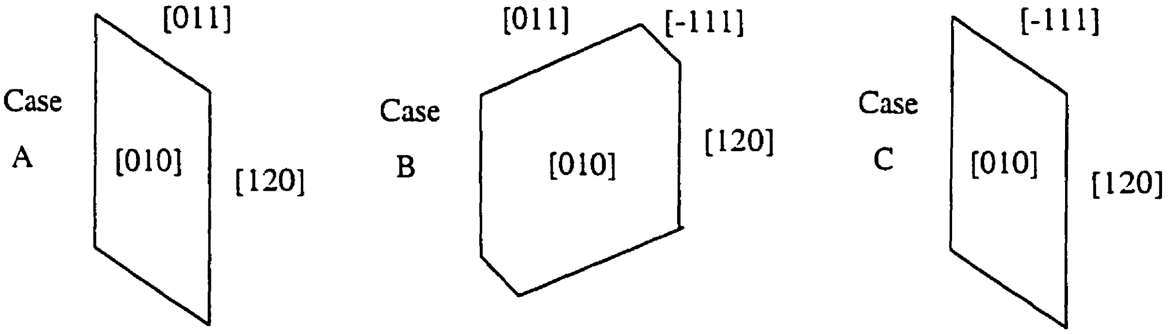

Van der Voort and Hartman (1991) used the energy of the face-solvent interactions to calculate theoretical gypsum face sizes, and generated a morphology similar to the one calculated by Heijen and Hartman (1991). This paper suggests that the morphology of gypsum may also be affected by the presence of adsorbed water on the crystal faces, which could affect the face growth rate. They argue that the growth of faces that do not have crystallographic waters on the surface would be slowed by the presence of adsorbed water. The [120] and [-111] faces do not present crystallographic water; this could explain the dominance of the observed [-111] face over the [011] face in solution. Weissbuch et al. (1995) discuss the idea put forth by others that favourable interactions between solute and solvent on specific faces can lead to faster surface growth.

If the Ising, or roughening temperature is used to predict the gypsum morphology, a morphology similar to that produced by the PBC theory results, as the Ising temperature for each face decreases from [010]>[120]>[-111]>[011]. A comparison of interfacial tensions for each face also indicates a similar theoretical model, with a similar trend in values (Weijnen et al. 1987).

It is proposed that the population of the face-specific growth units in the adsorption layer could also affect the rate of face growth. It has been proposed by Van der Voort et al. (1991) that the [-111] and [011] faces require Ca-SO_4-$2H_2O$ (½d) building units, while the [120] and [010] faces require Ca-SO_4-$2H_2O$- Ca-SO_4-$2H_2O$ (d) building units. The composition of the supersaturated solution may decrease or increase the probability of "d" growth unit arrangement, affecting the growth rate of that face.

For example, the semi-batch neutralization of acidic solutions (pH 0.5-1), takes place in solutions with a very low free sulphate concentration, and high bisulphate concentration. The needles produced in this environment may be indicative of the higher probability of a "½d" growth unit populating the adsorption layer instead of a "d" growth unit, resulting in higher growth rates for the [011] and [-111] faces. A relatively low population of these "½d" growth units, combined with the low activity of water may make the availability the "½d" growth unit the factor that determines the growth rate on the [011] and [-111] faces. This could contribute to the explanation of the presence of the arrowhead needle tips shown in Section 4-4-3-1-4, as if the water adsorption was an important factor, the growth of the [011] face would be favoured.

The active growth on the [120] and [010] gypsum faces grown in controlled neutralization conditions in the simulated zinc plant effluent may be related to the high sulphate concentration, and complexing power of the Ca^{2+} ion to form ion-pairs with sulphate. Both of these factors may affect the availability of "d" growth units, and the growth rates of the [010] and [120] faces. The growth rates of these faces are faster in the simulated zinc plant solution, resulting in crystals with lower aspect ratios.

In conclusion, there appears to be a complex relationship between the solution chemistry and crystal properties that makes the prediction of gypsum morphology difficult. However, the active growth on the [010] and [120] faces of gypsum grown in simulated zinc plant effluent produces thick gypsum crystals with low aspect ratios, which are expected to settle well from solution and pack efficiently.

Appendix H– The formation and effect of cluster crystals

Precipitation tests performed without seeds often produced gypsum crystals with stellate (radial aggregates radiating from a "star" like point) or divergent (crystals radiating from a center without producing stellate forms) morphologies (Figure H-1). It is proposed that these clusters are the result of discontinuous epitaxial growth of gypsum on foreign nuclei.

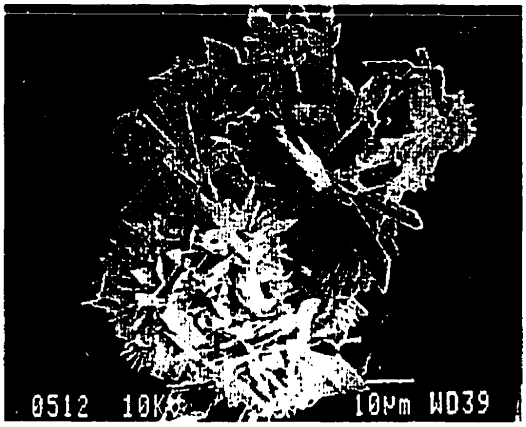

Figure H-1: SEM image of gypsum crystal cluster, precipitated with slaked lime from a seeded neutralization of sulphuric acid solution from pH 1 to 7

Epitaxy and crystal growth

Epitaxy signifies the oriented overgrowth of a crystal A upon the surface of a second phase B (Bloss, 1971). This overgrowth may be fairly continuous if the lattice dimension of the two phases are similar. If the lattice dimensions of solid A cannot be altered to permit continuous contact, then only small crystals of A will develop on substrate B. The small crystals that were oriented correctly could then continue to grow into the supersaturated solution, producing the observed clusters.

Systems that produce stellate gypsum

The evaporation of an unseeded solution saturated with gypsum at room temperature and pressure produced different gypsum morphologies^{A}. The precipitate morphologies were a combination of mostly needle and some stellate forms. The larger stellate crystals were taken apart, and in some cases, a foreign solid was observed in the middle of the cluster.

The divergent morphologies were also observed in particular precipitation tests. Large numbers of these morphologies were observed during the neutralization of unseeded acid solutions from pH 1-7 with dry lime or calcium carbonate (Figures H-2 and H-3). It is postulated that the slow dissolution of the neutralizing agents results in epitaxial growth of gypsum on the undissolved solids. Amatieu et al. (1988) postulated that the slow dissolution of calcium sulphate hemihydrate ($CaSO_4.\frac{1}{2}H_2O$) solids caused the heterogeneous nucleation of gypsum precipitation on the hemihydrate solids.

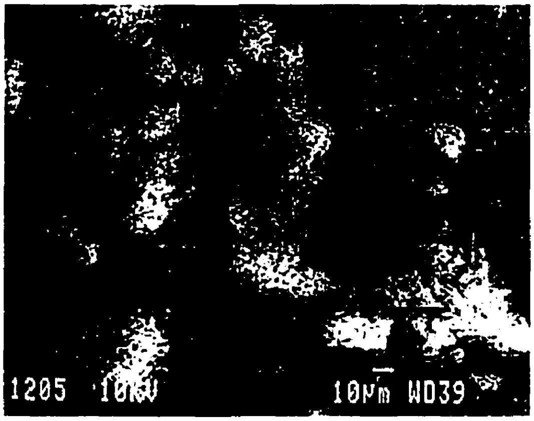

Figure H-2 – SEM image of gypsum crystals produced by neutralization of sulphuric acid solutions from pH 1-7 with dry lime

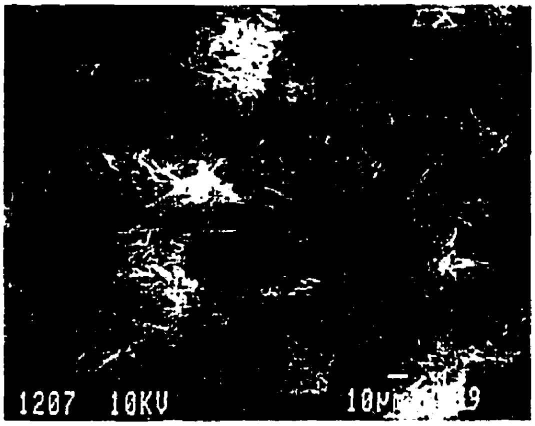

Figure H-3 – SEM image of gypsum crystals produced by neutralization of sulphuric acid solutions from pH 1-7 with dry calcium carbonate

Similar neutralizations of unseeded acid solutions from pH 0.5-1 with dry lime or calcium carbonate produced small, thin solids (Figures H-4 and H-5) however, stellate crystals were not apparent amongst the precipitated solids. This could be due to the rapid dissolution of the dry neutralizing agents in the more acidic solution.

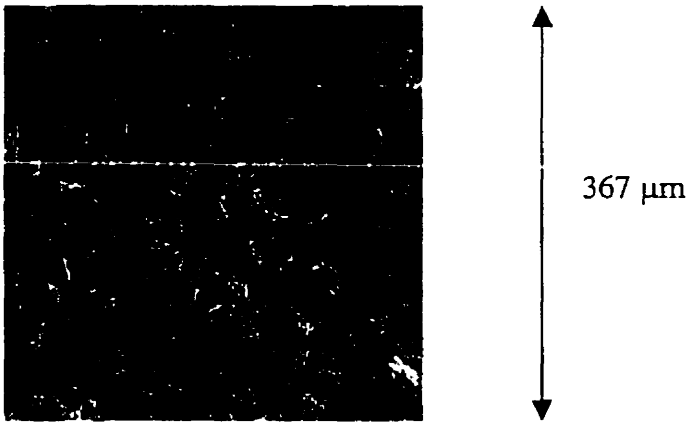

Figure H-4 – SEM image of gypsum crystals produced by neutralization of unseeded sulphuric acid solution from pH 0.5-1 with dry lime

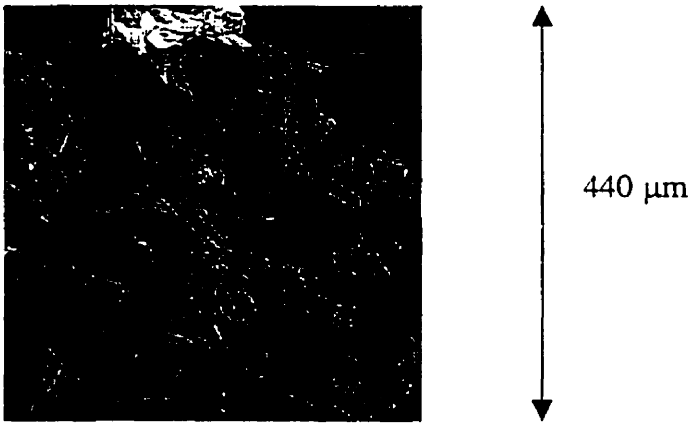

Figure H-5 – SEM image of gypsum crystals produced by neutralization of unseeded sulphuric acid solution from pH 0.5-1 with dry calcium carbonate

Other precipitation systems produced smaller numbers of clusters amongst the bladed or needle crystals (Figure H-6). It is presumed that the production of some divergent clusters is inevitable, as a wastewater treatment system will not be free of foreign solid impurities. However, these clusters may be crushed or shorn apart during the neutralization process, resulting in the release of smaller, well-grown crystals that can act as nucleation sites when recycled back to the process. Their production is not considered detrimental to the neutralization process, and preliminary results did suggest that they are not formed to any large extent during the continuous, staged neutralization (pH 1-5) with solids recycle and slaked, not dry, lime.

Figure H-6: SEM image of a combination of bladed and stellate gypsum precipitated with slaked lime from a seeded neutralization of sulphuric acid solution from pH 1 to 7

A – This experiment was performed as part of a chemical engineering undergraduate lab project by Angel Leung et al.

Appendix I – Twinning and gypsum growth

A crystal is said to be twinned if there is an intergrowth in which all crystallographic directions of the first crystal form are related to the corresponding crystallographic directions of the second crystal form by a geometric operation: a mirror plane of symmetry, a two (or more)-fold axis of symmetry, or a center of symmetry (Bloss, 1971). The type of symmetry operation classifies the different types of twins. Gypsum is well known for forming contact twins, which are mirror images of the crystal across a composition plane (Mineralogy, 1998).

Twins may from for a variety of reasons. Transformation and deformation twins may be formed when outside forces act on a crystal structure, causing a change in the crystal lattice along a plane. Growth twinning is caused by an error in stacking of unit cells when the crystal first begins to grow (Mineralogy, 1998). This error may be caused by the structure of the growth units in the adsorption layer of the crystal surface, or by the structure of water or other ionic molecules on the surface of the crystal that may interfere with crystal growth. The environment near the crystal surface in the adsorbing layer may orient a growth unit such that the unit joins with the crystal structure in a less-favourable orientation; if this incorrectly aligned nuclei continues to grow, a twin may result.

Publications concerned with gypsum crystal twinning (Rinaudo et al., 1985, 1992) highlight that the gypsum twin plane is usually (100) with a 180° rotation, and that hydrodynamics may have an effect on twin growth (Rinaudo et al., 1985). This type of twin was often grown in neutralization experiments with calcium carbonate (Figure 4-27), producing the "swallow-tail" morphology common for gypsum. Gypsum crystals produced by primary nucleation (without seed) by the neutralization through pH 0.5-1 with slaked calcium carbonate also exhibit many "swallow-tail" twins (Figure H-5).

Another predominant twin observed in gypsum crystal growth experiments was the nucleation of new islets on the [010] face (Figure 4-8) that are not aligned with the parent crystal growth axis, but grow approximately 60° to it. If the growth mechanism is polynuclear (birth and spread) on this face, as opposed to the spiral growth mechanism proposed for the growth of the other faces, then twinning may be due to the incorrect orientation of the birth nuclei on the [010] face.

Scanning force microscopy work on the gypsum [010] face (Hall et al. (1996), Bosbach et al. (1994)) revealed pits on the otherwise smooth face. Perhaps the twins on this plane were also induced by these pits, as it has been noted that some nucleation centers for twinning are positions of highly localized strain in the lattice (Reed-Hill, 1992). No evidence of this was presented in the SFM publications, as the SFM experiments only reported crystal growth in supersaturated solution by migration of elementary steps across the field of view.

Appendix J – Calculation of actual mean residence time and theoretical minimum mean residence time for adequate micromixing of the reactors used in the continuous tests

Residence time is defined:

$$\tau = \frac{V}{\dot{V}_A + \dot{V}_B + \dot{V}_C}$$

where V is the reactor hold-up, V_A is the acid (influent) flow, V_B is the slaked lime (influent) flow, and V_C is the recycled slurry flow to the reactor during steady-state conditions.

For the average continuous reactor conditions, the residence time varied from 15 to 25 minutes. The theoretical time for adequate macromixing was defined by Mersmann (1995, p. 231):

$$\tau_{macro} = 7.3\sqrt[3]{\frac{T^2}{\bar{\varepsilon}}}$$

where T is the tank diameter, and epsilon bar is the mean specific power input. The mean specific power input is calculated with the height of the reactor vessel (H), the vessel diameter (T), the stirrer diameter (D), the rotor speed (s) and a factor that is related to the stirrer Reynolds number (p_o):

$$\bar{\varepsilon} = \frac{4}{\pi} p_o s^2 D^2 \left(\frac{E}{T}\right)^2 \frac{D}{H}$$

p_o is 1 for the best stirred case, and ~0.04 for the worst case. As the characteristic number for the tested system is not known, both cases were calculated.

For the experimental setup, T = 10.5 cm, D = 4 cm, H = 10 cm, and s was estimated to be 300 rpm. The best case macromixing time was calculated to be 5.4 minutes, and the worst case macromixing time was calculated to be 15.8 minutes.

The calculated worst macromixing time was half of the average experimental residence time, therefore is could be assumed that the residence time was sufficient for good macromixing.

Appendix K: Zeta potential tests to determine the adsorption mode of zinc on gypsum

Zinc is the most valuable and abundant metal cation in the simulated zinc plant wastewater, therefore its inclusion in the precipitating gypsum structure is undesirable if it can be recovered. Tests were undertaken to determine if the incorporation of zinc in the precipitating gypsum structure was chemically favoured, or if its incorporation would be due to its random entrainment in the precipitating solid. These tests examined the zeta potential (ξ) of gypsum to determine if the zinc ion has a chemical or physical affinity for the gypsum surface. If the affinity of zinc cations to the gypsum surface is chemical in nature, zinc would likely be incorporated in the growing solid. If not, zinc ions by the gypsum surface might be displaced by the gypsum growth units, and zinc-free gypsum would precipitate.

The zeta potential is the measurable potential at the edge of the Stern layer (Israelachvili, 1991). The Stern layer is the layer of adsorbed ions that is very closely associated with a charged surface in solution. Specific adsorbing ions penetrate the Stern layer, affect the zeta potential, but do not change the surface potential. Potential-determining ions react chemically with the solids surface and affect both the zeta and surface potentials (Figure K-1). If zinc is determined to be a potential-determining ion, it could be assumed that it has a chemical affinity for the gypsum surface, and would likely be incorporated into the growing gypsum crystal structure. The calcium cation is a potential determining ion for gypsum; an increase in its concentration as calcium nitrate increases the negative zeta potential of gypsum in pure water to a positive value (Figure K-2). A similar increase in zinc concentration as zinc nitrate results in the zeta potential tending zero (Figures K-2). The error bars (Figure K-2) represent the measurement error. The increased salt concentration and the corresponding increase in solution ionic strength compress the electrical double layer. As the gypsum zeta potential does not become positive with increasing zinc concentration, it was concluded that zinc ions do not change the surface charge. Zinc was therefore not considered a potential-determining ion for the gypsum surface. EDS analysis of gypsum precipitated in synthetic zinc plant effluent did not detect zinc in the individual gypsum crystals (Figure 5-21).

As zinc does not specifically adsorb onto the gypsum surface, it could be excluded from the precipitating gypsum under controlled growth conditions, as its association with the surface is chemically weaker than the association of calcium.

Figure K-1 – The effect of non- potential-determining ions (Zeta 1) and potential-determining ions (Zeta 2) on the zeta potential.

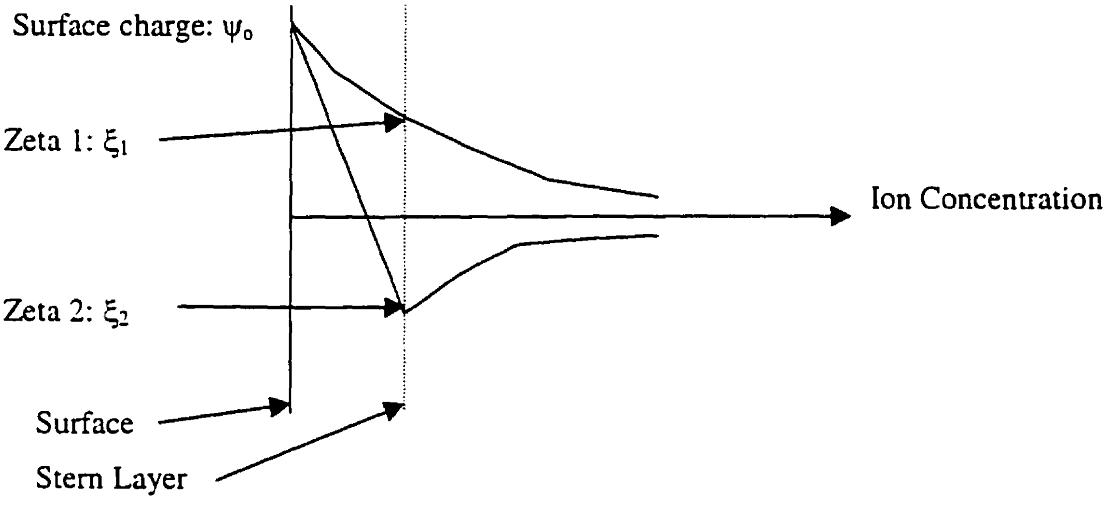

Figure K-2: The effect of calcium and zinc cations on the zeta potential of gypsum

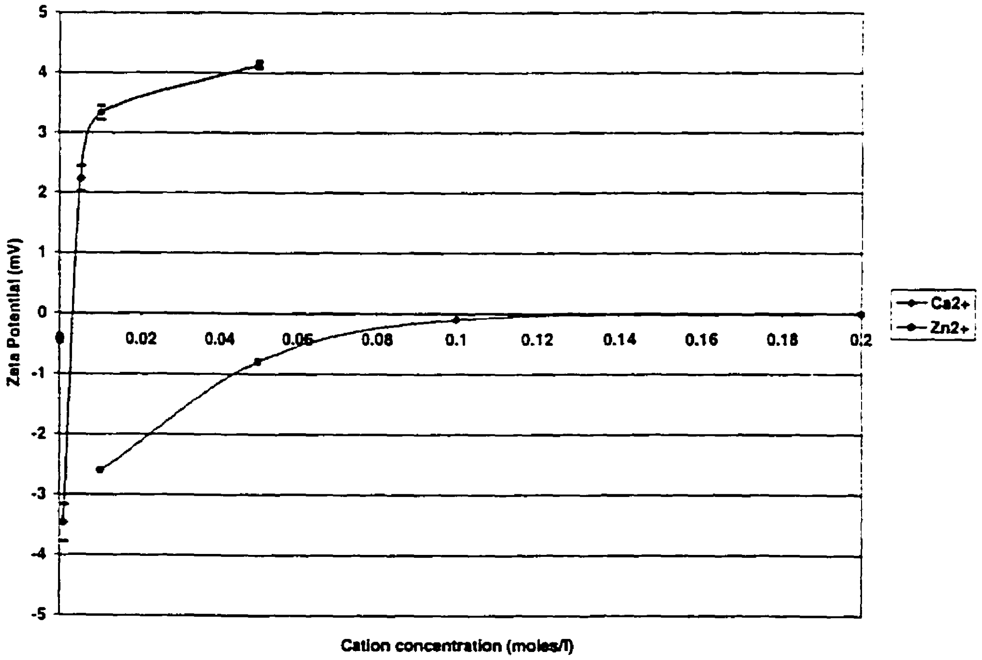

Appendix L - The effect of elevated temperatures on gypsum crystallization

Gypsum is the thermodynamically favoured calcium sulphate hydrate solid phase to exist in saturated systems at temperatures less than 40°C. Above that temperature, the calcium sulphate hemihydrate solid phase is favoured (Coburn et al., 1989); at even higher temperatures, the anhydride is the thermodynamically stable solid phase. The tests presented in this thesis were all performed at room temperature (20-25°C) and gypsum was precipitated from all tests.

Although it is not theoretically thermodynamically stable, gypsum has been reported to have spontaneously precipitated in solutions at 93°C (Furby et al., 1968) and solubility values for gypsum are available for up to 105°C (Nancollas et al., 1973). To briefly investigate gypsum precipitation at higher temperature, a short series of semi-batch tests were performed at 55°C with slaked calcium carbonate from pH 0.5-1 with the same methods outlined in Chapter 4 to investigate gypsum precipitation at this temperature[A].

The solids density improvement (Figure L-1) with the semi-batch recycle number is not as dramatic as the increase observed with the room temperature tests, as the solids density of the crystals produced at 55°C were consistently high.

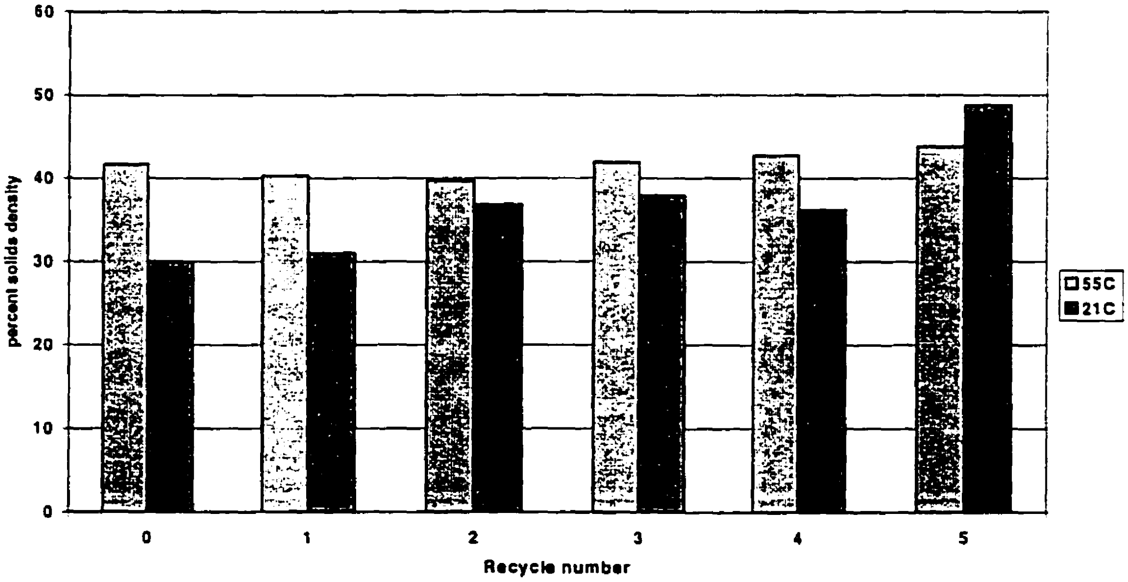

Figure L-1: Solids density of gypsum precipitated from pH 0.5-1 controlled, seeded neutralization with slaked calcium carbonate at 21°C and 55°C.

An inspection of the gypsum produced under high temperature showed crystals with needle morphology similar to that produced at room temperature at high acidity, but with smoother surfaces and sharper edges (Figure L-2 and L-3). Less twinning was noted amongst these crystals. An interesting surface roughening is presented in Figure L-4.

Figure L-2: SEM image of gypsum crystals precipitated from pH 0.5-1 controlled, seeded neutralization with slaked calcium carbonate at 55 °C (5th recycle).

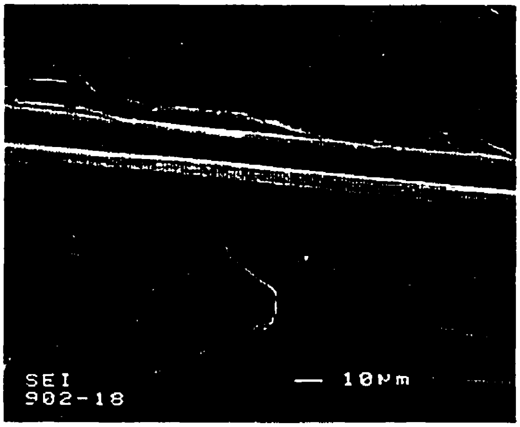

Figure L-3: SEM image of gypsum crystals precipitated from pH 0.5-1 controlled, seeded neutralization with slaked calcium carbonate at 55 °C (5th recycle).

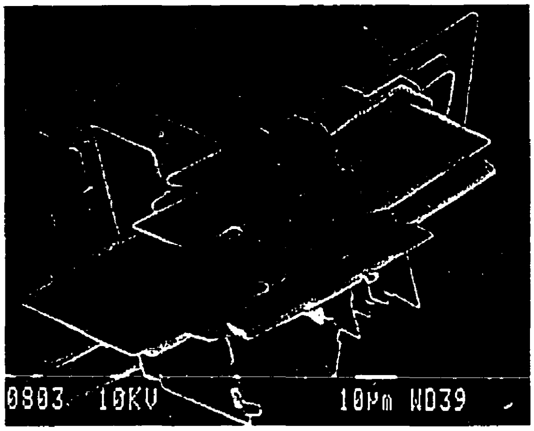

Figure L-4: SEM image of gypsum crystals precipitated from pH 0.5-1 controlled, seeded neutralization with slaked calcium carbonate at 55 °C (5th recycle).

The effect of temperature on the crystallization process is multi-faceted. In general it is usually easier to precipitate crystalline material from higher temperature systems, as the higher temperature facilitates the addition of growth units to an increased number of nucleation sites. The system temperature affects the "entropy factor", or concentration of kink sites where a growth unit can incorporate into the lattice (Söhnel et al., 1992):

$$\varepsilon = 4\omega / kT \qquad \text{(A-1)}$$

where ω represents the energy gain when a bond is formed between the solid and fluid phase, k is Boltzmann's constant, and T is absolute temperature. At low ε values/high temperature ($\varepsilon<3.2$), the crystal surface is very rough at the molecular scale, and the growth rate may reach its maximum value. A high probability exists that a growth unit will find a good kink site in which it may correctly incorporate into the crystal. As the value of ε increases, the surfaces become smoother, and steps are required for continuous crystal growth. The rate of two-dimensional surface nucleation is also a function of temperature through an exponential $\exp(-\Delta G/kT)$ term. As the temperature increases, the rate of two-dimensional surface nucleation increases.

An increase in temperature has other effects on the solution that facilitate the crystallization process. Increased temperature increases the exchange rate of the water in the solvation shell of charged species in solution; this could reduce the impedance of growth unit incorporation into the crystal lattice that comes from the required loss of solvation waters from the calcium ion. The calcium ion is surrounded by two water molecules in gypsum; a higher coordination number is possible in solution (van der Voort et al., 1991). Temperature also affects ion pairing equilibrium, and has been observed to affect the acid-base and speciation equilibrium in H_2SO_4-$ZnSO_4$ solutions (Filippou et al., 1995) of acidic zinc sulphate solutions. Temperature affects the activity of species in solution; the mean activity coefficient calculated by Meissner includes an equation to account for temperature.

A – These experiments were performed by Anne le Guen, an exchange student from Grenoble and a summer research associate extraordinaire.